DEVELOPMENT AND APPLICATION OF A PREDICTIVE MODEL TO DETECT ANALYTE CONCENTRATION FROM A QUARTZ CRYSTAL MICROBALANCE

By

WANG LIN

Bachelor of Science

Nanjing University

Nanjing, China

2000

Submitted to the Faculty of the
Graduate College of the
Oklahoma State University
in partial fulfillment of
the requirements for
the Degree of
DOCTOR OF PHILOSOPHY
May, 2005

DEVELOPMENT AND APPLICATION OF A

PREDICTIVE MODEL TO DETECT

ANALYTE CONCENTRATION FROM A

QUARTZ CRYSTAL MICROBALANCE

Thesis Approved:

Dr. Gary L. Foutch
Thesis Advisor

Dr. Russell Rhinehart

Dr. Arland Johannes

Dr. Martin S. High

Dr. Allen Apblett

Dr. A. Gordon Emslie
Dean of the Graduate College

PREFACE

This work characterizes a sensor technology employing thin coating film deposited on a Quartz Crystal Microbalance (QCM) device. The specific objective of this technology is to predict analyte concentration in rapid response. This work develops ion exchange / adsorption models to interpret sensor signal to analyte concentration. Several practical cases from industry or literature were studied. Emphasis has been placed on chemical and biochemical analyte detection.

Primarily, I would like to express my deepest appreciation to my advisor, Dr. Gary L. Foutch, for his guidance, inspiration, patience, and invaluable helpfulness throughout my PhD program. I would also like to thank the members of my dissertation committee, Dr. Russell Rhinehart, Dr. Arland Johannes, Dr. Martin S. High, and Dr. Allen Apblett for their helpful suggestions and invaluable insights.

Particular thanks goes to Dr. Dennis Hussey for his suggestions and previous work with the QCM model. I would also like to thank Dr. Jaehyun Lee and Mr. Yi Jia for their help and suggestions throughout my study.

Financial support from the School of Chemical Engineering and the Brims Ness Corporation is greatly appreciated.

I am grateful for the advice and assistance over the years from all the faculty, staff, and students I have met at Oklahoma State University. I would like to express my

special thanks to all my friends for their encouragement over the 4 years I have lived in Stillwater.

Finally, I want to express special gratitude and appreciation to my parents, Yiren Lin and Yun Yu, and to my brother, Zheng Lin, for their love, encouragement, and support over years. Nothing can exceed my appreciation to them except their love to me.

TABLE OF CONTENTS

LIST OF TABLES

LIST OF FIGURES

CHAPTER 1

INTRODUCTION

The focus of much of this thesis is on the investigation of theory and application of a quartz crystal microbalance (QCM) sensor. Precise measurement tools are necessary for successful scientific and engineering objectives. Over the past 20 years or so, research and development in the sensors area has expanded exponentially in terms of the number of papers published, the number of global active researchers, and financial investment. In addition, sensor technology has gained momentum from the enormous commercial potential for a variety of application, such as the hydrocarbon detectors used in the automobile industry, and sensors required for important clinical assays. Also, huge potential markets have been opened up in environmental monitoring, for example, environmental water monitoring or toxic gas and vapor monitoring in the workplace. Meanwhile, we will soon see devices that perform much better than the previous generations of sensors and are less expensive to purchase. In a word, we are on the verge of a "sensors revolution" (Diamond, 1998).

1.1 Characteristics of a sensor

The nature of sensors is that they produce an output signal in response to some input quantity. The output signal is usually electrical, including analog voltage or current, stream of digital voltage pulses, or possibly oscillatory voltage whose frequency represents the value of the input quantity. Factors that contribute to the suitability of a sensor for a particular assay may include physical parameters such as temperature, pressure, or even chemical interferences arising from the sample matrix. Desirable characteristics for a sensor are listed in Table 1.1, with some comments where relevant (Diamond, 1998). However, it should be pointed out that the "ideal" sensor does not exist—they all deviate from ideality to a more or less degree. In addition, the acceptable characteristics are often a function of the application. Hence, a sensor that performs well for detecting a particular analyte in a given matrix may be not suitable for detecting the same analyte in a different situation.

Table 1.1. Ideal Characteristics of a Sensor

Characteristic	Comments
Signal output should be proportional or bear a simple mathematical relationship, to the amount of species present in the sample	This is becoming less important with the advent of on-device electronics and integration of complex signal processing options to produce so-called smart sensors
No hysteresis	The sensor signal should return to baseline after responding to the analyte
Fast response times	Slow response times arising from multiple sensing membranes or sluggish exchange kinetics can seriously limit the range of possible application and prevent use in real-time monitoring situations
Good signal-to-noise (S/N) characteristics	The S/N ratio determines the limit of detection. S/N ratio can be improved by filter or impedance conversion circuitry built into the device ("smart" sensor)
Selective	Without adequate selectivity, the user can not relate the signal obtained to the target species concentration with any confidence
Sensitive	Sensitivity is defined as the change in signal per unit change in concentration (i.e., the slope of the calibration curve); this determines the ability of the device to discriminate accurately and precisely between small differences in analyte concentration

1.2 Trends in sensor study

The trends in sensor research can be obtained from the numbers of papers being published each year. Analytical journals are useful indicators of the research and development of sensor technology. A keyword based search of the *Analytical Abstracts* database revealed some insight into recent trends in this technology. The keywords used in this study are exactly the legends on the figure. Before examining these trends in

detail, it is worth nothing that variation in the number of papers may reflect changes in the popularity of terms rather than any fundamental changes in the research being carried out. An example of this is the growth in popularity of the term sensor, in contrast to the term electrode. This is because the term sensor is becoming more fashionable, although the same research groups may be involved in the publications (Diamond, 1998).

Figure 1.1 shows the number of papers for the term sensor for the period 1990-2003. The data are presented in terms of percentage of total number of sensor papers abstracted each year rather than in absolute number. The proportion of papers involving sensors grew from 3.25% to around 9%. This clearly shows a steady increase in the number of sensor papers. Over this period, the absolute number of sensor related papers rose from 484 to 1174.

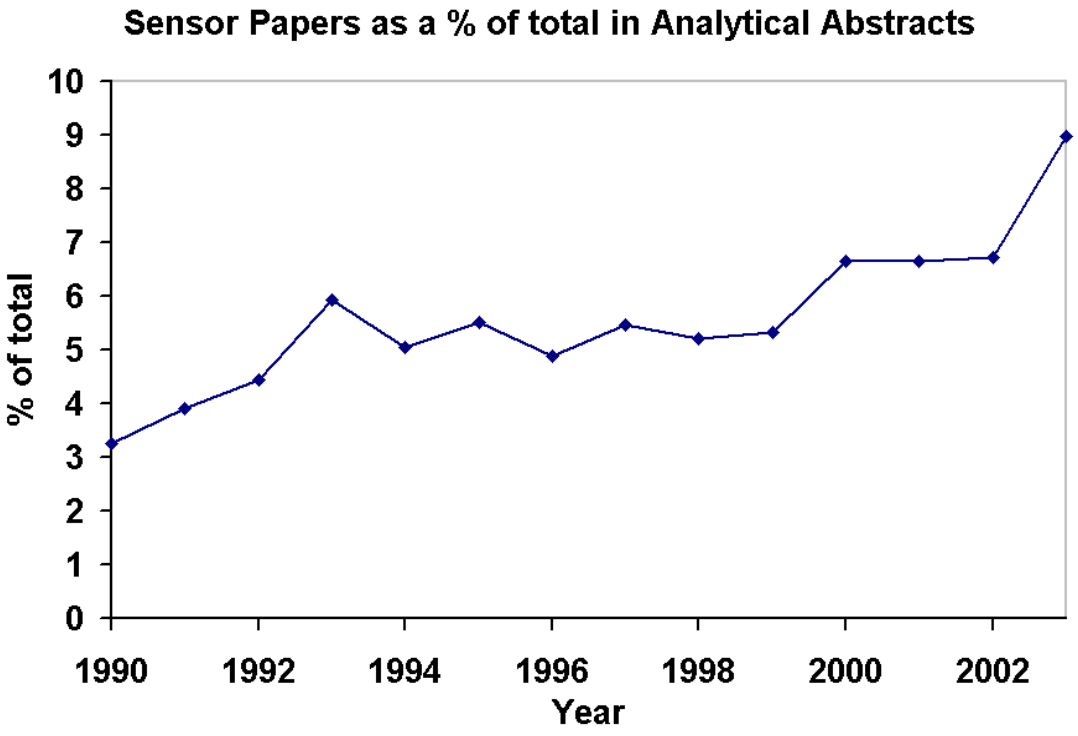

Figure 1.1. Papers searched using the keyword sensor expressed as a total of the number of papers in Analytical Abstracts from 1990 to 2003.

Figure 1.2 shows the absolute number of papers being published involving Quartz Crystal Microbalance (QCM). Clearly there has been a significant increase of QCM papers from 1995. This demonstrates a huge research effort, revealing the importance of current research, and the forecast of future application from it. Figure 1.3 demonstrates the number of papers for various subgroups of sensors, including ion selective electrodes, optical sensors, biosensors, acoustic sensors, and QCM sensors. Biosensors demonstrated their increasing importance from 1990. Also, ISE sensors lost their dominance from the 1980s, because ISE technology is mature compared to other sensor types, and publications tend to be much more on the applications side rather than fundamental.

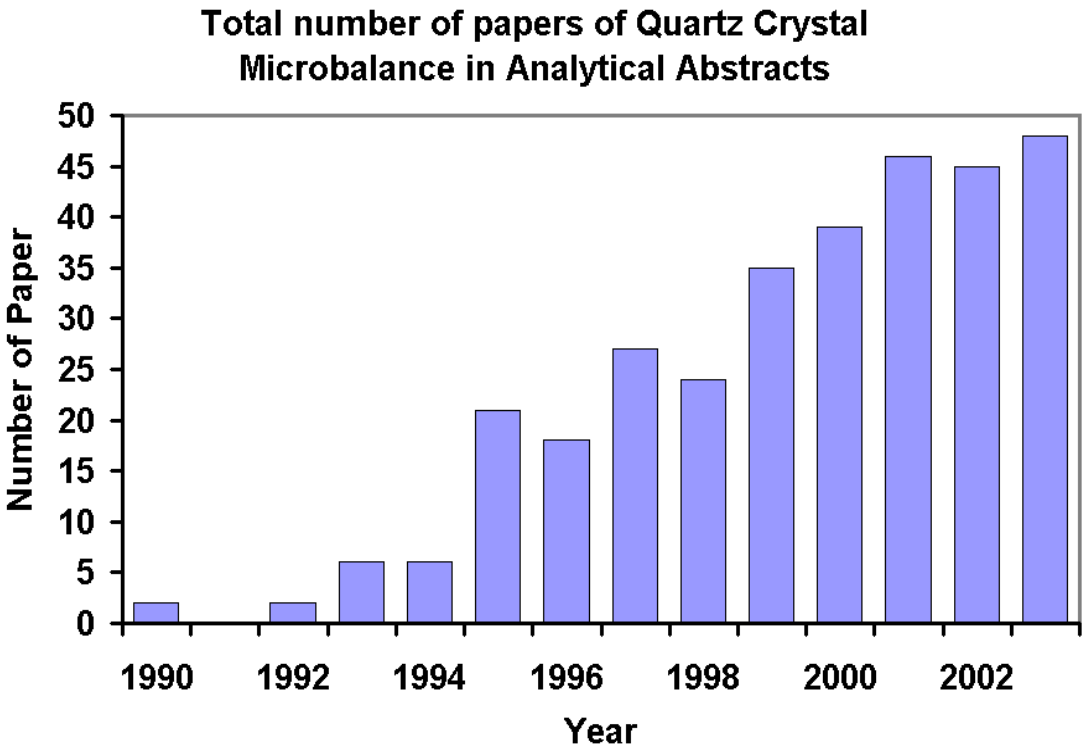

Figure 1.2. Absolute number of paper published with a keyword "Quartz Crystal Microbalance" from Analytical Abstracts over the period 1990 to 2003.

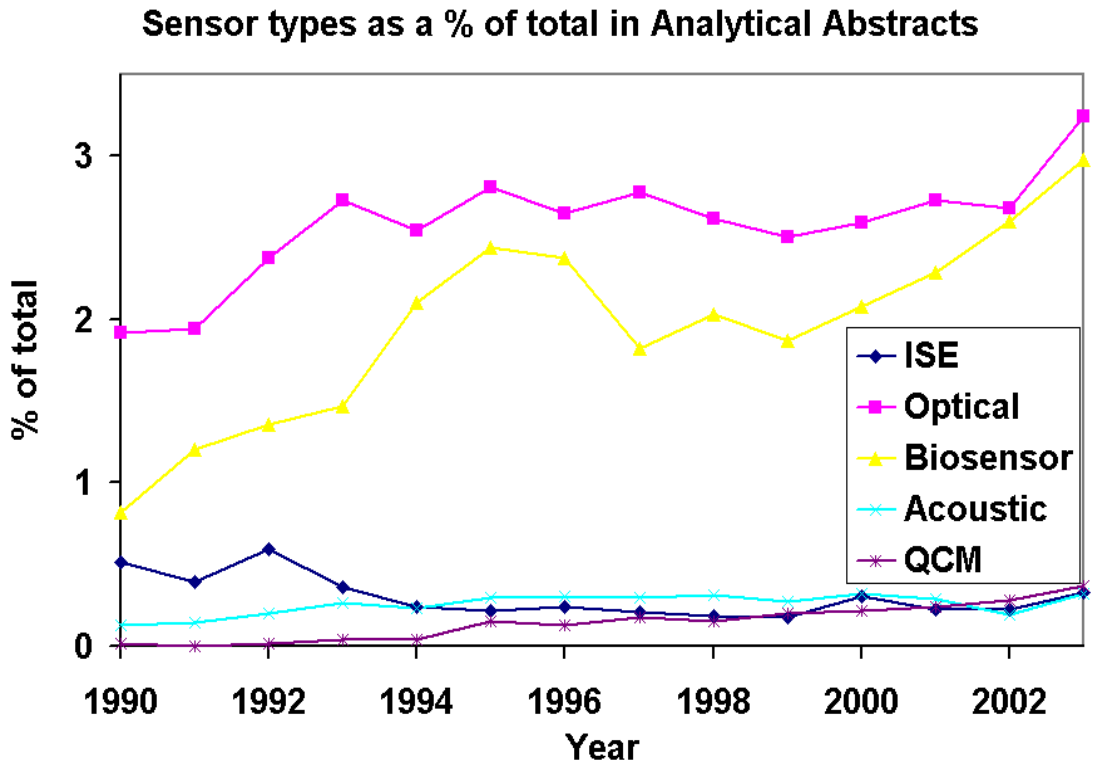

Figure 1.3. Trends in the proportion number of papers for each sensor type searched from Analytical Abstracts from 1990 to 2003.

1.3 The sensor market

Sensors based on MEMS technologies (microelectromechanical systems) and smart sensors are at the focus of current sensor development. MEMS technologies allow miniaturization of sensors and, at the same time, integration of their sensor elements with microelectronic functions in minimal space. The greatest progress in innovation, however, will happen where MEMS technologies overlap with smart technologies. The main goal of smart sensor development is to improve the reliability of these sensors and to make them more easily adaptable to new functions and conditions during the operating phase.

The non-military world market for sensors reached $32.5 billion in 1998. According to a newly released report, "Sensor Market 2008" by the Swiss company Intechno Consulting (Schröder, 1999), under very conservative assumptions it is expected to reach $50-51 billion by 2008; assuming more favorable but still realistic economic conditions, the global sensor market volume could even reach $54 billion by 2008. The expected price slump for many of these sensors is taken into account in these market figures. Shown as Figure 1.4, Western Europe is the leading consumer in 1998 with 31.7% of the world market, followed by the USA with 31.0% and Japan with 19.4%. The other countries account for approximately 17.9% of the world market.

Sensor types with the highest demand worldwide are temperature sensors, pressure sensors, flow sensors, binary position sensors (proximity switches, light barriers, reflectortype photosensors), position sensors, chemical sensors for measurement in liquids and gases, filling sensors, speed and rpm-sensors, flue gas sensors and fire detectors. The fastest growing types of sensors include rain sensors, thickness sensors, sensors that measure the quality of liquids, navigation sensors, tilt sensors, photodetectors, glass breakage sensors, biosensors, magnetic field sensors, and motion detectors. The worldwide sensor demand $32.5 billion in 1998 comprises around $29.3 billion for housed and ready-to-use sensors and $1.7 billion for sensor elements without housing. Worldwide demand for sensor modules was approximately $0.6 billion, and for complete sensor systems, $0.9 billion.

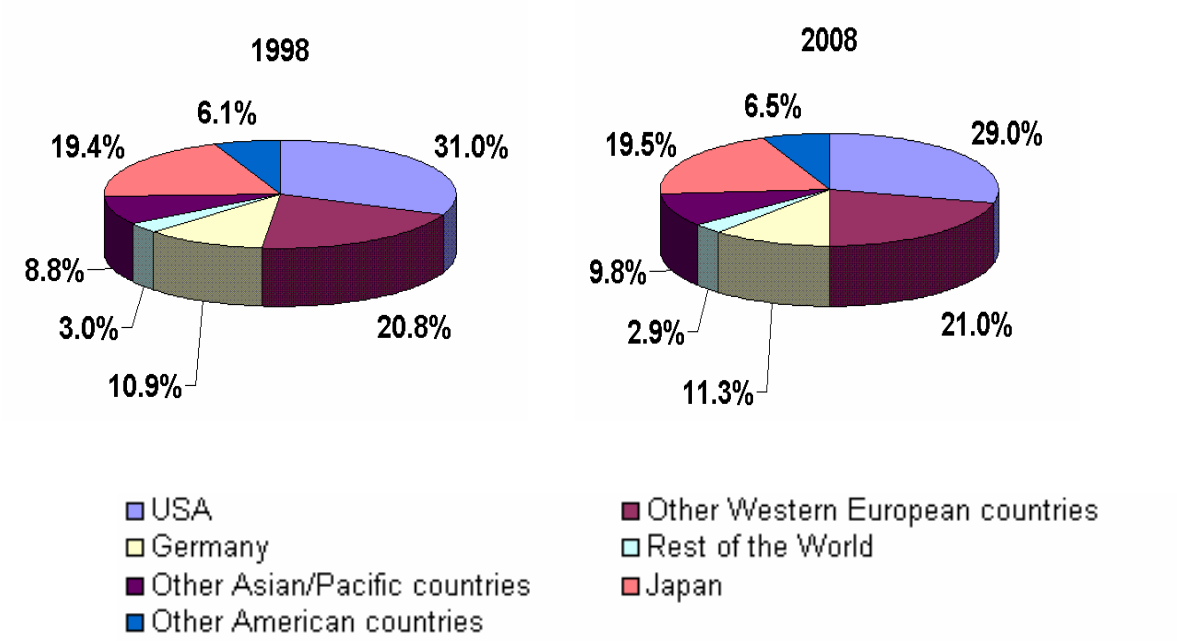

Figure 1.4. Development of the sensors market until 2008 (from Intechno Consulting).

The major success factors for sensor manufacturers specialized in mass applications are highly efficient mass production facilities, an increasingly internationalized distribution, and absolute customer orientation. The sensor product to be marketed in the future will be less and less just sensor hardware, but will include more and more software, service, and consulting. Chances in this field result from the ever-changing customer requirements, which become more differentiated and more complex. One example is remote-monitored storage tanks. In addition to supplying just filling sensors, sensor manufacturers can develop to become external service suppliers who take charge of procurement, maintenance, cleaning and even safety and security services. Through specific cooperation as well as for the single sensor company, the future might

hold interesting diversification opportunities, in line with the development from a technology provider to a service provider.

1.4 Technology trend in sensor research

The history of the development of sensor technology is a fascinating topic. To the present day, this technology is still an active area of research, particularly with respect to new products based on entirely different fabrication technologies. Process in sensor development increasingly requires a multidisciplinary effort and access to more complex fabrication technologies. Traditional sensor manufacturers have tended to specialize in a few products, and with low turnover and high profit margins. Although the traditional markets for conventional probes will undoubtedly remain, this situation is changing rapidly. Research, development, and the commercialization of sensor technology will accelerate over the coming years, and we can look forward to exciting new developments in this very dynamic area of scientific research. Some important areas of research contributing to progress in sensor development include (Diamond, 1998):

1. Improving the recognition mechanism is of fundamental importance as it is the basis of the signal that will be obtained from the sensor. Researchers are synthesizing new molecular receptors with better selectivity, as well as sensors that respond to new target species.

2. New materials are being investigated for use as a matrix in which to immobilize the receptor molecule. Important contributions are from new polymer materials with attractive properties—easily handled as monomer (nonviscous), a wide

variety of polymerization initiation mechanisms (e.g., photoinitiation, electropolymerization), rapid setting, and good stability in different environments.

3. New sensor substrates (i.e., materials constituting the body of the sensor, or on which the device is built) are being investigated, arising mainly from a need for new planar fabrication designs.

4. There is great interest in adapting planar fabrication technologies for sensor manufacture with the goal of producing devices that are as similar as possible to each other, as this will hopefully lead to products with predictable characteristics.

5. Improvements in signal processing technologies and instrumentation are making important contributions to the quality of sensor information. For example, smart sensors are being developed with a variety of signal processing options built in, ranging from impedance conversion to digitization and telemetry circuitry. In addition, the use of sensor arrays to analyze target, rather than single electrodes, can give important advantages such as multicomponent information, dynamic compensation for sample matrix effects, device malfunction-deterioration detection, and improved selectivity through the interpretation of response patterns obtained from the array.

1.5 Acoustic wave sensor

In 1880, Jacques and Pierre Curie discovered that a mechanical stress applied to the surfaces of quartz crystal produced an electrical potential across the crystal with a magnitude that was proportional to the applied stress. This behavior is referred to as the piezoelectric effect. Piezoelectricity literally means “pressure electricity”, derived from the Greek prefix *piezein*, “to press”.

The piezoelectric property exists only in ionic crystalline solids that crystallize in structure lacking a center of inversion. A crystal of an acentric material posses a polar axis due to dipoles associated with the arrangement of atoms in the crystalline structure. Therefore, considering a planar molecule of a hypothetical ionic solid that presents three electric dipoles of equal magnitude at 120° intervals, a net dipole moment will appear if the molecule is stretched or compressed along a direction parallel or perpendicular to one of the three vertices. Meanwhile, an electric field applied parallel to one of the three vertices will cause a distortion of each molecule. A quartz crystal provides the necessary combination of mechanical, electrical, chemical and thermal properties required for an acoustic device. However, piezoelectricity is not a unique characteristic of quartz. Crystallographers recognize 32 classes of crystals, of which, 20 are noncentrosymmetrical piezoelectric crystal. Not all crystals belonging to these 20 classes have an observable piezoelectric response, because it may be too small to detect.

Quartz crystal is made of silicon and oxygen and has the chemical formula SiO_2. Quartz is not the only mineral composed of SiO_2. SiO_2 is also found abundantly as the main component of sand. Although the crystalline form of quartz can be found in nature, its high cost has cultured the development of the quartz industry.

The combination of piezoelectricity with microelectronics began in the 1960s. In this period White and Voltmer (1965) demonstrated that photolithographic techniques could be employed to deposit interdigital transducers on piezoelectric substrates to excite and couple to elastic surface waves. Devices based on piezoelectric crystals, which allow transduction between electrical and mechanical acoustic energies, have been constructed in a number of configurations for sensor applications and materials characterization. The

development of integrated circuits reduced the cost of computing, storing, and transmitting information. It also made possible economical systems to process signals from sensors. The success of this effort has resulted in the availability of a growing number of sensors that are now moving from the research laboratories into development, commercialization, and application (Muller, 1990). Besides quartz crystal microbalance (QCM), sensing application of those devices also include the acoustic plate mode (APM) device, the surface acoustic wave (SAW) device and so on.

Figure 1.5. Quartz crystal microbalance unit (from Brims Ness Corporation).

Acoustic wave sensors are sensitive to perturbations of many physical parameters, both intrinsic to the sensor and extrinsic (Ballantine, 1997). Generally, both mass accumulation and changes in coating film properties can contribute to the response. Chemical sensitivity is typically introduced by depositing a thin coating film to the piezoelectrically active region of the sensor surface. As discussed in Chapter 5, important sensor parameters such as sensitivity, selectivity, reversibility, repeatability, and durability are critically dependent on this coating film. The coating film serves as a

chemical-to-physical transducer — one or more of its physical properties must change in response to the presence of the chemical species to be analyzed. The most commercially developed of the acoustic wave sensors is the quartz crystal microbalance. This sensor is often used in a deposition systems where it measures the mass accumulation of a deposited film. This device was analyzed and improved by a succession of workers starting in the 1950s (Sauerbrey 1959, King 1964). In a typical vapor detection application, the sorption of vapor molecules in a polymeric coating applied to one surface of the crystal increases the mass loading and lowers its vibration frequency.

The acoustic wave devices are conveniently small, relatively inexpensive, highly sensitive and selective, and inherently capable of measuring a wide variety of different input quantities.

1.6 Acoustic chemical sensors and biosensors

The definition by Janata and Bezegh (1988) sums up the role and the fundamental elements of chemical sensor: “a chemical sensor is a device which furnishes the user with information about its environment; it consists of a physical transducer and a chemically selective layer”. While a chemical sensor may contain a physical transducer, its basic character is usually determined by some type of chemically selective membrane, film or layer. Acoustic chemical sensors and biosensors most often employ the mass sensitivity of the vibration frequency in order to detect selectively adsorbed chemical species. Therefore, a coating film must be attached to the vibrating surface of the device which attracts molecules of the target species. The composition and form of this layer is of crucial importance in determining the effectiveness of the sensor, because it controls the

selectivity, sensitivity, lifetime, and response time of the sensor. In addition, a sensor is expected to detect target species in real time and provide a feedback signal for control purposes. Chemical sensors based on quartz crystals can be applied to both gas and liquid states (Lucklum 1991, Muramatsu 1988, 1990).

Biosensors are similar to chemical sensors, but they utilize biological molecules as the selective coating (Thompson 1987, Guilbault 1983). One definition of a biosensor is a sensing device that incorporates a biological entity (enzyme, antibody, bacteria tissue, protein etc.) as a fundamental part of the sensing process. Extreme selectivity is obtained by bioreaction, such as antibody-antigen reaction. However, a major problem associated with biosensors is that they usually work non-reversibly and the crystals can be reused only after repeating a sophisticated preparation procedure before each new detection.

CHAPTER 2

PRINCIPLES AND THEORIES OF QUARTZ CRYSTAL MICROBALANCE SENSOR

In the previous chapter, a quartz crystal resonator was introduced as an application in sensor field. The resonant frequency of a typical QCM device is determined by, along with some other physical parameters, the total mass of the vibrating body. When materials are added or removed from the vibrating body, a frequency change of the quartz crystal can be detected. The application of acoustic waves in solids at ultrasonic frequencies depends on the conversion of electromagnetic into mechanical energy. This process may involve inherent electromechanical mechanisms in piezoelectric materials or coupling of nonpiezoelectric solids with transducers capable of generating acoustic fields. The physics of propagation of acoustic waves in various materials is exceedingly complex in that it involves crystallography, electromechanical phenomena, wave engineering, and tensor mathematics, among a number of subdisciplines (Thompson, 1997). The emphasis in this chapter is to explain the piezoelectric effect and to give the theory and practice of piezoelectric quartz crystal resonators, modes of vibration and applications with different materials.

2.1 Piezoelectricity

Curies (1880) published the first description of the phenomenon of piezoelectricity. Piezoelectricity is associated with the instigation of electric polarization when a particular material is subjected to mechanical stress, and with the onset of deformation in the material when placed in an electric field. When the structure of a crystal lacks a center of inversion symmetry, the application of strain changes the distribution of charge on the atoms and bonds comprising the crystal in such a manner that a net, macroscopic, electrical polarization of the crystal results. This relationship is shown in Figure 2.1. The direct piezoelectric effect is the production of the electric displacement by the application of a mechanical stress; the converse piezoelectric effect results in the production of a strain when an electric field is applied to a piezoelectric crystal. The relation between stress and strain is indicated by the term “Elasticity”. Note that one could expand this representation to include magnetic variables (Nye, 1957).

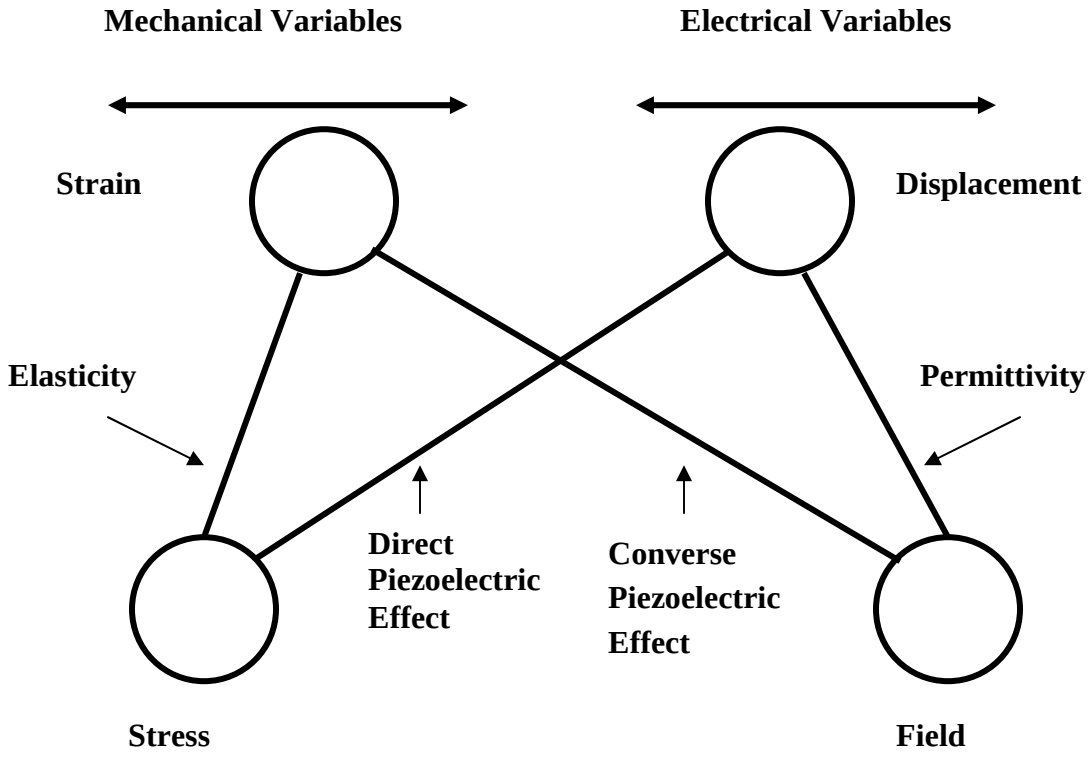

Figure 2.1. Relations among mechanical and electrical variables for a crystal. (Nye, 1957)

Generally speaking, when a pressure is applied to a piezoelectric material, an electric field is developed and the magnitude of the field is proportional to the mechanical stress (the piezoelectric effect). The converse is also true, i.e., the application of an electric field across a piezoelectric material induces a deformation of that material (the converse piezoelectric effect). Placing a piezoelectric crystal in an alternating electrical field causes it to oscillate in a mechanically resonant mode and results in a standing acoustic shear wave in the bulk of the quartz wafer (Lu, 1984).

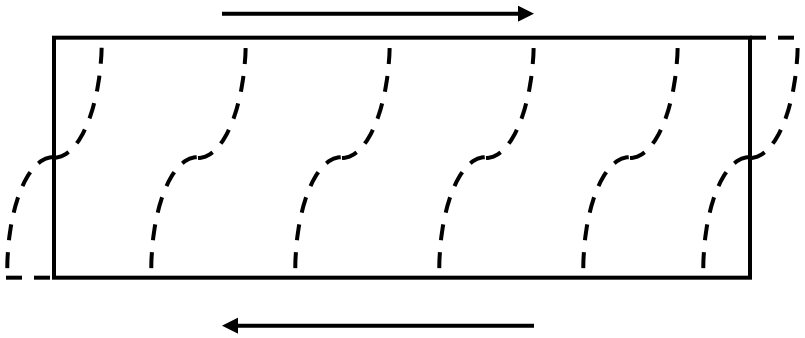

Figure 2.2. Schematic representation of a quartz crystal oscillating in the fundamental mode.

2.2 Piezoelectric materials

The origin of the piezoelectricity is from the interaction of Coulombic charge forces and elastic restoring forces that arise under such circumstances. An important factor in determining whether a particular material exhibits a piezoelectric property is the crystallographic nature of the solid. Piezoelectricity can not exist in solids with central symmetry (Thompson, 1997). Of the 32 crystal classes, 20 exhibit the piezoelectric effect (Lu 1984, Bottom 1982).

Crystalline quartz (silicon oxide), which is the principal piezoelectric material used commercially, has one axis of threefold symmetry, three axes of twofold symmetry and does not possess a central symmetry. Shearing stress produces motion of oxygen and silicon atoms. This deformation results in a separation of the charge centers and electric polarization. These electrical, mechanical and chemical properties of quartz crystal make it the most useful as a commercial piezoelectric material (Lu, 1984).

The quartz crystal has a natural vibration frequency (fundamental frequency) that depends on its chemical nature, shape and size, and mass. The cut of the crystal (the specific orientation with respect to the crystal axes) has an effect on the resonance

frequency (Heising, 1946). An AT-cut crystal is made by slicing through a quartz crystal at an angle of 35°15′ about the length direction (x-axis). The AT-cut quartz crystal plate is shown in Figure 2.3.

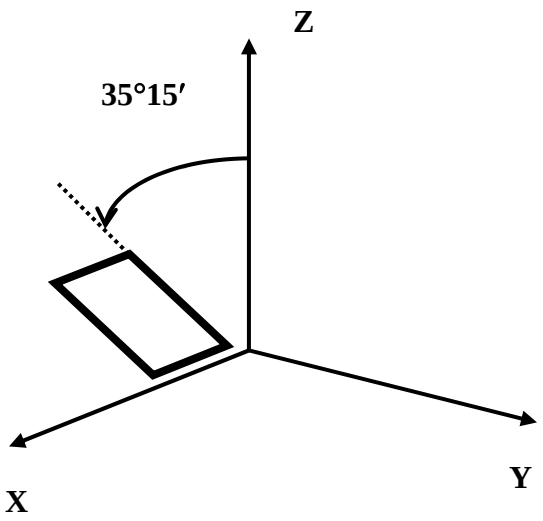

Figure 2.3. AT- cut quartz crystal plates.

A slight change in the orientation of a quartz crystal plate with respect to the crystallographic axes generally does not alter the mode of resonance. However, the effects of temperature and stress to the resonant frequencies are found to be highly sensitive to the crystallographic orientation (Lu, 1984). The advantage with the standard AT-cut quartz crystal is that it has nearly zero frequency drift with temperature around room temperature. This is a highly desirable feature for applications that requires the resonator to operate at, or near, room temperature.

2.3 Modes of vibration of piezoelectric quartz crystal

Quartz crystal is capable of transforming electrical energy to mechanical energy and vice versa. A piezoelectric quartz crystal resonator is a precisely cut slice from a single crystal of quartz. When a periodic voltage is applied to a quartz crystal unit, the quartz crystal may vibrate at the frequency of the exciting voltage.

At the resonant frequencies, a piezoelectric quartz crystal resonator can have many modes of resonance. A rectangular solid bar can vibrate in three types: longitudinal (extensional), lateral (flexural and shear), and torsional (twist). Meanwhile, the crystal can also vibrate at the overtone based on the three fundamental vibration modes. Also, some vibration modes can combine to form a much more complicated vibration. The need to have the quartz crystal oscillating at only one particular mode requires that the quartz crystal slice be cut at a specific crystallographic orientation with the proper shape. Among these types of vibrations, the high frequency thickness-shear mode is most sensitive to the addition or removal of mass for a quartz crystal resonator. The electrodes on the crystal, the QCM circuit and the supporting structure can also affect the mode of resonance (Lu, 1984).

2.4 Sauerbrey equation

For the application of piezoelectric quartz resonators for quantitative mass measurements, it is necessary to develop a quantitative relationship between the relative shift of the resonant frequency and the added mass. Before 1959, the understanding of this mass induced frequency shift was only known on a qualitative basis. However, Sauerbrey (1959) first showed that the frequency shift of a quartz crystal resonator is

directly proportional to the added mass. Sauerbrey's work is generally taken as the breakthrough and the first step towards a new quantitative tool to measure very small masses, i.e., the quartz crystal microbalance. If one assumes that the addition of a foreign mass can be treated as an equivalent mass change of the crystal itself, a fractional change in the mass results in a fractional change in the resonant frequency of the crystal.

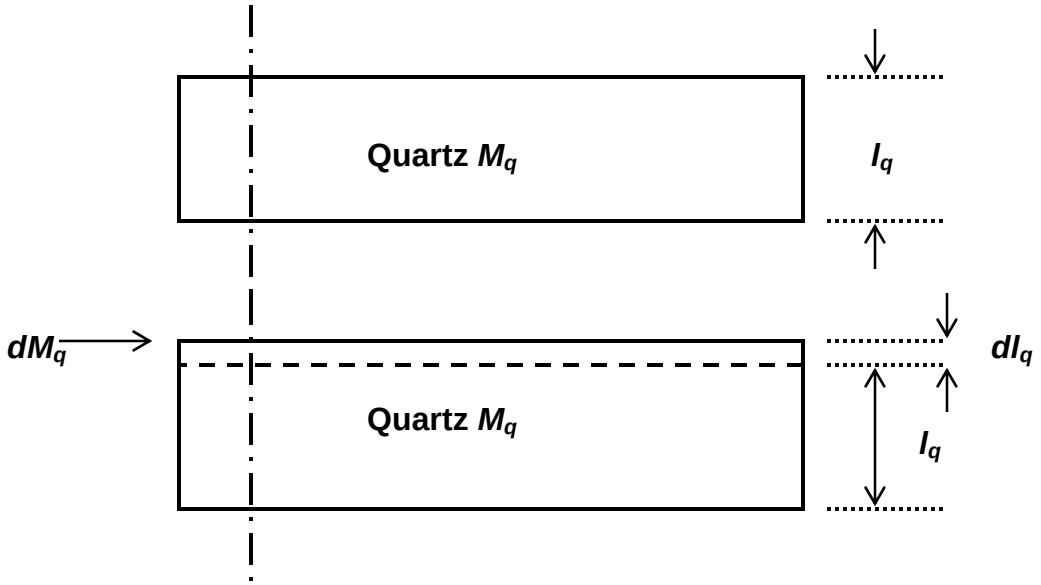

Figure 2.4. A simplified model of quartz crystal microbalance. An increase in the quartz plate mass results in a decrease in the resonant frequency.

Figure 2.4 shows the operating principle of shear-mode vibration quartz crystal of mass M_q and thickness l_q. For a quartz crystal plate to oscillate in the fundamental mode, the resonant frequency can be expressed as (Lu, 1984)

$$f_q = \frac{v_q}{\lambda_q} = \frac{v_q}{2l_q} \qquad (2\text{-}1)$$

where f_q is the resonant frequency, v_q is the shear wave velocity, and λ_q is the wavelength and is equal to 2 l_q.

The vibration frequency shift df_q caused by an infinitesimal change in the crystal thickness dl_q is found to be

$$df_q / f_q = -dl_q / l_q \tag{2-2}$$

Equation (2-2) can also be expressed in terms of the quartz crystal mass M_q, and its mass change dM_q

$$df_q / f_q = -dM_q / M_q \tag{2-3}$$

A combination of Eqs. (2-1) and (2-3) gives

$$\Delta f_q = -\left(\frac{2 f_q^2}{\rho_q v_q}\right)\frac{\Delta M_q}{A} \tag{2-4}$$

where Δf_q is the frequency change, f_q is the resonant frequency of the resonator before this change, ΔM_q is the change in mass, A is the area of the quartz plate undergoing oscillation, and ρ_q is the density of quartz. Substituting numerical values for ρ_q (2.648 g cm^{-3}) and v_q (333600 cm s^{-1}) in Eq. (2-4) yields

$$\Delta f_q = -2.26 \times 10^{-6} f_q^2 \frac{\Delta M_q}{A} \tag{2-5}$$

If one assumes only small added loading on the crystal, Eq. (2-5) can then be written in the form of

$$\Delta f_q = -2.26 \times 10^{-6} f_q^2 \frac{\Delta M}{A} \tag{2-6}$$

Thus, the interfacial mass change ΔM is related to the change in vibration frequency Δf. Eq. (2-6) serves as the principal basis of most QCM measurements. Typical operating frequencies of the QCM range from 5-15 MHz. The negative sign in Eq. (2-6) indicates that an addition of mass to the crystal results in a decrease in its resonant frequency and vice versa. The experimental data carried out by Mueller (1968, 1969), Stockbridge

(1966), Niedermayer (1966) supported the equation for a small loading. The mass added should not experience any shear deformation during oscillation. Since the mass sensitivity of a quartz crystal can be calculated from its resonant frequency and intrinsic properties of the quartz crystal, no individual calibration is required as long as the deposited material entirely covers the active vibration area. Furthermore, it should be noted that the mechanical damping and temperature also influence the resonant frequency (Lu, 1984). Sauerbrey (1959) found that the experimentally obtained loading sensitivity of 14 MHz AT-cut quartz crystal microbalance was accurate to within 2% of the theoretical value for loading mass of up to 20 $\mu g/cm^2$. McSkimin (1965) obtained a much better loading sensitivity using an AT-cut quartz crystal, where v_q = 3340 m/s. His work showed that the quartz crystal detector can have a resolution of better than 1 Hz at 5 MHz.

2.5 Equivalent circuit

It is convenient to use an equivalent circuit model to describe the electrical and mechanical behavior of the quartz crystal vibration. Coupling between mechanical displacement and electrical potential in the piezoelectric quartz crystal causes mechanical interactions between the QCM and contacting film to influence the electrical characteristics of the QCM. With only a few lumped elements, the equivalent circuit model can simulate the electrical characteristics of the QCM over a range of frequencies near resonance. An advantage of an equivalent circuit model is that standard circuit analysis software can be used to extract information from electrical measurements (Martin, 1991).

The Butterworth-Van Dyke (BVD) equivalent circuit typically used to describe the unperturbed QCM (without mass or liquid loading) is shown in Figure 2.5. The vibrating mass, the mechanical elasticity of the vibrating body, and the friction energy loss are represented by *L*, *C* and *R*, respectively (Lu, 1984). C_0 represents the capacitance between the electrodes when the resonator is perturbed at a frequency far from the resonance where it acts as a passive dielectric.

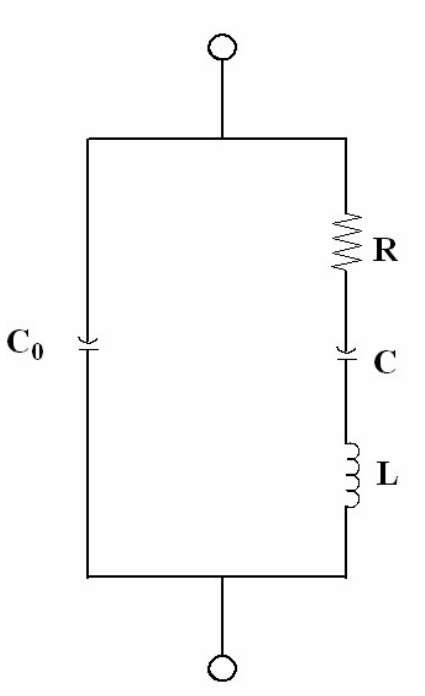

Figure 2.5. The equivalent circuit of a quartz crystal resonator.

For a resonance to occur, the complex impedance of the quartz crystal oscillator at the resonant frequency must be resistive only. There are two frequencies at which the complex impedance is resistive (Lu, 1984)

$$f_S = (1/2\pi)(1/LC)^{1/2} \tag{2-7}$$

$$f_P = (1/2\pi)\left[(1/LC) + (L/LC_0) + (R^2/L^2)\right]^{1/2} \tag{2-8}$$

where f_S and f_P are series and parallel resonances respectively. Quartz crystal resonators used for microbalance purpose operate in the series resonance mode. Therefore, it is obvious from Eq. (2-7) that f_S is not affected by the capacitance C_0. The mass sensitivity of a QCM can be directly related to the perturbation on the motional inductance L. An increase or decrease in the mass of quartz crystal is equivalent to a corresponding change in the value of L. Such a principle provides a phenomenological model for the operation of the quartz crystal resonator as a microbalance. However, it is worthy noting that, although the electrical characteristics can be measured precisely, the exact value of L and C in the equivalent circuit cannot be easily derived from the physical properties of the resonator (Lu, 1984).

A modified Butterworth-Van Dyke (BVD) can be applied to describe the electrical characteristics of the QCM under mass and contacting media loading conditions (Martin, 1991). This modified lumped element equivalent circuit model has circuit elements that are explicitly related to physical properties of the quartz, perturbing mass layer, and contacting liquid. Detailed discussion and application of modified BVD model in QCM is demonstrated in Chapter 3, and 5.

2.6 Effect of operating temperature

It is well known that temperature can have a considerable effect on performance of QCM devices, since many of the material constants involved are themselves temperature dependent. Different piezoelectric materials, propagation directions, and cut all show different temperature dependencies over different ranges (Thompson, 1997). Therefore, it is possible to develop a quartz crystal resonant device to have specific

temperature characteristics, which has led to the development of several quartz crystal based temperature sensors (Hauden 1981, Neumeister 1990, Viens 1990).

Hauden (1977) has studied the effect of temperature in terms of the corresponding frequency shift relative to fundamental frequency at 20°C. For ST-cut (42.75°) quartz, frequency shift shows a square dependence on the temperature centered at 20°C. In fact, the ST-cut quartz showed little or no temperature dependence at room temperature. Table 2.1 gives calculated frequency shift for a 52 MHz ST-cut quartz crystal device.

Table 2.1. Calculated frequency shifts due to temperature for a 52 MHz ST-cut quartz crystal device (Hauden, 1977).

T (°C)	$-\Delta f$ (kHz)
20	0.00
30	0.33
50	2.25
100	14.31
150	36.77
200	69.64

The effects of temperature to the resonant frequencies are found to be sensitive to the crystallographic orientation (Lu, 1984). For the standard AT-cut quartz crystal resonators, the resonant frequency is rather insensitive to temperature change in a region around room temperature. The frequency shift over temperature of AT-cut (35°10′) quartz crystal resonator is shown in Table 2.2.

Table 2.2. Frequency shifts due to temperature for AT-cut (35°10′) quartz crystal resonator (Lu, 1984).

T (°C)	$-\Delta f / f$ (ppm)
20	0
30	0
60	4
80	18
100	45

2.7 Applications of quartz crystal microbalance

QCMs have been employed for a wide variety of applications in analytical chemistry over the past few decades. Although QCMs have traditionally been used exclusively in vacuum deposition systems, i.e., binding of an analyte to a selective film deposited on a quartz crystal surface, other areas of applications have appeared in recent years: thin film deposition control; estimation of stress effects; etching studies; space system contamination studies and aerosol mass measurement to name but a few (O'Sullivan, 1999). An example is the recognition that these devices respond not only to simple mass changes, but also to other interfacial parameters such as acousticelectric effect, electrical conductivity. It was also known at a relatively early stage that sorption of analyte molecules into polymer films imposed on a quartz crystal surface could lead to changes in certain film properties such as viscoelasticity. This phenomenon has been turned to advantage in recent years through a number of studies on thin-film chemistry (Thompson, 1997).

With respect to chemical technology, in 1980, Nomura designed a quartz crystal microbalance device and showed that the oscillations of the quartz could be maintained in a liquid environment. Kanazawa and Gordan (1985) demonstrated that the high mass sensitivity of QCM, formerly used in gas phase, is also effective in solution.

This section will concentrate on a selected number of applications, rather than try to cover all possible studies in this area. A more detailed discussion of different coating films and applications can be found in Chapter 5.

2.7.1 Chemical sensors

King (1964) is recognized as the first to utilize a piezoelectric quartz crystal in an analytical chemical application. He developed and commercialized a piezoelectric detector, which could detect moisture to 0.1 ppm and hydrocarbons such as xylene to 1 ppm. Over the following two decades intensive research led to the development of many gas phase piezoelectric crystal detectors for organic vapors. For information on QCM techniques other than biosensing applications refer to the reviews by Alder and McCallum (1983), Guilbault and Jordan (1988), McCallum (1989), and Janta et al (1994).

Recent advances in gas phase detection systems focus on modification of the crystal surface with organic compounds or biological components that will bind a particular gaseous substrate which can provide enhanced detection sensitivity (Bunde, 1998).

Early attempts to apply the QCM device to liquid phase measurement failed because the crystal ceased to oscillate when submerged in solution. The first attempt to

use a piezoelectric quartz crystal device as a liquid phase sensor was by Nomura (1980). The resonant frequency of a QCM in air was compared with the frequency response when the whole crystal was immersed in 17 non-conducting organic liquids. They developed an empirical equation which related the frequency response to the square root of the viscosity and density of the solution.

In 1985, Kanazawa and Gordon reported a theoretical model which described the frequency response in liquid phases in terms of the physical parameters of the QCM device and the contacting solution. They showed that a QCM in solution is sensitive to the density and viscosity of the contacting solution. However, viscous coupling of the solution to the crystal surface results in both a decrease of vibration frequency of QCM and the dampening of the resonance. Therefore, their model cannot distinguish changes in mass accumulation from changes in solution properties, because the resonant frequency results from both mass and liquid loading.

Subsequent researchers experimentally demonstrated the validity of Kanazawa's theory for selected solutions but found deviations for highly viscous or conducting solutions (Barnes 1991, Muramatsu 1987). Although they clearly showed the frequency response is affected by the viscosity and density of the solution, the response is not controlled exclusively by these factors (Bunde, 1998). Later work demonstrated many parameters associated with the physical and chemical nature of the liquid/solid interfacial environment that influences the frequency. The frequency response is affected by interfacial interactions such as the surface roughness, conductivity, solution polarity, interfacial viscosity, surface free energy, temperature, and the extent of crystal contact

with the solution phase (Bunde, 1998). These factors indicate the need for characterizing the QCM device with the respective sensing environment.

2.7.2 Biosensors

The general approach to exploiting the piezoelectric effect for use in a biosensor is to coat a QCM with bioactive materials. Biologically active materials, such as antibodies and enzymes that are very selective and specific can greatly enhance the selectivity of piezoelectric crystal sensor. Two general experimental designs are used in most QCM biosensing applications. One method is to measure the resonance frequency of the crystal in air prior to the addition of sample. Then the QCM is immersed in the reaction solution for a time period sufficient to allow for the target substance in solution to bind to the immobilized coating materials. As the analyte interacts with the coating material on the QCM, the crystal may then be dried, any change in resonant frequency due to biospecific binding can calculated. This is known as the 'dip and dry' method (Guilbault 1992). The second method uses a flow cell to provide real time data on the time course of binding events on the QCM surface. The analysis is conducted completely in the solution phase. However, adsorption of the analyte on the QCM surface results in a change in the viscoelastic properties of the interfacial structure which are recognized by a decrease in the resonant frequency (Bunde, 1998).

An area which has captured a lot of attention has been the use of antibodies as the crystal coating. These antibody coated crystals are termed as QCM-based immunosensors (O'Sullivan, 1999). The first piezoelectric immunosensor was developed by Shon (1972). The crystal was coated with Nyebar C and BSA and was used to detect

BSA antibodies. Some recent developments are close to commercialization. For example, excellently performing blood-group detection in the ABO system has been reported (Tessier, 1993). One side of the quartz crystal sensor is coated with blood-group antibodies in order to allow blood cells to interact with the quartz crystal surface according to their group. Another example is human immunodeficiency virus (HIV) infection immunosensor (Aberl, 1994). Using this analytical system, antibodies specific against HIV can be detected in human serum samples within a few minutes and with a selectivity comparable to that of a licensed enzyme-linked immunosorbent assay (ELISA) (Benes, 1995).

Fawcett (1988) was the first to describe a QCM biosensor for DNA by immobilizing single stranded DNA on quartz crystals and detecting the mass change after hybridization. Over the past many years, much has been conducted on DNA/RNA detection using the QCM device. Aslanoglu (1998) adsorbed DNA onto a QCM and studied the metal complex binding projection of the immobilized DNA. Storri (1998) developed a piezoelectric quartz biosensor for DNA detection based on hybridization with an immobilized single stranded oligonucleotide. The biosensor detected DNA which was complementary to the immobilized oligonucleotide and was able to distinguish between DNA molecules of different lengths.

An exciting new application of piezoelectric quartz sensor is in the determination of pharmaceutical compounds and drugs. An example is that Attili (1996) applied the piezoelectric quartz sensor for detection of cocaine using the benzoylecyanine antibody coating.

It is obvious that the QCM has found a wide range of applications in biotechnology area of food, environmental and clinical analysis since its discovery, due to its inherent ability to detect analytes in real time. However, to produce commercially viable device, the re-usability of the piezoelectric crystal remains an important issue that is currently receiving a large amount of interest from many research groups (O'Sullivan, 1999).

CHAPTER 3

MODELING QUARTZ CRYSTAL MICROBALANCE SENSOR WITH AN ION EXCHANGE PROCESS

3.1 Introduction

In the previous chapter, the electrical and frequency responses of QCM device operation were examined. To produce practicable chemical sensors, it is necessary to coat the surface of the QCM with thin-film materials to obtain chemical selectivity and sensitivity. The ability of the QCM to rapidly monitor frequency changes permits their application for detecting dynamic ion exchange processes.

This chapter characterizes sensor technology employing ion exchange functional groups deposited on a QCM device. The primary hypothesis in using QCM as an analytical technique is that change in the vibrational frequency of the QCM cell can be reliably and reproducibly related to target analyte concentration. The ion exchange functional group is used to attract ions in the analyte. The QCM device is sensitive to the mass loading of the ions on the functional group layer, providing a measurable frequency drops when the QCM mass increases. As mass is added to a harmonic oscillator, the frequency of oscillation is reduced.

The potential benefit of using QCM coated with an ion exchanger is that the sensor is less expensive than competitive monitoring devices. QCM methods utilize the intrinsic selectivity of an adsorption process to create relatively simple, low cost, analytical alternatives for a variety of applications.

The applications of this sensor technology include:

- ***Industrial process control***

Major applications for ultrapure water (UPW) monitoring include semiconductor fabrication and nuclear power that require pure water. Over the past several decades, controlling the level of contaminants in ultrapure water has enabled semiconductor manufacturers to improve product quality and maximize chip yields. Another leading application of ultrapure water is nuclear power. The major concerns of the power industry include corrosion, scale formation and structural defects. To meet improved industrial requirements, advanced instrumentation for monitoring water contaminants is important in improving and measuring the quality of ultrapure water.

Over the past two decades, the Oklahoma State University Ultrapure Water Research Group has collaborated with the ultrapure water industry. The QCM monitor is an identified interest of practitioners and researchers in the ultra-pure water and semiconductor industries that participate in this Consortium.

- ***Drinking water and environmental water contaminants monitoring***

Environmental water monitoring, comprising about 1.5 million sites in the U.S., is done by drawing samples and submitting them to laboratories for analysis. The application of QCM to drinking water monitoring has the potential to ensure quality and alert possible contaminants.

- ***Environmental contaminants monitoring***

Environmental applications include surface and ground water, wastewater treatment plants, municipal water utilities and industrial users. The QCM technology may provide a low-cost sensitive means of contamination detection.

The work began with Hussey by applying a liquid film expression assuming no reaction in the film. He applied the flux equation developed by Franzreb (1993) to correlate the frequency change to the bulk concentrations of the solution flowing into the cell. The diffusion path was simplified to stagnant film diffusion; the path through the coating film was not included. However, it is Hussey's opinion this expression is too complex for modeling, not to mention the system is unspecified for multicomponent systems.

This chapter presents a literature review of the solid phase ion exchange model and the QCM response for liquids, qualitatively derives an approximate kinetics model of solid phase ion exchange, lists the assumptions required for completion of the model, applies the kinetics diffusion model to QCM frequency response, and allows for the prediction of the liquid phase concentration of target analytes. The theoretical QCM frequency response is estimated from literature data. In this chapter, the primary focus is on liquid phase ion exchange systems. Liquid phase adsorption systems are discussed in the next chapter.

3.2 Literature review

3.2.1 Literature review of solid phase ion exchange modeling

Ion exchange is a stoichiometric competitive process of ionic species by diffusion between an exchanger and a contacting solution (Helfferich, 1962). The rate of ion exchange is usually controlled by the resistance inside the exchanger particle or through an adherent liquid film. Diffusion rates are generally described by the Nernst-Planck equations (Helfferich, 1962).

For particle diffusion control Helfferich et al. (1962, 1958) developed a mathematical model to predict the ion exchange rate for binary systems. Later, the model was extended to ternary systems (Bajpai, 1974). Hwang and Helfferich (1987) developed a numerical solution for multi-species ion exchange. Their studies replaced the electrical potential gradient with a combination of concentration gradients. Also, their work is regarded as the most rigorous model for particle diffusion controlled ion exchange. However, because of its numerical complexity, simplified models of particle diffusion kinetics are proposed by other authors. Dolgonosov et al. (1995) developed a "macroscopic model" in comparison with the "local determinate" model described by Hwang and Helfferich (1987). Their model assumed that the concentration profiles are parabolic, similar to the well-known E. Glueckauf (1955 a,b) kinetics approximation used in adsorption. They showed that their approximation agreed well with their data, although they pointed out that the equivalent conductivity of ions must be corrected empirically. Carta and Lewus (1999) also give an analytical model for homovalent ion exchange and an approximate solution for heterovalent ion exchange. In their work, mass transfer is assumed as a pseudosteady-state diffusion through a flat solid film of the

particle. However, their solution must be calculated numerically for multi-component systems. Also, for the case of heterovalent exchange, a trial and error procedure must be used to find a constant that satisfies their model.

3.2.2 Literature review of QCM application in liquid

Around 1980, researchers began to investigate the effects of liquids on QCMs. Konash and Bastiaans (1980) first reported the liquid-phase detection involving the use of a piezoelectric crystal with a reactive or absorbent functional group. Nomura et al. (1980) succeeded in making a crystal vibrate with the exposure of only one surface of the crystal to a solution. Nomura et al. (1986, 1985) also demonstrated the selective sorption of ion in solution using coated quartz crystals. Therefore, the major deficiency of the QCM, namely, the absence of selectivity, is alleviated by the application of selective sorbents based on the functional polymers deposited on the crystal.

Kanazawa and Gordan (1985) demonstrated that the high mass sensitivity of QCM, formerly used in gas phase, is also effective in solution. They showed that QCM in solution is sensitive to the density and viscosity of the contacting solution. They derived a theoretical model which predicts the frequency change in terms of the properties of the solution and quartz crystal. However, viscous coupling of the solution to the crystal surface results in both a decrease of vibration frequency of QCM and the dampening of the resonance. Therefore, their model cannot distinguish changes in mass accumulation from changes in solution properties, because the resonant frequency results from both mass and liquid loading.

Martin et al. (1991) derived an equivalent electrical circuit for an AT-cut QCM simultaneously loaded by a surface mass layer and a contacting Newtonian liquid. With their model, the effect from mass change can be differentiated from change in liquid properties.

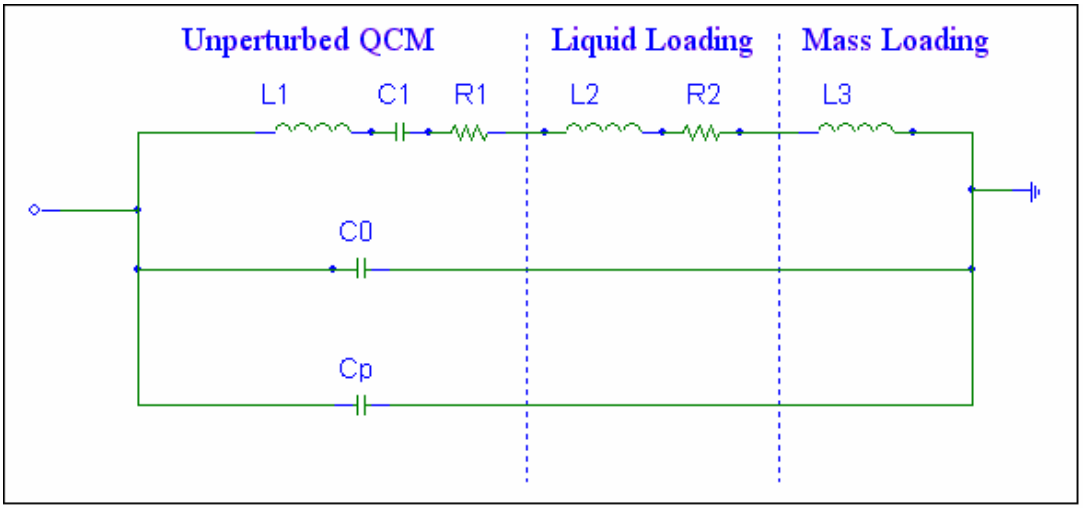

Figure 3.1. Equivalent circuit for a QCM under mass and liquid loading (Martin, 1991).

Figure 3.1 shows the equivalent circuit that approximates the admittance of a QCM perturbed by a thin mass layer and a contacting liquid with circuit element. L_1, R_1, and C_1 denote inductance, resistance, and capacitance for unperturbed QCM. L_2 and R_2 denote inductance and resistance due to liquid loading, and L_3 denotes inductance due to mass loading. Beck et al. (1988) argued that liquid loading causes an increase in both the inductance L_1 and resistance R_2. Martin (1991) also showed that, in contrast, mass loading increases only the inductance, contributed by L_3. When mass and liquid loading are small, the change in resonant frequency is

$$\Delta f = -\frac{2 f_0^{\,2}}{N\sqrt{\mu_q \rho_q}} \frac{\Delta m}{A} - \frac{2 f_0^{\,2}}{N\sqrt{\mu_q \rho_q}} \left(\frac{\rho \eta}{4\pi f_0} \right)^{1/2} \qquad (3\text{-}1)$$

where f_0 is the fundamental resonance frequency of the QCM crystal, μ_q is the shear modulus of quartz, ρ_q is the density of the quartz, ρ is the liquid mass density, η is the liquid viscosity, N is the overtone or harmonic number = 1, 3, 5,…, A is the electrode area. The first term of Eq. (3-1), related to the mass loading on the surface, is equivalent to Sauerbrey's (1959) equation. The second term is equivalent to the model given by Kanazawa and Gordan (1985) for a liquid loaded QCM operating at the fundamental resonance, with N=1.

3.3 Theory

The integral modeling of QCM to predict the concentration includes two aspects: first, a relationship between the resonance frequency change as well as mass accumulation and properties of the contacting liquid; second, the ion exchange rate on the polymer coating of crystal. The model currently developed is based on a solid-phase control ion exchange process.

The QCM surface is coated with a thin ion exchanger. The planar ion exchange model assumes that the ion exchanger film is composed of an inner film with homogeneous concentration distribution and an outer film with parabolic concentration distribution.

3.3.1 Diffusion model

3.3.1.1 Model assumptions

To simplify the mathematical derivation, the following assumptions were made based on the system conditions.

(1) isothermal, isobaric operation.

(2) negligible swelling and shrinking changes of the ion exchanger

(3) electrical neutrality

(4) complete Donnan exclusion, no net co-ion flux within the film

(5) constant individual diffusion coefficients of the ions

(6) constant activity coefficients

(7) quasi-stationary or pseudo steady state liquid film diffusion

(8) ion exchanger film is assumed to be composed of an inner film with homogeneous concentration distribution and an outer film with parabolic concentration distribution.

Moreover, in order to simplify the mathematical model, coupling of ion fluxes other than by electric diffusion potential is neglected. Figure 3.2 shows a schematic diagram of concentration profiles in the exchanger film.

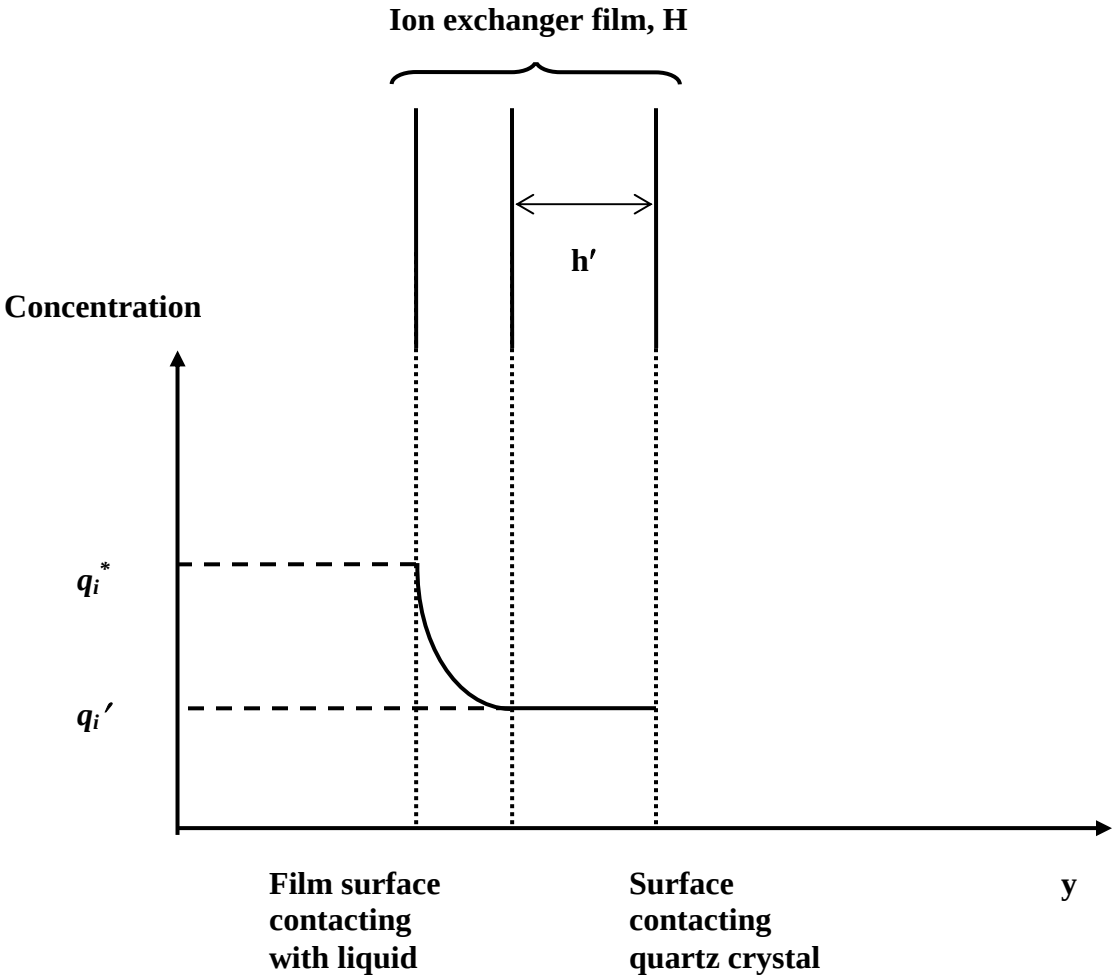

Figure 3.2. Schematic diagram of concentration profile in planar ion exchanger film. The inner film has homogeneous concentration distribution. The outer film has parabolic concentration distribution.

3.3.1.2 Mathematical model

We consider an ion exchange system with *n* counterions. The flux of ion *i* in the ion exchanger is described by the Nernst-Planck equation

$$J_i = -D_i\left[\frac{\partial q_i}{\partial h} + z_i \frac{q_i F}{RT}\frac{\partial \Phi}{\partial h}\right] \qquad (3\text{-}2)$$

$i = 1, 2, \ldots, n$ counterions

where D_i is the effective diffusivity of *i*th ions in the exchanger, z_i is the electrochemical valence of ion *i*, *F* is Faraday constant, Φ is electric potential, and q_i is the concentration of *i*th ions in the exchanger.

The condition of no net electric current can be expressed by

$$\sum_{i=1}^{n} z_i J_i = 0 \qquad (3\text{-}3)$$

The corresponding initial conditions are

$$\text{at} \quad t = 0, \qquad q_i = q_i^0 \qquad i = 1, 2, \ldots, n \qquad (3\text{-}4)$$

Boundary conditions are

$$\text{at} \quad h = h', \qquad \frac{\partial q_i}{\partial h} = 0 \qquad (3\text{-}5)$$

$$\text{at} \quad h = H, \qquad q_i = q_i^* \qquad i = 1, 2, \ldots, n \qquad (3\text{-}6)$$

where q_i^* is the concentration of *i*th ions at the boundary condition.

If the ion exchanger is assumed to be composed of an inner film with homogeneous concentration distribution and an outer film with parabolic concentration distribution, one has

$$q_i = q_i' + a(h - h')^2 \quad \text{for} \quad h' \le h \le H \qquad (3\text{-}7)$$

where *a* is arbitrary function of time. On the external surface of ion exchanger, by substituting boundary condition, Eq. (3-7) becomes

$$q_i^* = q_i' + a(H - h')^2 \qquad (3\text{-}8)$$

hence

$$a = \frac{q_i^* - q_i'}{(H - h')^2} \qquad (3\text{-}9)$$

The external surface concentration gradient is

$$\left.\frac{\partial q_i}{\partial h}\right|_{h=H} = 2(H-h')\frac{q_i^{*}-q_i'}{(H-h')^2} \tag{3-10}$$

The average concentration of ion *i* in ion exchanger can be obtained by carrying out the integration.

$$\bar{q}_i = \frac{1}{V_0}\int_0^{V_0} q_i\, dV \tag{3-11}$$

where $\bar{q}_i$ is the average concentration of ion *i* in the exchanger.

Same as the derivation in Appendix D, Eqs (3-12, 13, 14, 15, 16) are formulated for various parabolic profile thickness of ion exchanger.

$h' =$ 0, $$\frac{d\bar{q}_i}{dt} = \frac{3}{H^2}D_i\left[(q_i^{*}-\bar{q}_i) - z_i q_i^{*}\frac{\sum z_i D_i (q_i^{*}-\bar{q}_i)}{\sum z_i^2 D_i q_i^{*}}\right] \tag{3-12}$$

$h' =$ 0.2*H*, $$\frac{d\bar{q}_i}{dt} = \frac{3.4091}{H^2}D_i\left[(q_i^{*}-\bar{q}_i) - z_i q_i^{*}\frac{\sum z_i D_i (q_i^{*}-\bar{q}_i)}{\sum z_i^2 D_i q_i^{*}}\right] \tag{3-13}$$

$h' =$ 0.4*H*, $$\frac{d\bar{q}_i}{dt} = \frac{4.1667}{H^2}D_i\left[(q_i^{*}-\bar{q}_i) - z_i q_i^{*}\frac{\sum z_i D_i (q_i^{*}-\bar{q}_i)}{\sum z_i^2 D_i q_i^{*}}\right] \tag{3-14}$$

$h' =$ 0.6*H*, $$\frac{d\bar{q}_i}{dt} = \frac{5.7692}{H^2}D_i\left[(q_i^{*}-\bar{q}_i) - z_i q_i^{*}\frac{\sum z_i D_i (q_i^{*}-\bar{q}_i)}{\sum z_i^2 D_i q_i^{*}}\right] \tag{3-15}$$

$h' =$ 0.8*H*, $$\frac{d\bar{q}_i}{dt} = \frac{10.7143}{H^2}D_i\left[(q_i^{*}-\bar{q}_i) - z_i q_i^{*}\frac{\sum z_i D_i (q_i^{*}-\bar{q}_i)}{\sum z_i^2 D_i q_i^{*}}\right] \tag{3-16}$$

3.3.2 Frequency response of QCM coated with ion exchanger

The load from the mass accumulation and liquid shear displacement are approximately additive, shown as Martin's (1991) equation

$$\Delta f = -\frac{2 f_0^{\,2}}{N\sqrt{\mu_q \rho_q}}\left[\frac{\Delta m}{A} + \left(\frac{\rho\eta}{4\pi f_0}\right)^{1/2}\right] \tag{3-17}$$

where f_0 is the fundamental resonance frequency of the QCM crystal, μ_q is the shear modulus of quartz, ρ_q is the density of the quartz, ρ is the liquid mass density, η is the liquid viscosity, N is the overtone or harmonic number = 1, 3, 5,…, A is the electrode area.

To simplify the model, it is necessary to make the assumption that the density and viscosity of liquid as well as the density and the elastic constant of quartz are constant. Thus, the equation can be simplified to

$$\Delta f = K\Delta m + k_0 \tag{3-18}$$

Suppose that the ion exchanger is initially in the A form and the counter ion in the solution is B. Exchange equilibrium between two monovalent ions can be defined by

$$\mathrm{A_R} + \mathrm{B_S} \Leftrightarrow \mathrm{A_s} + \mathrm{B_r} \tag{3-19}$$

The loading of ion on the quartz crystal is directly related to the fractional attainment of functional group deposited on the crystal. The mass change, i.e. loading, is equal to the number of molar multiplied by the difference of molecular weight of the two counter ions, defined by

$$\Delta m = Q\frac{m_r}{1000}\bar{q}_B(M_B - M_A) \tag{3-20}$$

where m_r is the mass of ion exchanger, Q is the capacity of ion exchanger, $\bar{q}_B$ is the dimensionless concentration of ion B, M_A and M_B are the molecular weight of ion A and B respectively.

In this work, to predict analyte concentration, ion concentration in ion exchanger film is assumed to be parabolic distribution, i.e. ion exchange rate is defined by Eq. (3-12) with $h' = 0$.

$$\frac{d\bar{q}_i}{dt} = \frac{3}{H^2} D_i \left[(q_i^* - \bar{q}_i) - z_i q_i^* \frac{\sum z_i D_i (q_i^* - \bar{q}_i)}{\sum z_i^2 D_i q_i^*} \right] \tag{3-21}$$

For monovalent ions, Eq. (3-21) becomes

$$\frac{d\bar{q}_i}{dt} = \frac{3}{H^2} D_i \left[(q_i^* - \bar{q}_i) - q_i^* + q_i^* \frac{\sum D_i \bar{q}_i}{\sum D_i q_i^*} \right] \tag{3-22}$$

or in the approximate form

$$\frac{d\bar{q}_i}{dt} = \frac{3}{H^2} D_i \left[\frac{q_i^*}{\sum q_i^*} - \bar{q}_i \right] \tag{3-23}$$

In practical applications, equilibrium can be conveniently expressed in terms of the distribution coefficients of the counter ions. The distribution coefficient can be defined by

$$\lambda_i = \frac{q_i^*}{q_i} \tag{3-24}$$

therefore Eq. (3-23) can be defined as

$$\frac{d\bar{q}_i}{dt} = \frac{3}{H^2} D_i \left[k_3 q_i - \bar{q}_i \right] \tag{3-25}$$

where $k_3 = \dfrac{\lambda}{\sum q_i^*}$

With initial condition,

at $t = 0$, $\qquad \bar{q}_{i,n} = \bar{q}_{i,n-1}$ (3-26)

where $\bar{q}_{i,n}$ and $\bar{q}_{i,n-1}$ are the average solid phase concentration of *i*th ion in *n*th and $(n-1)$ th introduction of new analyte. Eq. (3-25) can be integrated as

$$-\ln(k_3 q_i - \bar{q}_{i,n}) = \frac{3}{H^2} D_i t - \ln(k_3 q_i - \bar{q}_{i,n-1}) \tag{3-27}$$

Liquid phase concentration of ion *i* can be expressed as

$$q_i = \frac{EXP(\frac{3}{H^2} D_i t)\bar{q}_{i,n} - \bar{q}_{i,n-1}}{\left[EXP(\frac{3}{H^2} D_i t) - 1\right] k_3} \tag{3-28}$$

When substituting Eq. (3-18) and Eq. (3-20), liquid phase concentration can be related to frequency change

$$q_i = \frac{EXP(k_2 t_n)\Delta f_n - \Delta f_{n-1}}{\left[EXP(k_2 t_n) - 1\right] k_1} \tag{3-29}$$

where $k_1 = KQ \frac{m_r}{1000}(M_B - M_A)k_3$

$$k_2 = \frac{3}{H^2} D_i$$

$\Delta f_{n-1} = f_{n-1} - f_0$ is the frequency change from baseline at the moment of exposure to (*n*-1)th analyte.

$\Delta f_n = f_n - f_0$ is the online frequency change from baseline after time t_n exposure to *n*th analyte.

t_n is the time after exposure to *n*th analyte.

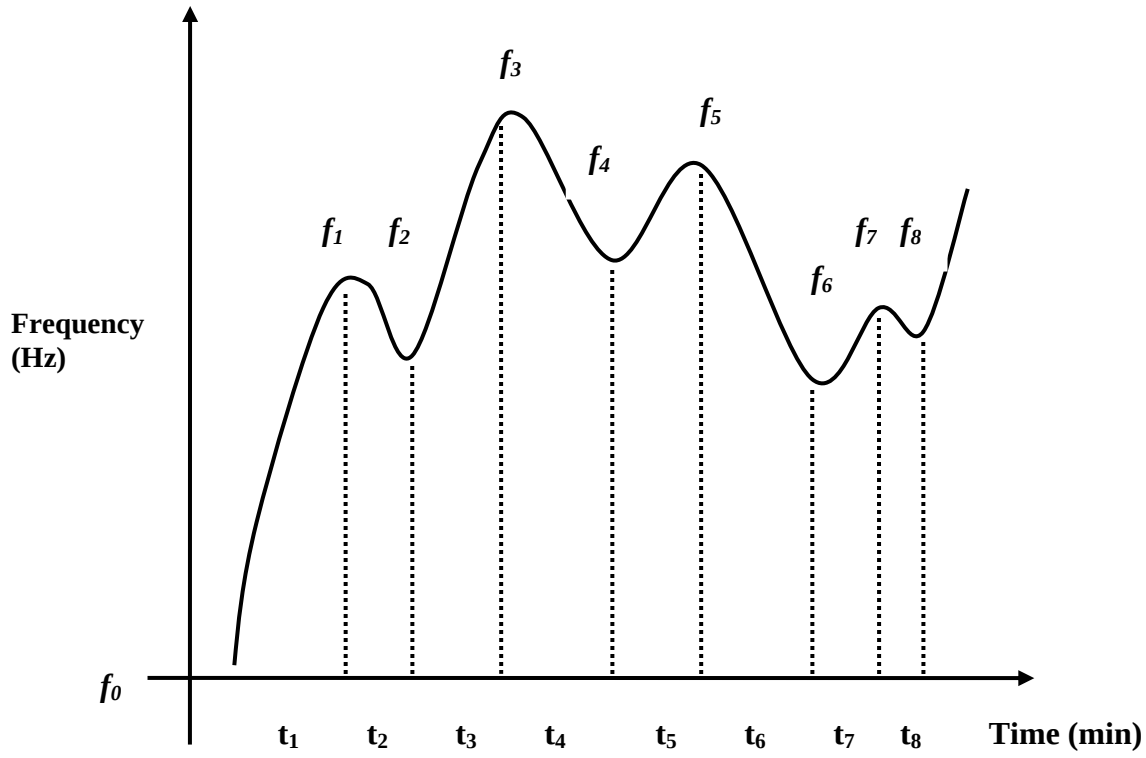

Figure 3.3. Frequency response profile of QCM sensor to sample solution with varying concentrations.

In the model, H is the thickness of ion exchanger material attached to the surface of the QCM. Also, M_B, M_A, m_r, Q, K are constant for specific ions. The diffusivity, D_i, is constant at a specific temperature — a property of the ions being monitored. Therefore, all two coefficients, k_1 and k_2 are constant, shown as Eq. (3-29).

Figure 3.3 shows a frequency response of QCM as a function of time and varying solution concentrations. The introduced solutions are composed of the same ion with varying concentration. The frequency shift increases for a higher concentration solution entering the QCM, and decreases for lower concentration solution.

Eq. (3-29) and Figure 3.3 show that predicted ion concentration in solution is a function of time, frequency change and frequency change of previous running cycle. From a measurement perspective, to instantly predict the ion concentration, instant frequency change Δf_n with corresponding time t_n after exposure to new solution, and frequency change Δf_{n-1} of previous cycle ending point are needed, provided constant k_1 and k_2 are known.

The application of this kinetic model can be used to predict solution phase concentrations of the same constituents for both increasing and decreasing concentrations. The ion exchanger loading and frequency response vary with time and solution concentrations; hence we can calculate solution concentration at a specific time based on the ion exchanger loading and/or frequency response.

3.3.2.1 Effect of concentration

A higher concentration of competing ions means a higher ion exchange rate, thus results in larger frequency response. Figure 3.4 shows the effect of various solution concentrations on the frequency response with $k_1 = 1000$, $k_2 = 0.1$. The predictions show that, at equilibrium, frequency change is directly related to solution concentration. This phenomenon can be found by analyzing Eq. (3-29). When time interval is infinite, Eq. (3-29) becomes

$$q_i = \frac{\Delta f_n}{k_1} \qquad (3\text{-}30)$$

Therefore, it is obvious that the model will handle both ion exchange rate and equilibrium.

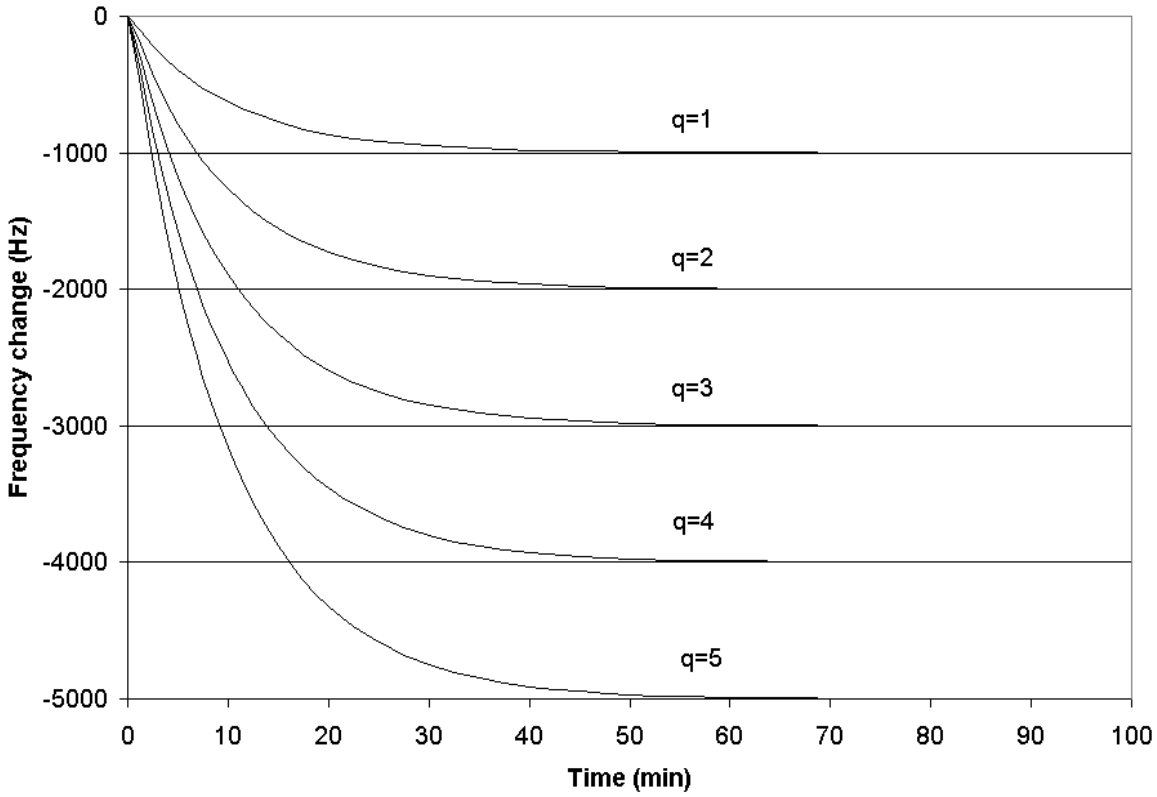

Figure 3.4. Plot of the various solution concentrations and frequency changes as a function of time according to Eq. (3-29).

3.3.2.2 Effect of capacity

Each ion has an affinity for the ion exchange functional group. This preference for the ion exchanger is often expressed by the separation factor or selectivity coefficient. However, for practical applications, equilibrium is most conveniently expressed as distribution coefficients of the counter ions. As some authors (Helfferich, 1962, Chap. 5) pointed out, the application of the distribution coefficient is particularly advantageous if the species is only a trace component. In this work, for simple discussion, we applied this concept to the model and assumed distribution coefficient is a constant.

Consider a single counter ion species entering the QCM test cell with a uniform velocity. The new counter ion A moves within the ion exchanger and replaces the original counter ion B. If there is no ion B in the solution phase, then ion A continuously migrates from the solution into the ion exchanger, until the pores of the ion exchanger are completely occupied by ion A. At this time, ion exchange equilibrium is attained.

Ion exchange capacity can be defined as the number of counter ion equivalents in a specified amount of ion exchanger. Figure 3.5 shows that when capacity increases or decreases 10 percent, the frequency response baseline changes correspondently. The sensor responses appear to follow the concept exactly; large capacity will result in fast ion exchange rate and large frequency equilibrium baseline.

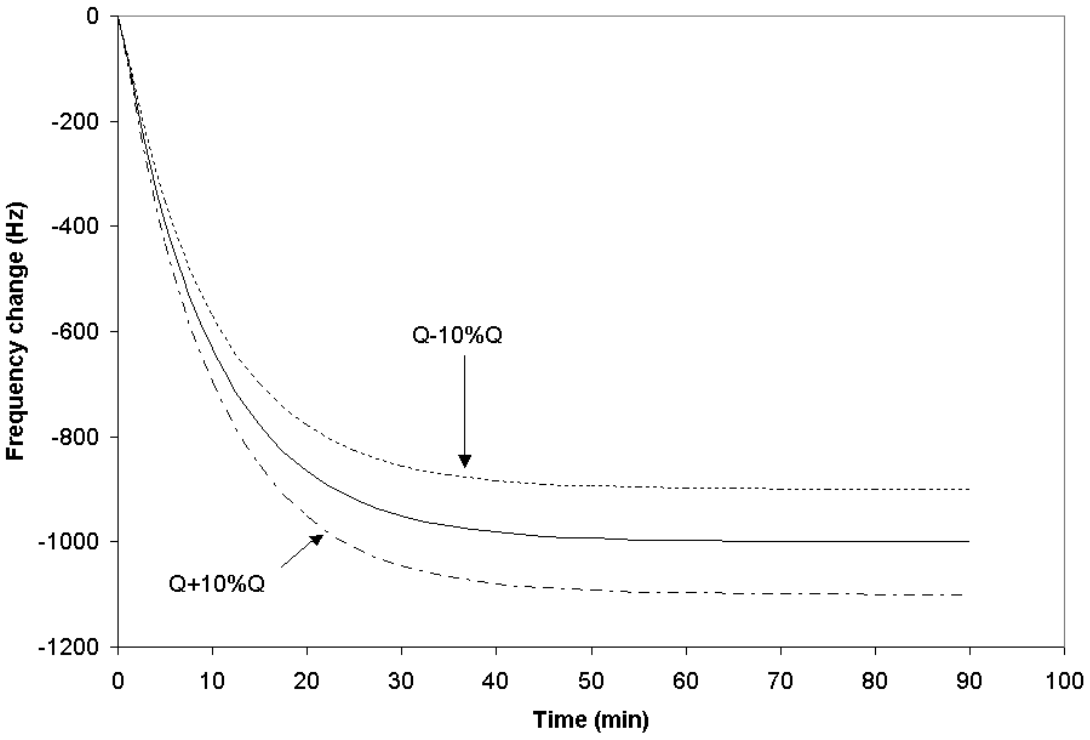

Figure 3.5. Effect of the capacity of ion exchanger in the simulation of QCM response.

3.3.2.3 Effect of diffusivity

The three frequency change curves in Figure 3.6 show the effect of changes in diffusivity. The lower curve shows that when diffusivity of the counter ion is high, the frequency change curve drops sharper and earlier. All three frequency change curves level off and reach the same equilibrium. This is due to the same concentration and capacity.

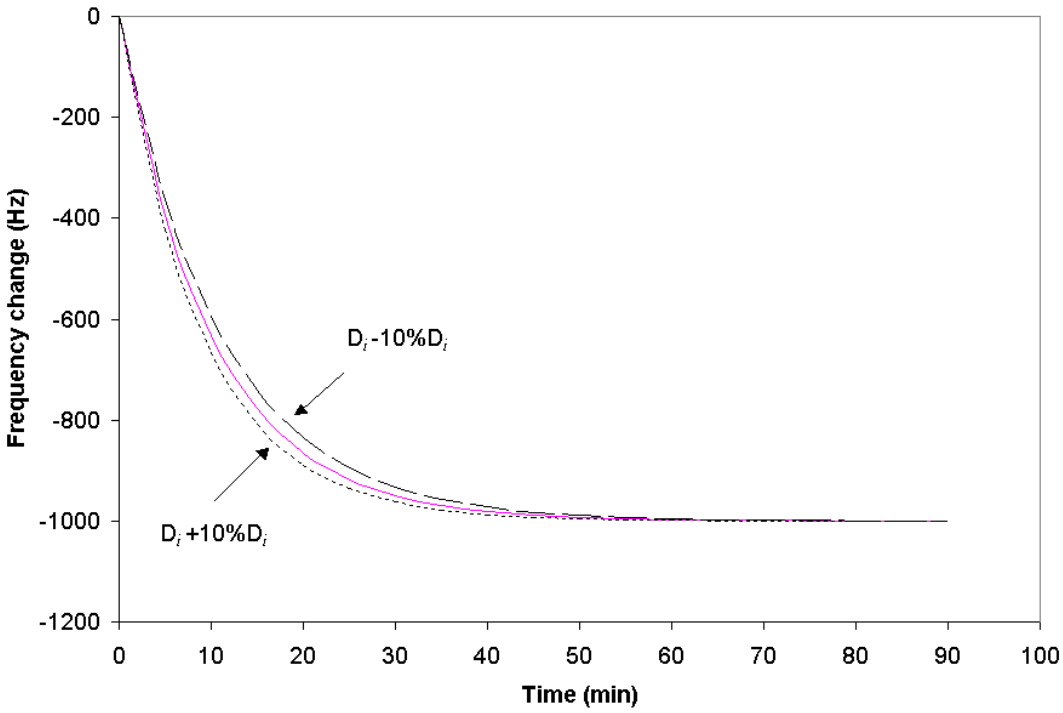

Figure 3.6. Effect of diffusivity in the simulation of QCM response.

3.4 Brims Ness Corporation ion exchange case

In December 2001, Brims Ness Corporation completed the dual-cell sensor system. The sensor system consists of sensor cell, oscillator, frequency counter, controller, ultra stable clock and output PC. The sensor cell houses the crystals – the

input flow is directed across a single side of the crystal. The oscillator causes the crystals to oscillate, typically at about 10 MHz. When prompted by the controller, the microprocessor-based frequency counter counts the oscillations from the oscillator circuits. The microprocessor-based controller initiates the frequency counter (FC), receives the frequencies from the FC, and forwards them to the output PC. The ultra stable clock keeps the frequency counters and the controller operating with precise timing.

The quartz crystals used in this study were AT cut with a fundamental resonance frequency of 10 MHz. The crystals were obtained from International Crystal Manufacturing Co. Inc. (Oklahoma City, OK) with Cr/Au electrodes (0.2 cm^2). Coating film was prepared by spin coating a PAH (polyallylamine hydrochloride) / DadMac (diallyldimethylammonium chloride) solution on a polished crystal at 3000 rpm for 60 seconds. All measurements were carried out at room temperature. The data fed to the output PC consists of frequency readings taken every 7 seconds.

Figure 3.7 is the comparison of modeling and experimental data of frequency response. In this experiment, solution was changed between 1.61 mmol/L KCl and KH_2PO_4. In Figure 3.7, from hour 13 to hour 16.4, KH_2PO_4 was introduced. At hour 16.4, 1.61 mmol/L KCl solution was introduced and continued until hour 20. The simulation curve deviates a little from experiment data at the later phase, but it still shows the tendency toward equilibrium.

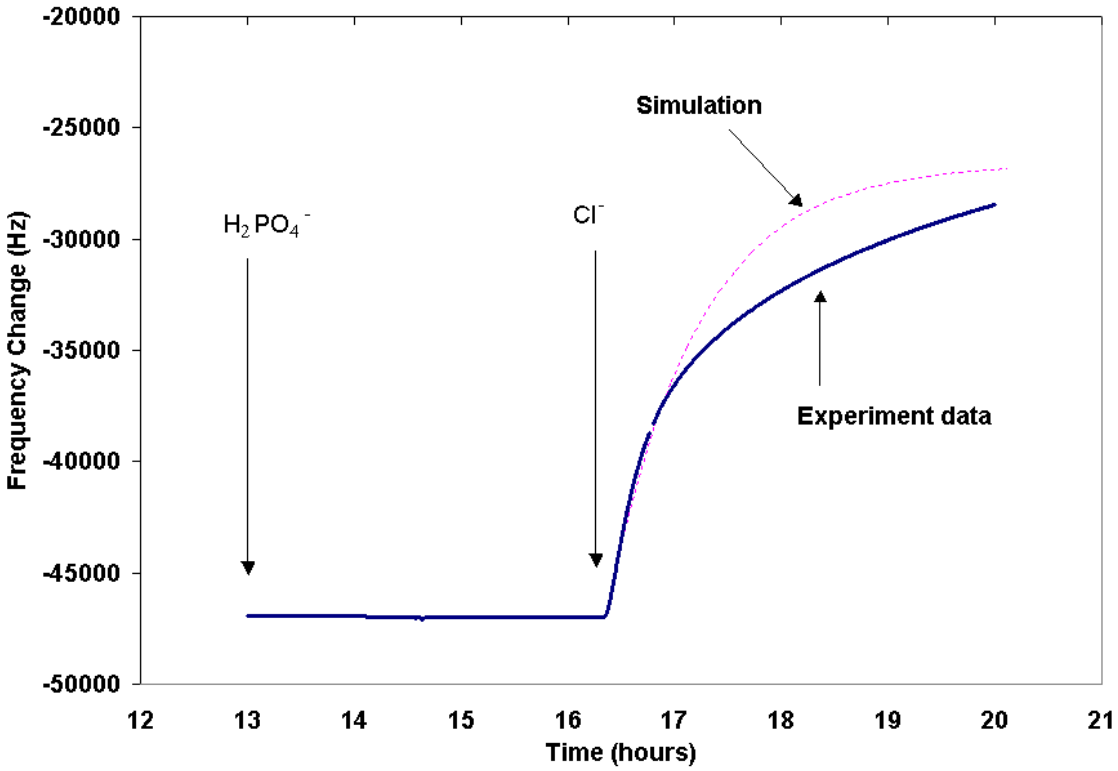

Figure 3.7. BNC KCl - KH_2PO_4 ion exchange frequency response profile.

Figure 3.8 shows the predicted analyte concentration at various time. The analyte concentration in the experiment is 1.61 mmol/L, shown as a straight line in Figure 3.8. The results show that the predicted concentrations are within or around 10% error of the exact value. The simulation errors from hour 1 to hour 3 are around 10%. These high errors agree with the result in Figure 3.7, because the simulation of frequency response deviates from the experiment data.

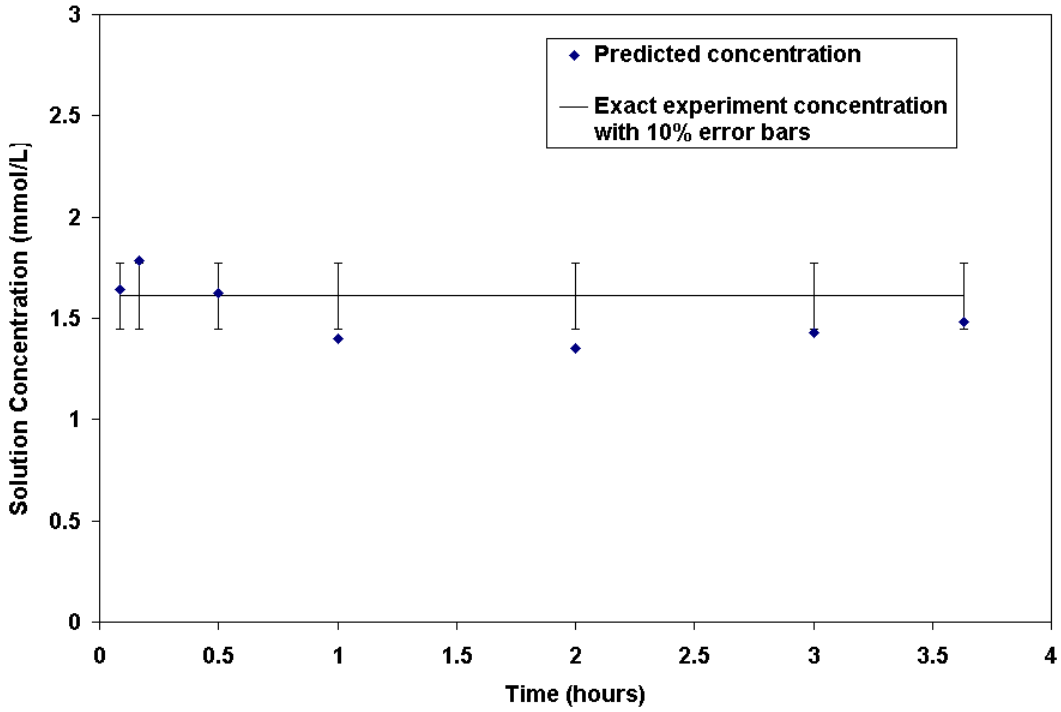

Figure 3.8. Prediction of solution concentration of BNC KCl - KH_2PO_4 ion exchange.

Figure 3.9 is the nitrate / chloride ion exchange profile for 45 hours. The experimental data are also provided by Brims Ness Corporation. Chloride was first introduced until approximate 3.33 hrs. Then 0.08 mmol/L KNO_3 follows chloride, steadily displacing chloride and using much of the exchange capacity. It is worth noting that there is a time lag between analyte introduction and frequency response. This time lag can be clearly demonstrated in Figure 3.10. Figure 3.10 shows that after 0.5 hour, the predicted concentrations are within 10% error of the exact value. However, there is no frequency response at 0.1 hour. This is probably because of the low concentration of nitrate.

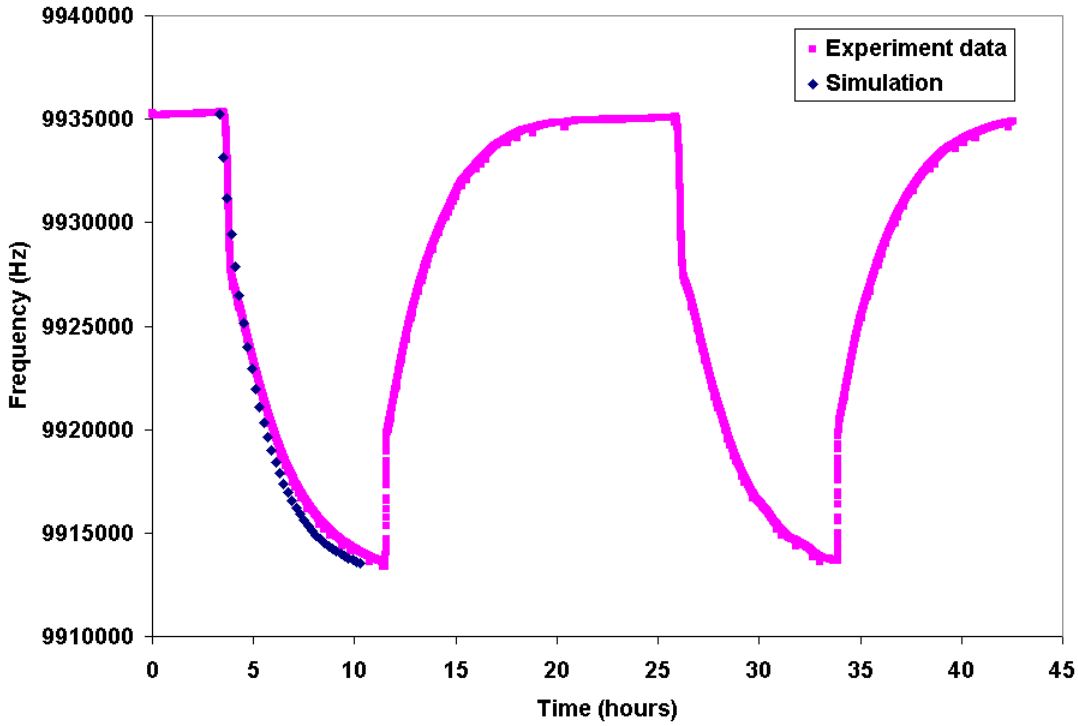

Figure 3.9. BNC KCl - KNO_3 ion exchange frequency response profile.

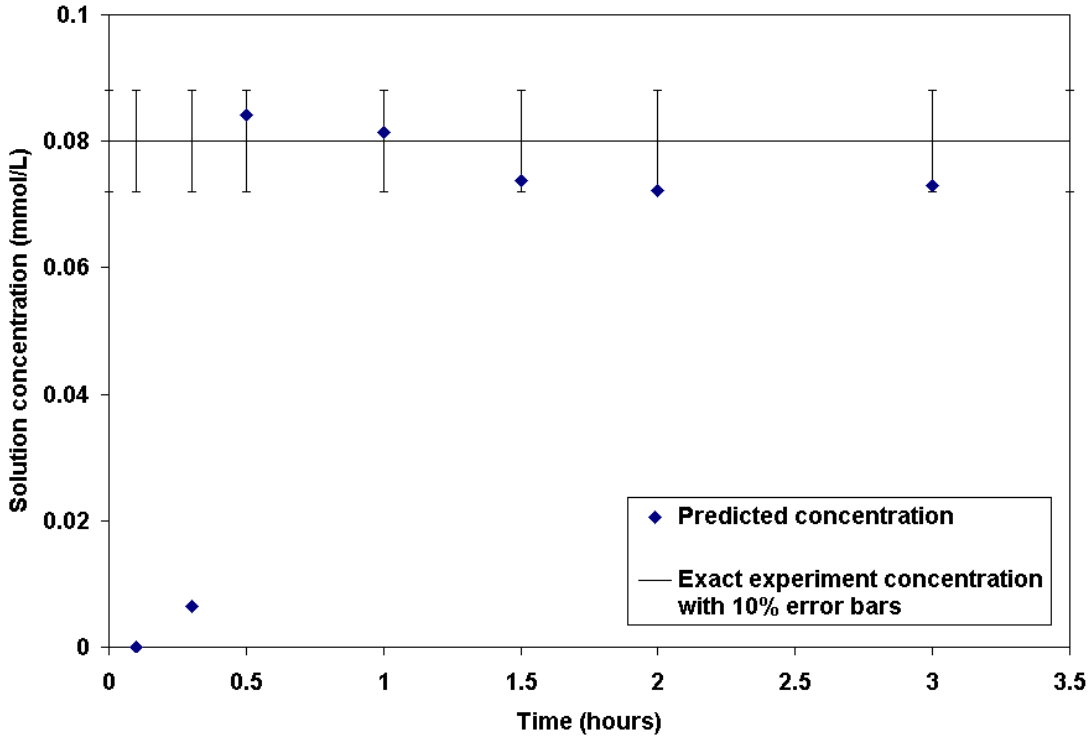

Figure 3.10. Prediction of solution concentration of BNC KCl - KNO_3 ion exchange.

3.5 University of Wyoming ion exchange case

Figure 3.11 shows the frequency response of QCM sensor corresponding to external potassium ion concentration (Lasky et al., 1990). The QCM electrode surface is coated with poly (vinylchloride) (PVC) film which contains plasticizer and crown ether for the potassium ion sensor. The coating films of 43% PVC, 56% dioctylsebacate, and 1% dibenzo-18-crown-6 were prepared by casting a tetrahydrofuran solution onto the QCM quartz surface. As Figure 3.11 shows, external potassium ion concentration was changed after the previous run reached equilibrium. The reverse profile continues from potassium ion concentration 5 mM to 0 mM. Figure 3.11 shows that the simulation curve is very close to the experiment data in the increasing concentration profile. Even the agreement between the simulation and experiments for the reverse exchange is acceptable, considering there are several different concentrations run before.

It is interesting to note that a frequency drop larger than expected occurred when 5 mmol/L was introduced. This behavior, however, is not predicted according to the simulation. This large frequency drop may be interpreted by sorption of chloride. The electric potential repels chloride from the coating film. Chloride uptake and electrolyte sorption are equivalent because of electroneutrality requirement. Hence, the electrolyte is partially excluded. The uptake of the chloride by the coating film increases with increasing concentration of the solution. This is because the electrolyte sorption is a function of the solution concentration and electrolyte exclusion is most efficient with dilute solutions.

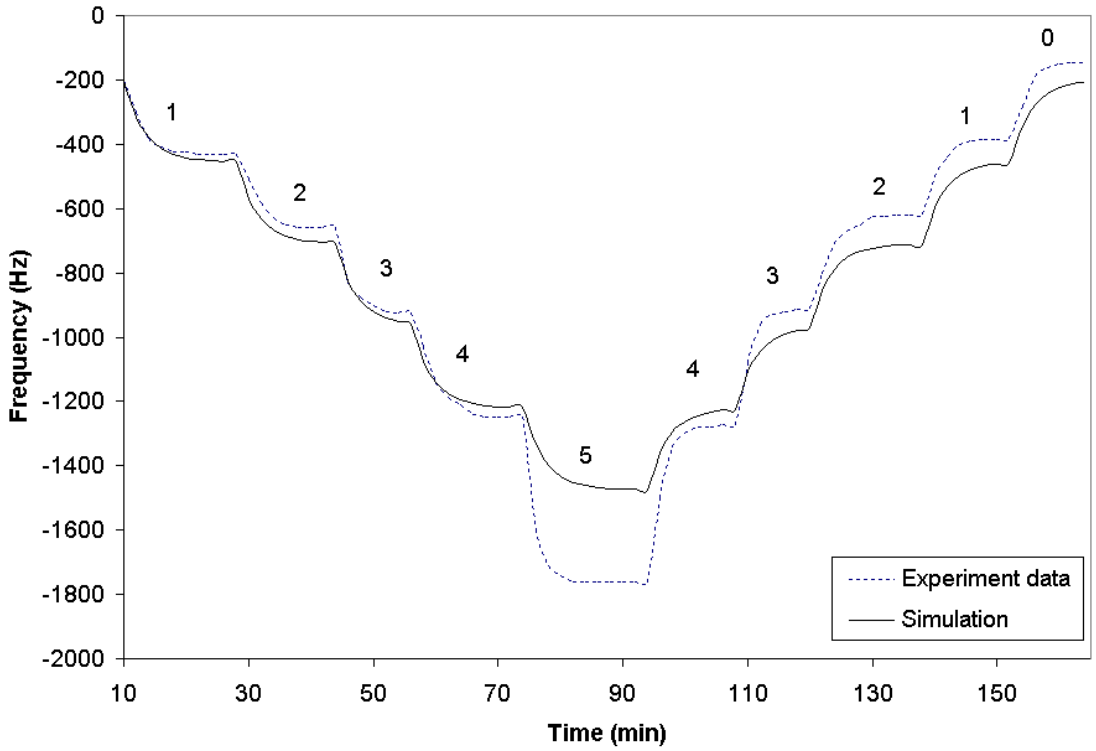

Figure 3.11. WU ion exchange case frequency response profile.

The results in Figure 3.12 are shown for the purpose of testing the accuracy of the simulation. The predicted concentration correspond to the increasing concentration profile case of concentration = 1, 2, 3, 4, and 5 mmol/L respectively, namely, the predicted concentration points are supposed to distribute around concentration = 1, 2, 3, 4, and 5 mmol/L respectively. Over the concentration range considered, the results show satisfactory agreement between simulation and experiment data for concentration = 1, 2, 3, 4 mmol/L. For concentration = 5 mmol/L, the simulation can not give quantitatively accurate results. As discussed previously, this is probably because of the sorption of anions, which increases with increasing concentration of the solution.

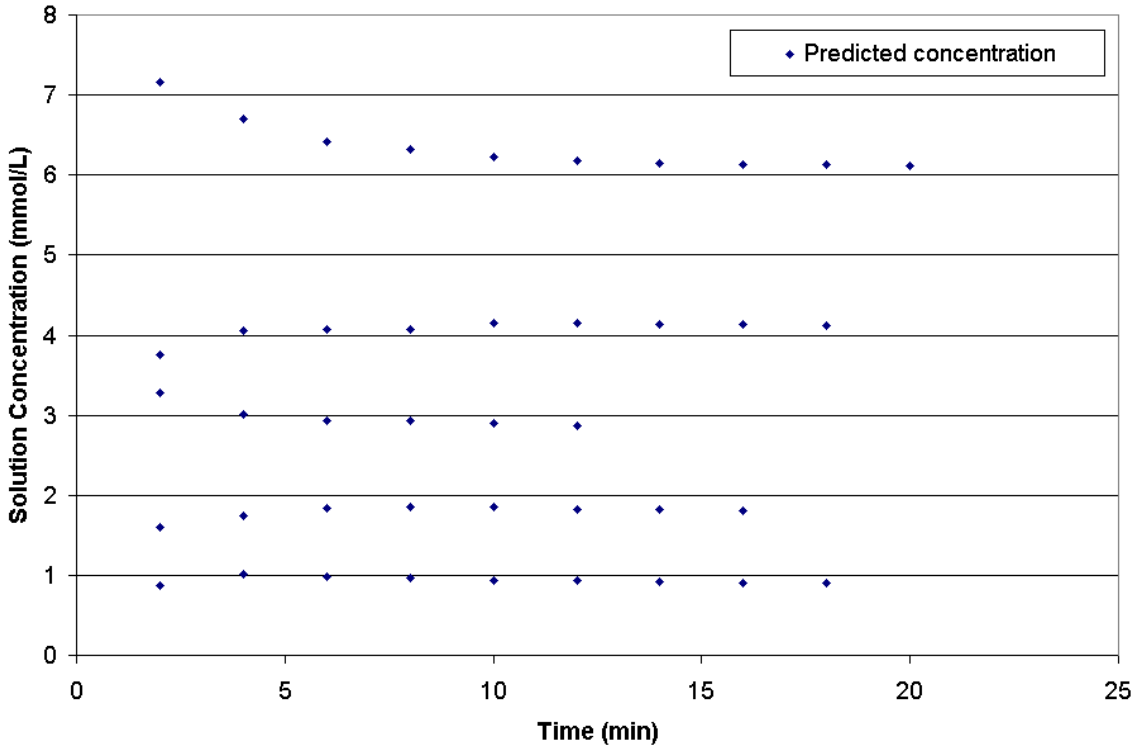

Figure 3.12. Prediction of solution concentration of WU ion exchange case.

CHAPTER 4

MODELING QUARTZ CRYSTAL MICROBALANCE SENSOR WITH AN ADSORPTION PROCESS

In the previous chapter the theory and operation of QCM, acoustic wave sensor responses are examined in some detail. To produce a viable chemical sensor, it is necessary to coat the quartz crystal surface with some film to achieve chemical selectivity and sensitivity. In real terms, we require the signal response from the sensor that can reliably and reversibly be related to the concentration of the target analyte. The response function depends on all the experiment condition and operation, i.e., pressure, temperature, mass, conductivity, dielectric constant, film thickness, diffusivity, viscoelasticity, and so on. Therefore, the successful application of QCM and other acoustic wave sensor depends on:

- Precise control of the experimental conditions
- Material properties and coating
- Adequate calibration

In this chapter, the adsorption rate model are discussed. The final section of this chapter consists of comparison of the predicted analyte concentration with literature data.

4.1 Introduction

In considering QCM sensor response to the adsorption of a particular analyte, it is necessary to realize that the processes involved are essentially kinetic in nature. For these applications, a method for rapidly evaluating the adsorption and diffusion properties in thin films is necessary. The expected flow path and distribution of adsorbate molecule entering and leaving the coating film can be described as follows:

1. The adsorbate concentration in solution changes.
2. The adsorbate transports from the bulk solution to the surface of coating film.
3. The adsorbate diffuses into the bulk of the coating film.
4. The adsorbate diffuses from the bulk of coating film to the surface and subsequently desorbs.

It is equally valid to envision the case where target adsorbate simply adsorbs to the surface before desorbing, which also causing acoustic wave perturbation (Thompson, 1997).

4.1.1 Surface adsorption and characterization of coating film

Adsorption from liquids generally involves both physisorption and chemisorption. Adsorption on a solid surface is the process by which a species for the gas or liquid phase "adheres" to the solid surface (Adamson, 1982; Hiemenz, 1986; Vold, 1983). If adsorption is characterized by relatively weak interactions, for example van der Waals force and hydrogen bonding interactions, the mechanism is called physisorption. Generally physisorption is due to molecular interactions between the adsorbate and solid. Heats of physisorption are of the same order of magnitude as heats of liquefaction.

Therefore, physisorption is similar to condensation. Chemisorption occurs due to strong interactions between the adsorbate and the solid surface, including ionic and covalent bonding and hydrogen bonding. Chemisorption is often irreversible and can occur even at very low concentrations. The endpoint for chemisorption is when all the active sites on the adsorbent are occupied by adsorbate (Ballantine, 1997). Meanwhile, for liquid adsorption, the molecular interactions between the adsorbate and the liquid, as well as those with the solid need to be considered. A straightforward example is the adsorption of water into the coating film, which results in a frequency drift from baseline.

According to Thompson (1997), we can categorize the QCM application into two measurement conditions:

1. Static monitor: The QCM sensor surface is exposed to the target analyte for a fixed amount of analyte in a fixed volume liquid.
2. Dynamic monitor: The QCM sensor surface is exposed to the continuous flowing bulk fluid.

We can further identify the dynamic monitor into two cases:

1. The bulk solution concentration is constant throughout the detection process.
2. The bulk solution concentration varies through a series concentration change.

In all categories of applications, the frequency response of QCM is measured as a function of time.

Static monitors are usually used to determine the properties and performance of the coating film. An example is to measure the diffusion coefficient of polymer film. For a dynamic monitor, there is a continuous flow of a suitable carrier fluid through the system. Sample introduction is achieved either by direct injection or stream switching.

Therefore, stable flow rates and correct calibration of flowing phase concentrations are essential.

4.1.2 Diffusion on the thin coating film of QCM

Studies on diffusion coefficient on the thin film of QCM have been carried out by many researchers. Carslaw's (1947, 1959) method originally derived for heat conduction in solids was applied to diffusion process.

Crank (1975) summarized Carslaw (1947)'s solutions for one-dimensional diffusion assuming a Fickian diffusion. For a constant diffusion coefficient, the derivation starts with the diffusion equation

$$\frac{\partial C}{\partial t} = D\frac{\partial^2 C}{\partial x^2} \tag{4-1}$$

where, $C(x,t)$ is the concentration of the adsorbing species in the polymer, x is the distance from the polymer/substrate interface, and t is time measured from the onset of the change in the partial pressure of the adsorbing species. The initial and boundary conditions for this equation are

$$C(x,0) = C_1 \tag{4-2}$$

$$C(L,t) = C_0 \tag{4-3}$$

$$\frac{\partial C}{\partial x}(0,t) = 0 \tag{4-4}$$

This boundary condition requires that, during the diffusion process, the fluid must maintain a constant concentration at the surface of the polymer film. Eq. (4-1) can be solved under these conditions to yield the following expression

$$\frac{C - C_1}{C_0 - C_1} = 1 - \frac{4}{\pi}\sum_{n=0}^{\infty}\frac{(-1)^n}{2n+1} e^{-D(2n+1)^2\pi^2 t/4L^2} \cos\frac{(2n+1)\pi x}{2L} \qquad (4\text{-}5)$$

Integration of Eq. (4-5) gives the ratio of the mass adsorbed by the polymer film at time t to the mass adsorbed by the film at equilibrium ($t = \infty$)

$$\frac{M_t}{M_{\max}} = 1 - \sum_{n=0}^{\infty}\frac{8}{(2n+1)^2\pi^2} e^{-D(2n+1)^2\pi^2 t/4L^2} \qquad (4\text{-}6)$$

where $M_{\max}$ is the incremental amount of species adsorbed in the film after equilibrium is attained. Although some researchers (Ballantine, 1997 and Willoughby, 1998) regarded Eq. (4-6) as Crank's (1975) work, Crank indicated that Eq. (4-6) is based on Carslaw's (1947) solution, which is originally derived for heat conduction. The detailed derivation of Carslaw's method is in Appendix A. It is obvious Eq. (4-6) is the same as Eq. (A-21). A technique for evaluating diffusivity coefficients is to use a QCM device to monitor adsorption process and then extract diffusivity coefficients by fitting the data to an equation similar to Eq. (4-6). Willoughby (1998) used a simplified expression of Eq. (4-6) to evaluate the diffusion coefficients. The diffusion coefficients can be calculated by determining the initial slope of the M_t/M_{max} vs. $\sqrt{t}$ curve. It should be noted that so far the applications of Eq. (4-6) with various simplified expressions are limited to the evaluation of diffusion coefficients. To rapidly predict analyte concentration, a concentration dependence expression must be developed to interpret frequency response in terms of target analyte concentration.

4.1.3 Kinetics of sorption into coating film

The ability of porous solids to reversibly adsorb vapor was discovered by Fontana (1777). In chemistry, adsorption is a surface phenomenon and refers to the accumulation

of adsorbate on the surface of adsorbent. The material that is adsorbed is called the adsorbate. The solid material upon whose surfaces adsorption takes place is called the adsorbent. According to Tien (1994), one may view the adsorption phenomenon as follows. "Consider a heterogeneous system composed of a fluid phase (liquid or gaseous) and a solid surface. Further assume that the fluid phase is a solution of several different chemical species and that the fluid and solid phases are under thermodynamic equilibrium. A species present in the fluid phase is said to be adsorbed on the solid surface if the concentration of the species in the fluid-solid boundary region is higher than that in the bulk of the fluid. Adsorption takes place because of the interaction between the species present in the fluid phase and the solid surface."

Mathematical simulations of adsorption process provides quantitative knowledge of an adsorption process. Many researchers have contributed to the modeling of adsorption process. Ruthven (1984) has given a complete review on the dynamics and mathematical modeling of isothermal adsorption. More recently, Tien (1994) have given a fairly complete coverage to adsorption modeling and calculations.

For an adsorption column system, adsorption models can be divided into three categories: equilibrium models, plate models and rate models. The first equilibrium theory of multicomponent isothermal adsorption was developed by Glueckauf (1949). Equilibrium models assume the solid phase and liquid phase reach direct local equilibrium, neglecting axial dispersion and mass transfer resistance. Although equilibrium models may effectively predict adsorption process with fast mass transfer rates, they are generally over-simplified. This is because that equilibrium models assume direct equilibrium in the mobile phase and the stationary phase, without regard to the

mass transfer rate through the stationary phase. For a chromatography adsorption system, the term "theoretical plate" is taken from plate theory, which relates the theory of adsorption to the theory of distillation. The plate models assume the adsorption column is divided into a series of small artificial cells. Rate models may be used to describe the adsorption kinetics. Rate models are significantly more accurate than equilibrium models with varying complexities. They generally assume a rate expression between the mobile phase and the stationary phase.

For QCM applications, the wide variability of adsorption and diffusional properties of chemical species in thin polymer coating film makes them useful as selective barriers. Even though adsorption in polymers is generally a complex process, it is reasonable to find a relatively dominant mechanism for the system. For these applications, adsorbent particles are inevitably microporous and adsorption takes place exclusively in the particle's internal void surface (Tien, 1994). Consequently, uptake of adsorbates requires their molecules to diffuse into the interior of the particles.

The simplest case to consider is a single microporous adsorbent particle. The adsorption starts when adsorbent particle is exposed to a step change in adsorbate concentration at the external surface of the particle at time zero. The mass balance equations for an adsorbent particle provide the starting point for development of a mathematical model to describe the dynamic behavior of the system. A quantitative description of adsorption rates processes can generally be obtained for different diffusion mechanisms by applying transient conservation equations in spherical coordinates for the particles and coupling these equations to overall transient balances through boundary conditions at the particle fluid interface (Ruthven 1984, Yang 1987). Generally,

diffusion mechanisms of spherical particles relevant to adsorption processes include pore and surface diffusion.

4.1.3.1 Pore diffusion

According to LeVan's (1997) theory, pore diffusion operates if the intraparticle mass transfer is due to the diffusion of adsorbate molecules through the pore fluid. For the simple case of single-species adsorption and assuming that Fick's law applies, the system is described by the following equation

$$\varepsilon_p \frac{\partial c}{\partial t} + \rho_p \frac{\partial q}{\partial t} = \frac{1}{r^2} \frac{\partial}{\partial r}\left[D_p r^2 \frac{\partial c}{\partial r} \right], \qquad 0 \le r \le a_p \qquad (4\text{-}7)$$

where c and q are the adsorbate concentrations in the pore fluid and of the adsorbed phase within the particle, ε_p is porosity, ρ_p is density, D_p is pore diffusivity.

Diffusion in liquid-filled pores includes both pore diffusion and molecular diffusion of adsorbate molecules in fluid systems. In molecular diffusion, the resistance to flow arises from collisions among fluid molecules. Under these conditions the free path of the molecules is small relative to the pore radius. However, in small pores and at low pressure, collisions between the fluid molecules and pore walls become dominant, and its effect must be considered, which is known as Knudsen diffusion. The Knudsen diffusivity may be estimated from the commonly accepted semiempirical expression (Kennard, 1938)

$$D_K = 9700 r_p \left(\frac{T}{M} \right)^{1/2} \qquad (4\text{-}8)$$

where r_p is the mean pore radius (cm), T is temperature in Kelvin, and M is the molecular weight of the diffusing species.

In reality, the actual diffusion path is randomly distributed and both pore collisions and intermolecular collisions contribute to the diffusional resistance. Therefore, the real diffusivity is from both the Knudsen and molecular diffusivities. Modification of D_p in Eq. (4-7) can be defined as (Scott and Dullien, 1962)

$$\frac{1}{\overline{\overline{D}}_p} = \frac{1}{D_p} + \frac{1}{D_K} \tag{4-9}$$

where D_K is Knudsen diffusion coefficient in Eq. (4-8). From Eq. (4-9), it is obvious that if either diffusivity is much smaller than the other one, the following diffusion mechanism will dominate.

4.1.3.2 Surface diffusion

In the case in which the intraparticle mass transfer is affected by the transport through the physically adsorbed layer on the surface of the particle, the adsorption mechanism is referred to as surface diffusion. For spherical particles, and assuming that Fick's law applies, the intraparticle adsorption may be expressed as

$$\left(\frac{\varepsilon_p}{\rho_p}\right)\frac{\partial c}{\partial t} + \frac{\partial q}{\partial t} = \frac{1}{r^2}\frac{\partial}{\partial r}\left[D_s r^2 \frac{\partial q}{\partial r}\right] \tag{4-10}$$

where ε_p is porosity, ρ_p is density, D_s is the surface diffusion coefficient.

In general, the adsorption mechanism occurring within the adsorbent particles includes pore diffusion of fluid and surface diffusion of adsorbed phase simultaneously. The combination of both mechanisms can be defined as (Tien, 1994)

$$\varepsilon_p \frac{\partial c}{\partial t} + \rho_p \frac{\partial q}{\partial t} = \frac{1}{r^2}\frac{\partial}{\partial r}\left[D_p r^2 \frac{\partial c}{\partial r}\right] + \frac{\rho_p}{r^2}\frac{\partial}{\partial r}\left[D_s r^2 \frac{\partial q}{\partial r}\right] \tag{4-11}$$

Due to the mathematical complexities associated with the combination of both mechanism of intraparticle adsorption, simple rate expressions are desirable.

The most widely used approximate rate model is the so-called linear driving force (LDF) approximation, which assumes the adsorption isotherm is linear and local equilibrium exists between the pore fluid phase and the adsorbed phase. The LDF approximation expresses the rate of interphase mass transfer as the product of a rate coefficient times a driving force of concentration difference. The LDF approximation was originally developed by Glueckauf (1955 a,b) for surface diffusion with a constant diffusivity. The LDF approximation can also be derived based on the assumption that the adsorbed phase concentration profile inside a sorbent particle is parabolic (Rice, 1982; Liaw 1979). Using the similar mechanism, Lai and Tan (1991) assumed parabolic and quartic profiles for the combined pore and adsorbed phase concentration inside the particle and extended the approximation model to nonlinear adsorption. Based on concentration layer concept, Yao and Tien (1993) derived an approximation for the adsorption rate of adsorbate in spherical adsorbent for both linear and nonlinear adsorption isotherms. Starting with the parabolic profile assumption for the combined pore fluid and adsorbed phase concentration, Zhang and Ritter (1997) developed an approximation for parallel pore and surface diffusion. Carta and Cincotti (1998) proposed an approximate model for nonlinear adsorption and diffusion in a spherical adsorbent particle based on an equivalent film resistance model. Although these new mechanisms are generally similar in form to the LDF approximation, they significantly introduce far more mathematical complexities into computation.

4.2 Model assumptions

To simplify the mathematical derivation, the following assumptions were made to satisfy physical requirements of the system and make the algorithm calculation feasible. They are listed below in no particular order.

1. Isobaric operation.
2. Isothermal operation. Heat transfer is sufficiently rapid, relative to the adsorption rate, so that temperature gradients both through the particle and between particle and surrounding fluid are negligible.
3. Negligible swelling and shrinking changes of the coating film.
4. Intraparticle mass transfer is the rate controlling step.
5. The uptake of adsorbate by the adsorbent is small relative to the total quantity of adsorbate introduced to the system. The ambient adsorbate concentration will remain essentially constant following the step change.
6. Constant individual diffusion coefficients of the chemical species.

4.3 Concentration prediction model development

The concentration prediction model of QCM is developed based on a planar coating film. The single microporous adsorbent particle provides the starting point for development of a mathematical model to describe the dynamic behavior of the system. The fundamental case to consider is a planar thin film exposed to step changes in adsorbate concentration at the external surface of the film at time zero. If the diffusivity is constant, the diffusion equation simplifies to

$$\frac{\partial q}{\partial t} = D\frac{\partial^2 q}{\partial x^2}, \quad 0 < x < L, \tag{4-12}$$

where D is the diffusion constant in the adsorbent and $q(x,t)$ is the adsorbed phase concentration. The bulk adsorbate concentration is assumed to remain essentially constant following the step change. Therefore, the appropriate initial boundary conditions are

$$q(x,0) = q_0 \quad \text{when time t = 0} \tag{4-13}$$

$$q(L,t) = q_1 \quad \text{when time t > 0} \tag{4-14}$$

$$\left(\frac{\partial q}{\partial x}\right)_{x=0} = 0 \tag{4-15}$$

The solution for the adsorption equation is given by the well-known expression (Carslaw and Jaeger, 1959). The detailed derivation is in Appendix (A).

$$\bar{q} = q_0 + (q_1 - q_0)\left\{1 - \frac{8}{\pi^2}\sum_{n=0}^{\infty}\frac{1}{(2n+1)^2}\exp\left[-(2n+1)^2\pi^2 Dt/4L^2\right]\right\} \tag{4-16}$$

where D = diffusion constant in the coating film

L = coating film thickness

$\bar{q}$ is the average internal concentration of the coating film, defined by

$$\bar{q} = \frac{1}{L}\int_0^L q\,dx$$

For single step change, Glueckauf (1947) and Vermeulen (1954) have suggested an approximation of Eq. (4-16)

$$\frac{d\bar{q}}{dt} = k(q_s - \bar{q}) \tag{4-17}$$

where $\bar{q}$ and q_s are average adsorbed phase concentration and the adsorbed phase concentration at the exterior surface of the coating film, respectively

The physical meaning of Eq. (4-17) is that the uptake rate of adsorbate by coating film is linearly proportional to the difference between the existing average concentration and that obtaining at the surface of coating film.

If we are considering a succession of step changes of surface concentration, instead of a single change

$$q_s = q_0 \qquad \text{for } t < 0$$

$$q_s = q_1 \qquad \text{for } t_1 > t > 0$$

$$q_s = q_2 \qquad \text{for } t_2 > t > t_1$$

$$q_s = q_3, \qquad \text{for } t_3 > t > t_2, \text{ etc.}$$

then, Eq. (4-16) changes to

$$\bar{q} = q_0 + (q_1 - q_0)\left\{1 - \frac{8}{\pi^2}\sum_{n=0}^{\infty}\frac{1}{(2n+1)^2}\exp\left[-(2n+1)^2\pi^2 D(t-0)/4L^2\right]\right\}$$

$$+ (q_2 - q_1)\left\{1 - \frac{8}{\pi^2}\sum_{n=0}^{\infty}\frac{1}{(2n+1)^2}\exp\left[-(2n+1)^2\pi^2 D(t-t_1)/4L^2\right]\right\}$$

$$+ (q_3 - q_2)\left\{1 - \frac{8}{\pi^2}\sum_{n=0}^{\infty}\frac{1}{(2n+1)^2}\exp\left[-(2n+1)^2\pi^2 D(t-t_2)/4L^2\right]\right\}$$

$$+\ldots\ldots \qquad (4\text{-}18)$$

If the surface concentration is subject to a continuous change, which may be an arbitrary function of time, Eq. (4-18) develops into

$$\bar{q} = q_s - \frac{8}{\pi^2}\int_0^t\left(\frac{dq_s}{d\tau}\right)\sum_{n=0}^{\infty}\frac{1}{(2n+1)^2}\exp\left[-(2n+1)^2\pi^2 D(t-\tau)/4L^2\right]d\tau \qquad (4\text{-}19)$$

Then the adsorption rate $\frac{d\bar{q}}{dt}$ can be obtained by differentiation of Eq. (4-19).

$$\frac{d\bar{q}}{dt} = \frac{8D}{4L^2}\int_0^t \left(\frac{dq_s}{d\tau}\right)\sum_{n=0}^{\infty} \exp\left[-(2n+1)^2\pi^2\left(\frac{D}{4L^2}\right)(t-\tau)\right]d\tau \tag{4-20}$$

According to successive integration by parts

$$\int f_1 f_2 d\tau = f_1\int f_2 d\tau - \frac{df_1}{d\tau}\int\int f_2 d\tau^2 + \frac{d^2 f_1}{d\tau^2}\int\int\int f_2 d\tau^3 - \cdots + \cdots \tag{4-21}$$

Eq. (4-19) may be integrated as

$$\begin{aligned} q_s - \bar{q} &= \frac{8}{\pi^2}\left\{\frac{dq_s}{d\tau}\sum_{n=0}^{\infty}\frac{1}{(2n+1)^2}\int_0^t \exp\left[-(2n+1)^2\pi^2\left(\frac{D}{4L^2}\right)(t-\tau)\right]d\tau\right\} \\ &\quad -\frac{8}{\pi^2}\left\{\frac{d^2 q_s}{d\tau^2}\sum_{n=0}^{\infty}\frac{1}{(2n+1)^2}\int_0^t\int_0^t \exp\left[-(2n+1)^2\pi^2\left(\frac{D}{4L^2}\right)(t-\tau)\right]d\tau^2\right\} + \cdots \\ &= \frac{8}{\pi^2}\left\{\left(A_2/\pi^2\right)\frac{dq_s}{d\left(Dt/4L^2\right)} - \left(A_3/\pi^4\right)\frac{d^2 q_s}{d\left(Dt/4L^2\right)^2} + \cdots\right\} \end{aligned} \tag{4-22}$$

where

$$A_2 = \sum_{n=0}^{\infty}\frac{1-\exp\left[-(2n+1)^2\pi^2\left(\frac{D}{4L^2}\right)t\right]}{(2n+1)^4}$$

$$A_3 = \sum_{n=0}^{\infty}\frac{1-\exp\left[-(2n+1)^2\pi^2\left(\frac{D}{4L^2}\right)t\right]}{(2n+1)^6}$$

Applying the same integration method, Eq. (4-20) can be given as

$$\frac{d\bar{q}}{d\left(Dt/4L^2\right)} = 8\left[\frac{A_1}{\pi^2}\frac{dq_s}{d\left(Dt/4L^2\right)} - \frac{A_4}{\pi^4}\frac{d^2 q_s}{d\left(Dt/4L^2\right)^2} + \cdots\right] \tag{4-23}$$

where

$$A_1 = \sum_{n=0}^{\infty}\frac{1-\exp\left[-(2n+1)^2\pi^2\left(\frac{D}{4L^2}\right)t\right]}{(2n+1)^2}$$

Under these conditions, an expression of the diffusion process can be given by combining Eqs (4-22) and (4-23)

$$\frac{d\bar{q}}{d\left(Dt/4L^2\right)} = \pi^2\left(q_s - \bar{q}\right) + \frac{8}{\pi^2}\left(A_1 - A_2\right)\frac{dq_s}{d\left(Dt/4L^2\right)} - \frac{8}{\pi^4}\left(A_2 - A_3\right)\frac{d^2 q_s}{d\left(Dt/4L^2\right)^2} + \cdots \tag{4-24}$$

According to Glueckauf (1955 b), unless q is an exponential function, this series converges quickly, not only because of $\frac{1}{\pi^2}$, but $A_n - A_{n+1}$ also decreases rapidly. Also, if $Dt/4L^2 > 0.1$, the value of $A_n - A_{n+1}$ may be approximate as

$$A_n - A_{n+1} \to \sum_{n=0}^{\infty}\frac{1}{(2n+1)^{2n}} - \sum_{n=0}^{\infty}\frac{1}{(2n+1)^{2n+2}} \tag{4-25}$$

therefore,

$$A_1 - A_2 = \sum_{n=0}^{\infty}\left[\left(\frac{1}{(2n+1)^2} - \frac{1}{(2n+1)^4}\right)\left\{1 - \exp\left[-(2n+1)^2\pi^2(D/4L^2)t\right]\right\}\right]$$

$$\cong \sum_{n=0}^{\infty}\left[\frac{1}{(2n+1)^2} - \frac{1}{(2n+1)^4}\right]$$

$$= \frac{\pi^2}{8} - \frac{\pi^4}{96} \tag{4-26}$$

or $$\frac{8}{\pi^2}(A_1 - A_2) \approx 0.1775 \tag{4-27}$$

Using the same method,

$$A_2 - A_3 \cong \sum_{n=0}^{\infty}\left(\frac{1}{(2n+1)^4} - \frac{1}{(2n+1)^6}\right) = \frac{\pi^4}{96} - \frac{\pi^6}{960} \tag{4-28}$$

$$\frac{8}{\pi^2}(A_2 - A_3) \approx 0.0107 \tag{4-29}$$

Under these conditions, an approximate expression of the diffusion is given by

$$\frac{d\bar{q}}{d\left(Dt/4L^2\right)} = \pi^2\left(q_s - \bar{q}\right) + 0.1775\frac{dq_s}{d\left(Dt/4L^2\right)} - 0.0107\frac{d^2q_s}{d\left(Dt/4L^2\right)^2} + \cdots \tag{4-30}$$

where the last term can usually be neglected. Thus by assuming that $\frac{dq_s}{dt}$ can be replaced by $\frac{d\bar{q}}{dt}$, Eq. (4-24) becomes

$$\frac{d\bar{q}}{d\left(Dt/4L^2\right)} = \frac{\pi^2\left(q_s - \bar{q}\right)}{1 - 0.1775} \tag{4-31}$$

which leads directly to

$$\frac{d\bar{q}}{d\left(Dt/4L^2\right)} = 12\left(q_s - \bar{q}\right) \tag{4-32}$$

or

$$\frac{d\bar{q}}{dt} = 3\frac{D}{L^2}\left(q_s - \bar{q}\right) \tag{4-33}$$

Eq. (4-33) can also be derived by assuming parabolic concentration profile within the coating film. This method has been used in Chapter 3 to derive the diffusion equation of ion exchange.

If the concentration in adsorbent is assumed to be parabolic, the concentration distribution is

$$q = q' + al^2 \tag{4-34}$$

where q' is the concentration at the bottom of the coating film and a is arbitrary function of time. The surface concentration can be expressed as

$$q_s = q' + aL^2 \tag{4-35}$$

where L is the height of coating film. The adsorption rate can be defined as a function of surface diffusion rate

$$\frac{d\overline{q}}{dt} = \frac{1}{L} D \left(\frac{dq}{dl} \right)_{l=L} \tag{4-36}$$

and from Eq. (4-35),

$$\left(\frac{dq}{dl} \right)_{l=L} = 2aL \tag{4-37}$$

The average concentration, $\overline{q}$, can be obtained by integrating Eq. (4-34)

$$\overline{q} = \frac{1}{L} \int_0^L \left(q' + al^2 \right) dl$$

$$= q' + \frac{L^2}{3} a \tag{4-38}$$

Thus,

$$q_s - \overline{q} = \frac{2}{3} aL^2 \tag{4-39}$$

By combining Eq (4-36), (4-37), (4-39), $\frac{d\overline{q}}{dt}$ can be shown as

$$\frac{d\overline{q}}{dt} = 2Da = \frac{3D}{L^2} \left(q_s - \overline{q} \right) \tag{4-40}$$

This diffusion equation is the same as Eq. (4-33).

4.4 Frequency response of QCM coated with thin adsorbent film

In the situation so far considered a thin coating film diffusion resistance has been regarded as rate controlling. Assuming a linear equilibrium relation and an infinitely large system, an analytical solution was derived for the adsorption curve assuming step change(s) concentration at the external surface of the coating film.

The frequency response of QCM can be obtained with the same mathematics used in Chapter 3. The load of mass accumulation and liquid shear displacement are shown as Martin's (1991) equation.

$$\Delta f = -\frac{2 f_0^{\,2}}{N\sqrt{\mu_q \rho_q}}\left[\frac{\Delta m}{A} + \left(\frac{\rho\eta}{4\pi f_0}\right)^{1/2}\right] \tag{4-41}$$

which can be simplified to

$$\Delta f = K\Delta m + k_0 \tag{4-42}$$

The mass change on the coating film is directly related to the amount of adsorbate in the solid phase.

$$\Delta m = Q\frac{m_r}{1000}\bar{q}M \tag{4-43}$$

where m_r is the mass of adsorbent, Q is the total adsorption in moles per unit mass of adsorbent, M is the molecular weight of adsorbate.

In this work, equilibrium is assumed between the solid phase and fluid phase at the surface of coating film and the equilibrium relationship is taken to be linear. The distribution coefficient can be defined as the concentration of a component on the stationary phase divided by the concentration of the component in the mobile phase in equilibrium conditions.

$$\lambda = \frac{q_s}{q} \tag{4-44}$$

Expressed in terms of distribution coefficient, Eq. (4-33) becomes

$$\frac{d\bar{q}}{dt} = 3\frac{D}{L^2}\left(\lambda q - \bar{q}\right) \tag{4-45}$$

With initial condition,

at $t = 0$, $\bar{q}_n = \bar{q}_{n-1}$ (4-46)

where $\bar{q}_n$ and $\bar{q}_{n-1}$ are the average solid phase concentration of *n*th and (*n*-1)th introduction of new solution. Thus, Eq. (4-45) can be integrated as

$$-\ln(\lambda q - \bar{q}_n) = \frac{3}{L^2} Dt - \ln(\lambda q - \bar{q}_{n-1}) \tag{4-47}$$

Based on Eq. (4-47), the liquid phase adsorbate concentration q can be conveniently correlated in terms of the average solid phase concentration of *n*th and (*n*-1)th introduction of new solution.

$$q = \frac{EXP(\frac{3}{L^2} Dt)\bar{q}_n - \bar{q}_{n-1}}{\left[EXP(\frac{3}{L^2} Dt) - 1\right]\lambda} \tag{4-48}$$

When substituting Eq. (4-42) and Eq. (4-43), liquid phase concentration can be expressed as a function of frequency change

$$q = \frac{EXP(k_2 t_n)\Delta f_n - \Delta f_{n-1}}{\left[EXP(k_2 t_n) - 1\right]k_1} \tag{4-49}$$

where $k_1 = KQ\frac{m_r}{1000} M\lambda$

$$k_2 = \frac{3}{L^2} D$$

$\Delta f_{n-1} = f_{n-1} - f_0$ is the frequency change from baseline at the moment of exposure to (*n*-1)th solution

$\Delta f_n = f_n - f_0$ is the online frequency change from baseline after time t_n exposure to *n*th solution.

t_n is the time after exposure to *n*th analyte.

Eq. (4-49) shows that predicted concentration of adsorbate is a function of time, frequency change and frequency change of previous running cycle. From a measurement perspective, to instantly predict the analyte concentration, instant frequency change Δf_n with corresponding time t_n after exposure to new solution, and frequency change Δf_{n-1} of previous cycle ending point are needed, provided constant k_1 and k_2 are known.

Same as in Chapter 3, this model can be used to predict solution phase concentrations of the same constituents for both increasing and decreasing concentrations for an arbitrary time. The mass loading and frequency response vary with time and solution concentrations; hence it can calculate solution concentration at a specific time based on the mass loading (frequency response).

Theoretically, this model can also be used for non-step changes. In Eq. (4-49), Δf_n exactly describes the sorption on the coating film instead of previous external analyte concentration, i.e., prediction of current analyte is based on the known previous sorption on the coating film, not the previous external analyte concentration. Thus, it actually does not matter if Δf_n is a frequency change for step change or an arbitrary non-step change point. Meanwhile, from a practical point, it is necessary to keep the time interval short to ensure the prediction is for current external analyte.

This model is self-correcting based on the previous running cycle. Theoretically, the model can predict the solution concentration based on any previous added input data. To make the simulation consistent, the previous equilibrium data are always used as the reference. This concept guarantees the model can keep the prediction current after several step changes.

4.5 Prediction of adsorbate concentration using QCM

4.5.1 Me-Cav coated QCM to detect toluene

Ferrari (2004) investigated AT-cut thickness-shear quartz crystal microbalance sensors coated with cavitand (Me-Cav) film to detect organic vapors toluene. Cavitands used in their study show supermolecular host properties which permit the adsorption of adsorbate with a suitable polarity and shape. Figure 4.1 shows Me-Cav which has a more accessible and electron-rich cavity. The QCM sensor used in this study has 10 MHz AT-cut 8 mm diameter crystals with 5 mm diameter gold electrodes.

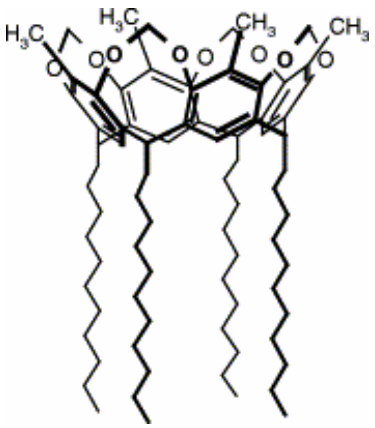

Figure 4.1. Me-Cav. (Ferrari, 2004).

The experiments consisted of the following procedure. The sensors were first exposed to nitrogen stream at a flux rate of 500 ml/min until the frequency baseline of the sensors reached steady state. While keeping the overall flux constant, the repeated exposure to toluene was run followed by flowing with nitrogen stream.

The measurement setup is described in Figure 4.2. The test toluene was generated from a bubbler system at ambient temperature using nitrogen as the carrier gas. The

toluene then was diluted to known concentration by computer-driven mass flow controllers. The output frequencies from oscillator circuits were taken as the sensor signal and fed to frequency counter. The sequential acquisition of the sensor signals was controlled by a PC under dedicated program.

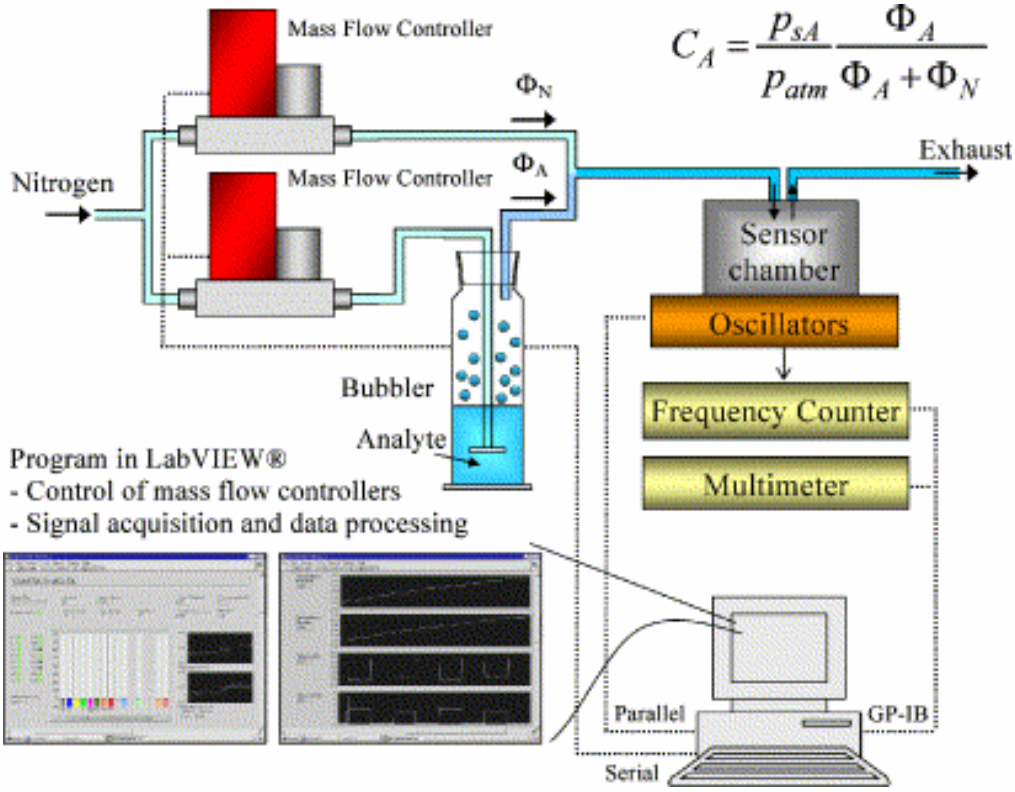

Figure 4.2. Block diagram of the measurement setup. (Ferrari, 2004).

Figure 4.3 is the typical time responses at room temperature of Me-Cav coated QCM sensors to different concentrations of toluene from 500 ppm to 2000 ppm followed by nitrogen stream. The frequency change demonstrates substantial reversibility. Figure 4.3 also shows the comparison of modeling and experimental data of frequency response.

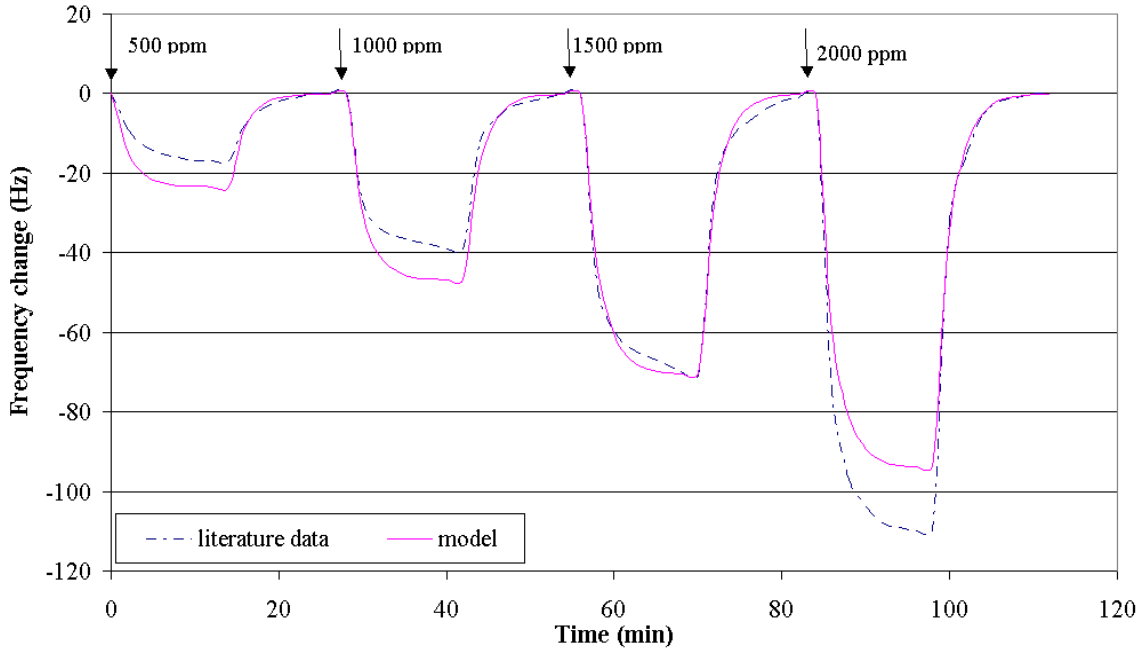

Figure 4.3. Me-Cav coated QCM to detect toluene case frequency response profile.

The results in Figure 4.4 are shown for the purpose of testing the accuracy of the simulation with 15% error bar. The predicted concentrations correspond to the increasing stepping change of concentration 500, 1000, 1500, 2000 ppm respectively. Predicted concentrations around zero are consistent with the exposure of nitrogen stream purging. Over the concentration range considered, the results show the predicted concentration is around 15% error of the experiment data.

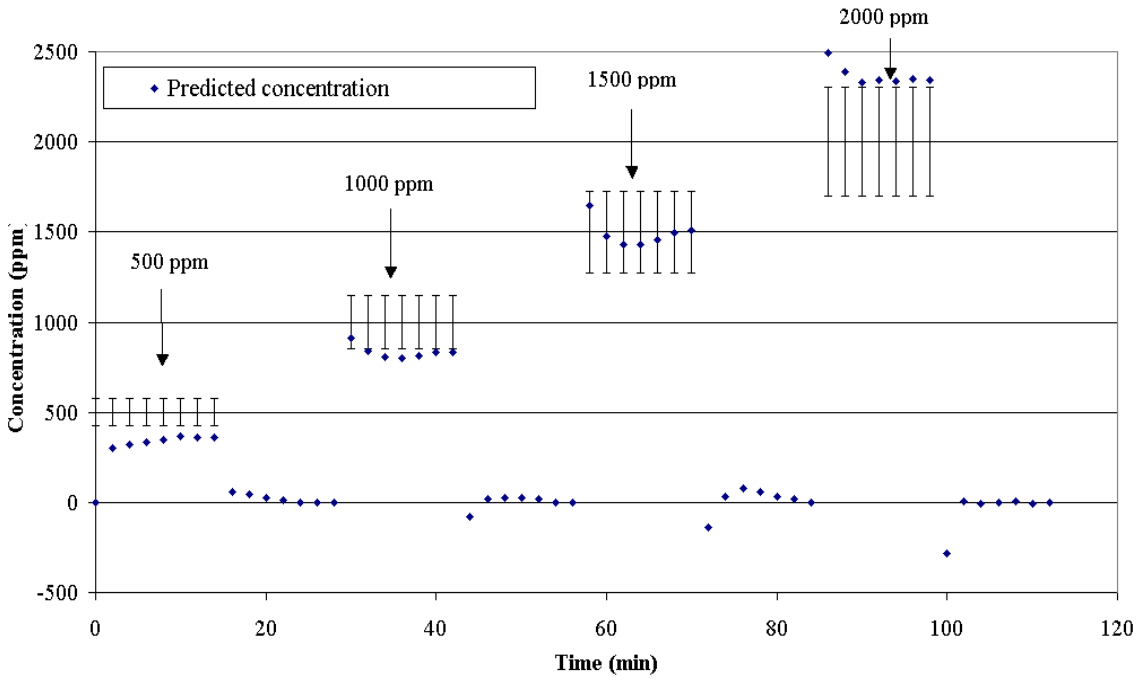

Figure 4.4. Prediction of concentration of Me-Cav coated QCM to detect toluene case.

4.5.2 Lysozyme coated QCM to detect DNA

Mao (2001) studied the formaldehyde (FA)-induced DNA-protein cross-linking process using QCM coated with lysozyme. FA is mainly from industrial processes, including motor vehicle exhaust, wood burning stoves and cigarette smoke. Therefore, human exposure to FA is extensive. Sufficient evidence demonstrates that FA is an animal carcinogen. As for people, although the evidence is not conclusive, several studies have suggested the possibility that FA causes carcinogenesis. The reactions of FA with DNA and proteins have been extensively investigated. Some researchers show that FA can induce the production of DNA-protein cross-linking, which may be a mechanism of FA carcinogenicity. The DNA-protein cross-links are constituted of the complexes of lysine in proteins and guanine in DNA molecules. First, a hydroxymethyl

intermediate is formed between FA and a primary amine of either lysine or guanine. Then, the intermediate is linked with second primary amine to form a methylene bridge.

The FA-induced DNA-lysozyme cross-linking reaction can be described by the following equation

$$[lysozyme - FA] + [DNA] \Leftrightarrow [lysozyme - FA - DNA]$$

The experiments were carried out at 37 ± 0.1 °C. Lysozyme was immobilized on the quartz crystal surface by means of adsorption. One face of the crystal was in contact with a lysozyme aqueous solution in TE buffer (10 $mmol^{-1}$ Tris, 1 $mmol^{-1}$ EDTA, pH 8) for a given time. Before the experiment, 30 min were needed to stabilize the whole experimental setup. 9 ml TE buffer (pH 8), warmed to 37 °C, was first placed in the detection cell, which was held at a constant temperature of 37 °C to mimic a biological environment. Then, with gentle stirring, 0.50 ml of 13.3 mol /L formaldehyde was added to the detection cell and about 15 min later 0.50 ml of DNA solution was introduced. The cross-linking process continues for about 20 min.

Figure 4.5 shows real time frequency response and fitted curves for FA-induced DNA-lysozyme adsorption at 60 μg/ml concentration. Figure 4.6 demonstrates that the predictions are in good agreement with the experiment value within 10% error.

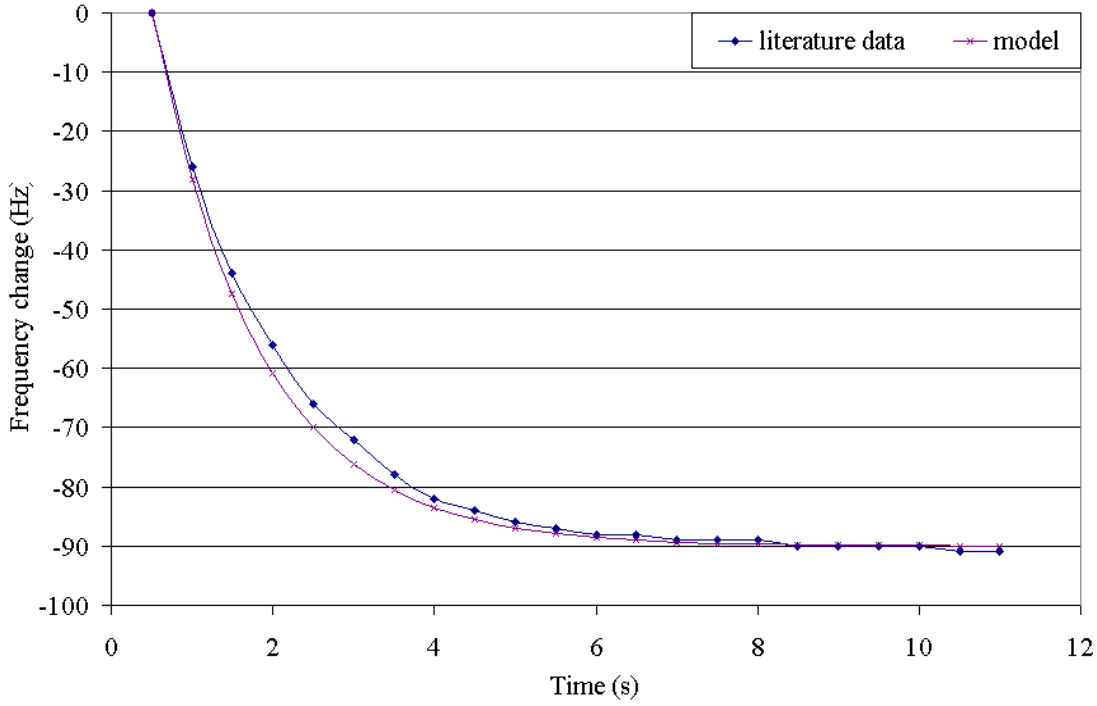

Figure 4.5. Lysozyme coated QCM to detect DNA case frequency response profile.

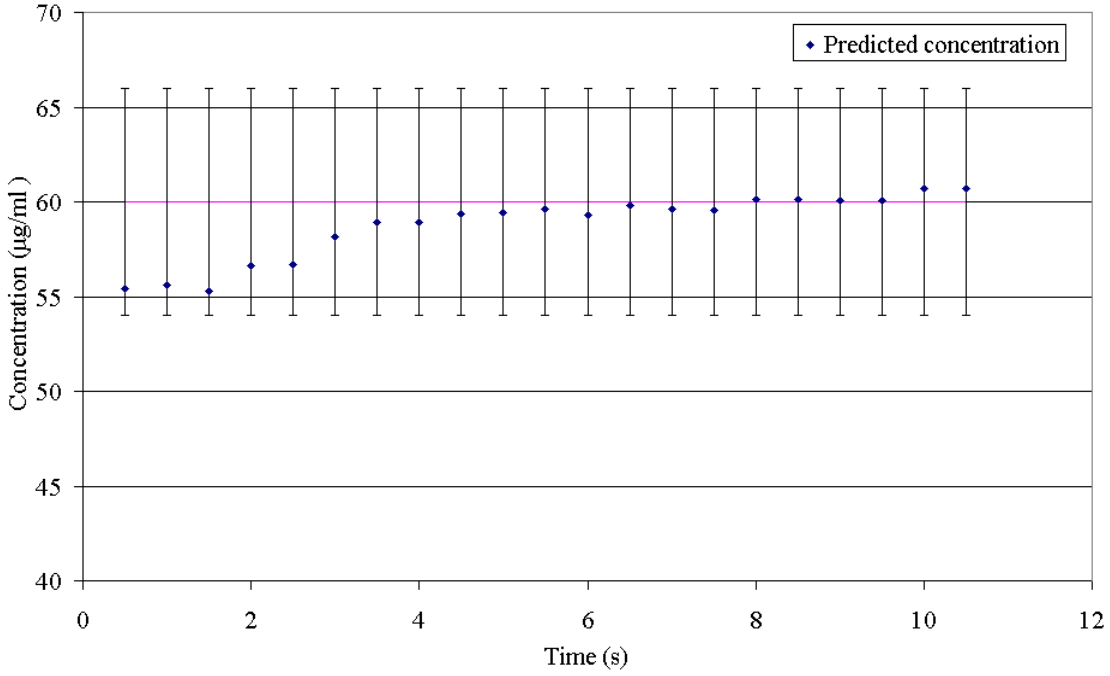

Figure 4.6. Prediction of concentration of lysozyme coated QCM to detect DNA case.

4.5.3 Polymethylmetacrylate (PMMA) coated QCM to detect phenol

Mirmohseni (2004) has investigated the determination of phenol in solution using Polymethylmetacrylate coated quartz crystal microbalance. Phenol is present in the environment as a result of industrial processes. Phenolic compounds act as intermediates in many industrial processes, including those in the petroleum and pulp and paper industry. Phenol and its derivatives are an important source of environmental pollutants. Phenolic compounds are listed in both Environmental Protection Agency (EPA) and the European Union as dangerous chemical species discharged into the aquatic environment (Wissiack, 2000). There are several methods to analyze phenolic compounds in aquatic environment including gas (Mussmann 1994, Louter 1997, Bao 1996) or liquid (Jauregui 1997, Masque 1998, Chung 2001) chromatography. However, the sample solution must be pre-concentrated before analysis due to the low level of their occurrence in the environment. This method is laborious and requires large volumes of expensive toxic organic solvents.

Quartz crystal microbalance device is based on the sorption of analyte on an adsorbent material. In this system, adsorption and detection are carried out simultaneously and there is no need for using expensive equipment such as gas or liquid chromatographs.

The polymer is coated on the surface of quartz crystal using solution casting method. Using a microliter syringe, 2 μL of 0.3% PMMA/chloroform solution was dropped on top of the surface of quartz crystal gold electrode. A thin coating of PMMA was obtained after solvent evaporation. Phenol solutions with various concentrations of

phenol were prepared by dissolving the phenol in distilled water. All experiments were carried out at room temperature.

PMMA coated quartz crystal electrode (approximately 400 nm in thickness) was directly exposed to various concentrations of phenol solutions ranged from 0 to 10 ppm. Figure 4.7 shows frequency changes and simulation versus time for various concentrations of aqueous phenol solutions. As the concentration of analyte increased the magnitude of the response also increased. Figure 4.7 shows that the simulation curves are very close to the experiment data for various concentrations profile.

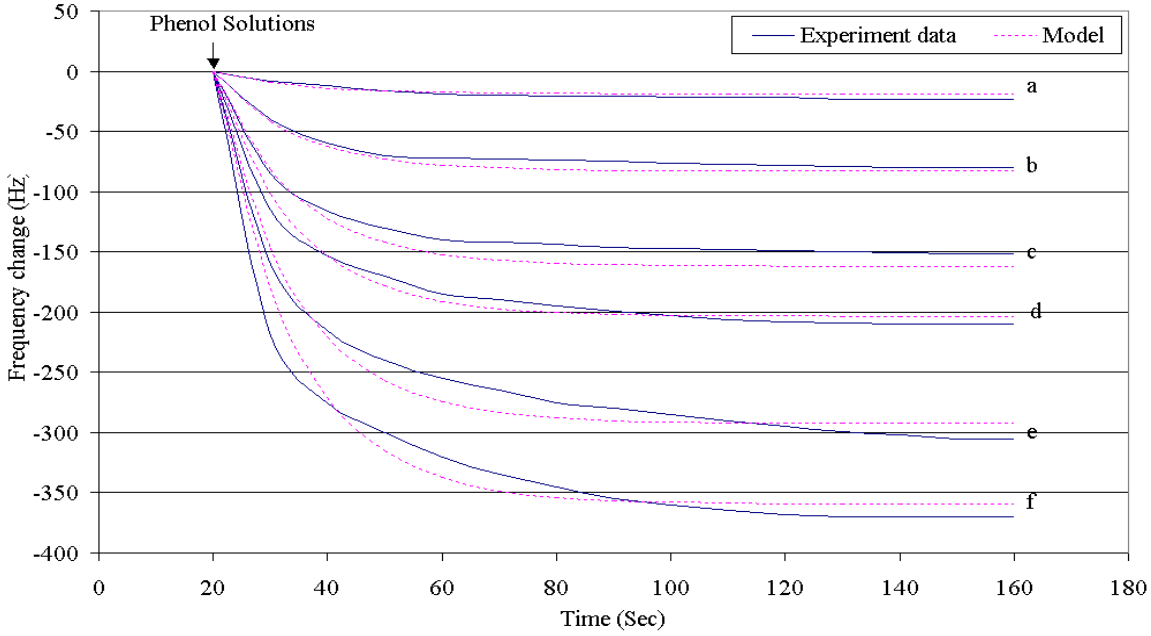

Figure 4.7. PMMA coated QCM to detect phenol case frequency response profile.

Frequency change of a PMMA modified quartz crystal electrode as a function of time in direct exposure to various concentrations of phenol solutions: (a) 0.52 ppm, (b) 2.3 ppm, (c) 4.5 ppm, (d) 5.65 ppm, (e) 8.12 ppm, (f) 9.98 ppm.

Figure 4.8 shows the predicted concentration and experiment data versus time in direct exposure to various concentrations of phenol solutions. The concentrations in the experiment are shown as straight lines with 10% error bars: (a) 0.52 ppm, (b) 2.3 ppm, (c) 4.5 ppm, (d) 5.65 ppm, (e) 8.12 ppm, (f) 9.98 ppm. In general, the predicted concentrations are within 10% error of the exact experiment value.

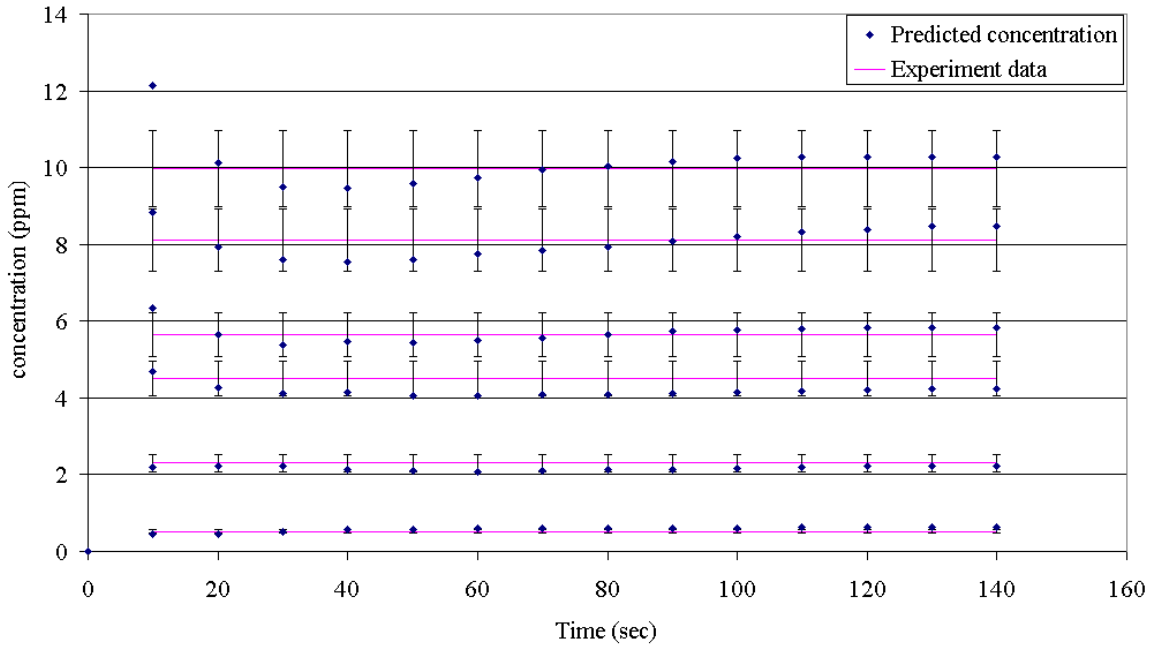

Figure 4.8. Prediction of concentration of PMMA coated QCM to detect phenol case.

4.5.4 BSA coated QCM to detect berberine hydrochloride

Mao (2002) studied the drug binding process to protein with quartz crystal microbalance device. The real time method was used to monitor the binding process of berberine hydrochloride to bovine serum albumin (BSA).

When a drug is introduced, it usually enters the blood stream and binds with plasma proteins to form a complex by covalent or noncovalent interaction (Kwong 1985,

Svensson 1986). This complex follows the blood cycling to the action site of the target organ, where the pharmacodynamic function of the drug is produced. Serum albumin is one of the most abundant and important proteins in the plasma. It can bind with small intrinsic and extrinsic compounds as storage and transfer protein. Therefore, it is crucial to investigate the drug binding process to serum albumin for better understanding of the metabolism, transportation, and pharmacodynamic properties of drug. The binding reaction of berberine to BSA immobilized on the sensor surface can be described by the equation

$$[\text{free binding site}]_s + [\text{berberine}]_l \leftrightarrow [\text{berberine-bound site}]_s$$

where $[\ ]_s$ and $[\ ]_l$ mean on the surface of the sensor and in the solution, respectively.

Many researchers have studied the ligand-protein binding using fluorescence, spectroscopy and chromatography method. QCM has advantage over other methods because QCM can obtain real time data about the binding process. Real time data are critical to understand the underlying chemical mechanisms involved in the process.

BSA was directly immobilized on the quartz crystal surface by means of adsorption. One face of the crystal was in contact with a BSA aqueous solution in phosphate-buffered saline (PBS). All experiments were carried out at the temperature 25±0.1 °C.

Figure 4.9 shows real time frequency response for the adsorption process of berberine hydrochloride to BSA at various berberine concentrations. Figure 4.10 demonstrates the predicted concentration and experiment data versus time in direct exposure to various concentrations of berberine solutions. The concentrations in the experiment are shown as straight lines with 10% error bars. The predicted concentrations

are generally within 10% error of the exact experiment value except in the early time of 60 μmol/L run. The above result further shows that the proposed method is an effective tool to predict solution concentration for bio-related adsorption or binding process.

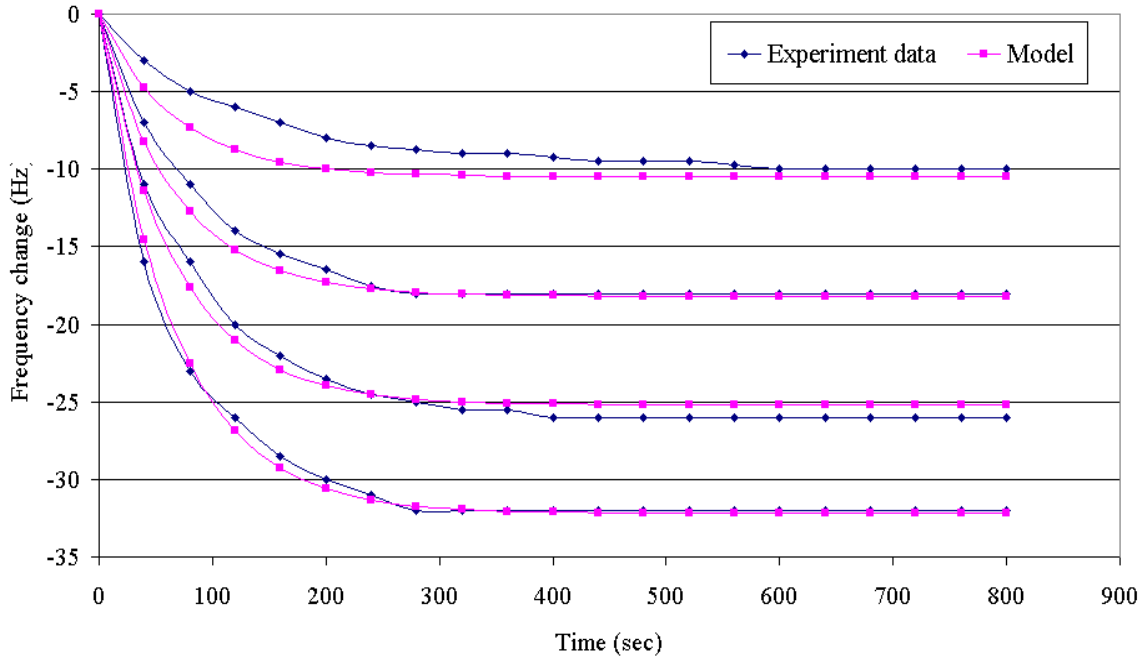

Figure 4.9. BSA coated QCM to detect berberine hydrochloride case frequency response profile.

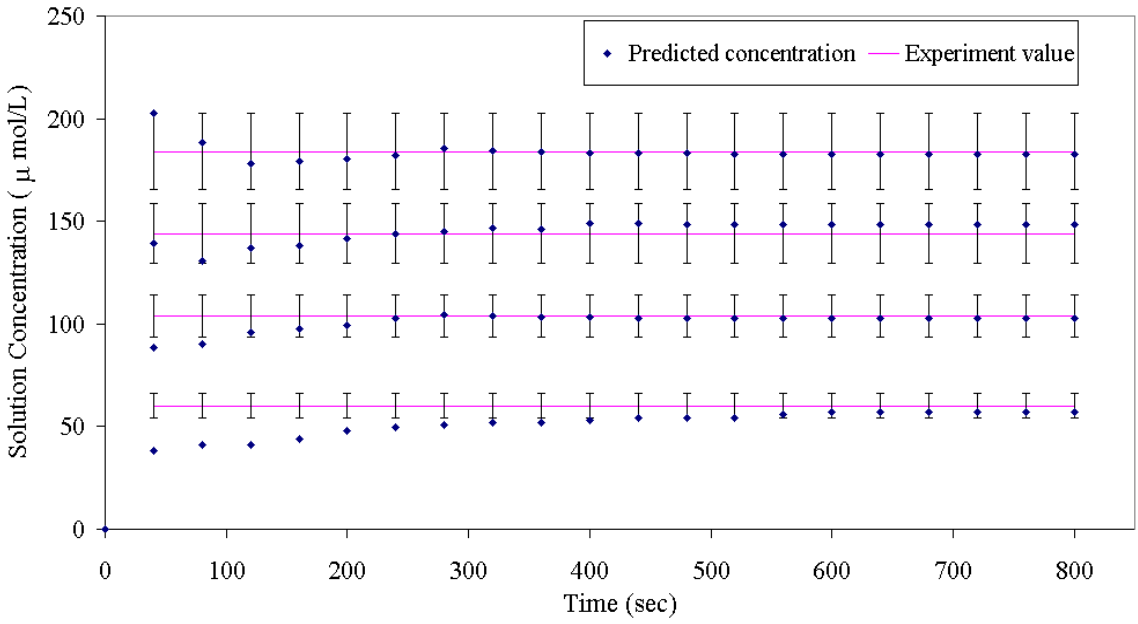

Figure 4.10. Prediction of concentration of BSA coated QCM to detect berberine hydrochloride case.

4.5.5 EDC coated QCM to detect Avidin

Caruso (1997) monitored the binding of Avidin to the pre-modified layer of QCM crystal surface, which had been attached to the QCM using a water-soluble carbodiimide hydrochloride (EDC). In this study, the QCM was exposed to an ethanolic 5 mM solution of 3,3′-dithiodipropionic acid for 20 min, followed by water rinsing. Five microliters of 100 mg/mL EDC solution was then placed on the surface, followed immediately by 5 μL of 100 mg/mL N-hydroxysuccinimide (NHS) solution. This solution was allowed to interact with the 3,3′-dithiodipropionic acid for 20 min in a 100% humidity environment to prevent solution evaporation. Then the surface was rinsed with water. This process is illustrated in Figure 4.11.

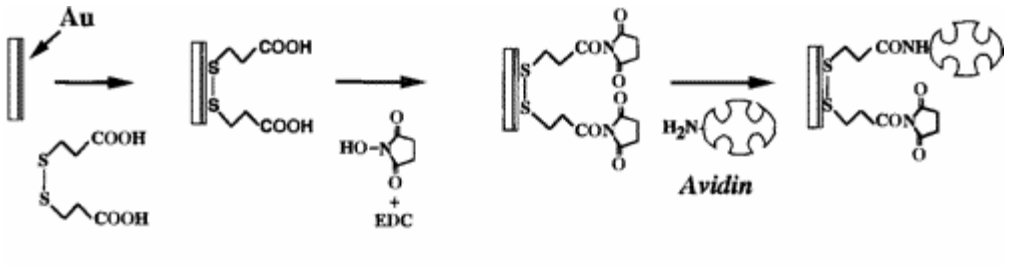

Figure 4.11. Immobilization of Avidin on QCM surface (Caruso, 1997).

Adsorption of avidin from a 0.2 mg / mL aqueous avidin solution onto QCM surface was monitored in situ, as shown in Figure 4.12.

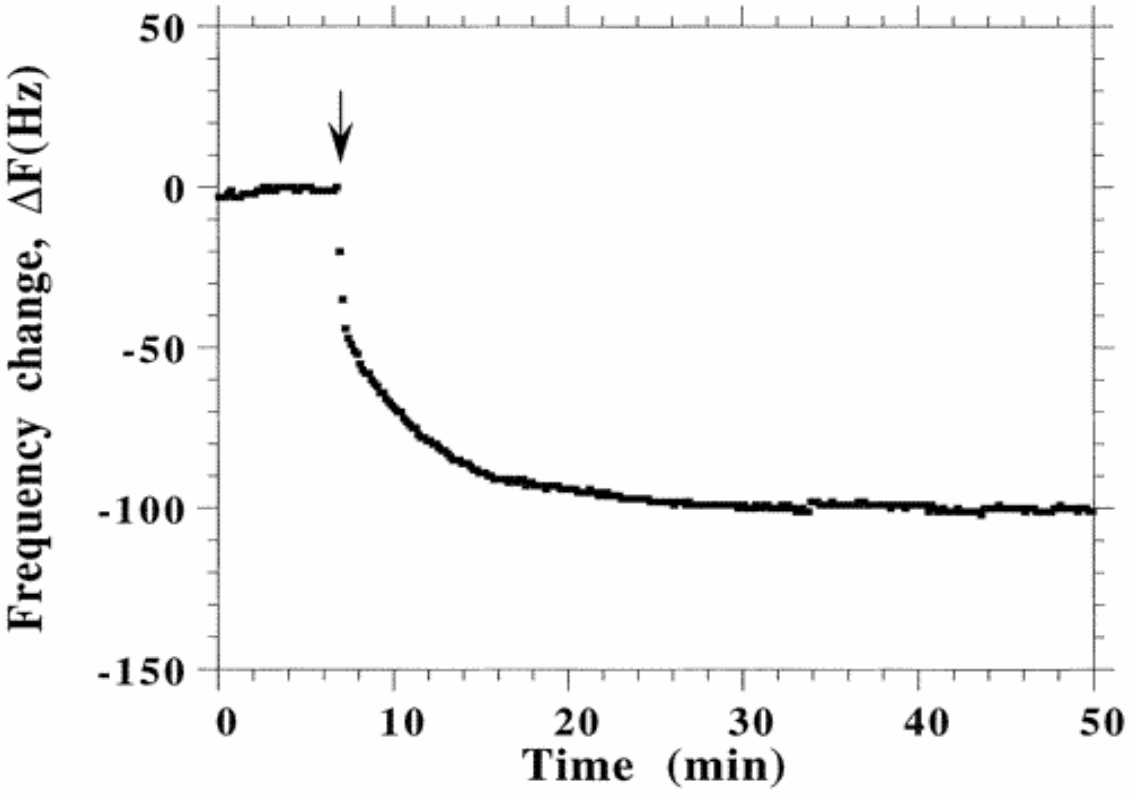

Figure 4.12. QCM frequency change as a function of time for the adsorption of avidin from a 0.2 mg mL^{-1} aqueous avidin solution onto QCM surface. The arrow indicates the time at which avidin was injected into the water solution. (Caruso, 1997)

Figure 4.13 shows the predicted concentration with time for the adsorption of avidin onto QCM surface. The concentration of avidin used in this experiment is 0.2 mg/mL. The predicted concentrations are within 10% error after 4 minutes introduction of avidin, although there is significant error in the initial period.

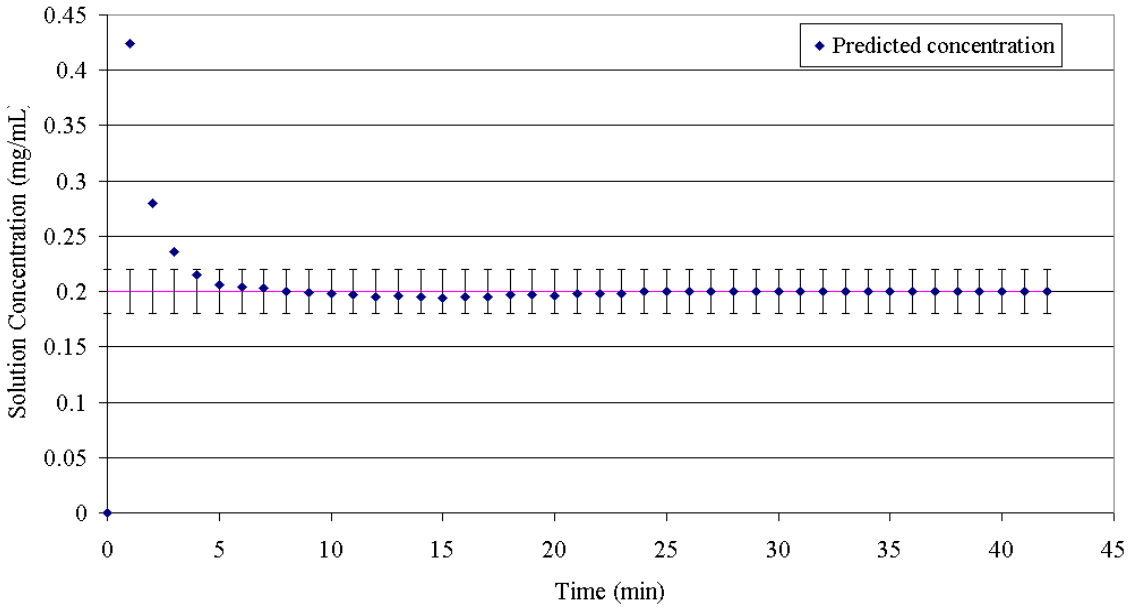

Figure 4.13. Prediction of concentration of EDC coated QCM to detect Avidin case.

CHAPTER 5

MATERIALS CHARACTERIZATION, PERFORMANCE, AND PATTERN RECOGNITION OF QCM IN ANALYTICAL CHEMISTRY

5.1 Introduction

In the previous two chapters, the mass and corresponding frequency changes were investigated for the application of concentration prediction. In this chapter, the materials characterization, pattern recognition, sensor array, and performance of QCM are examined.

QCM sensors are typically attached with a thin film to an acoustically active region of the device surface. The detection of chemical species can be based on changes in several physical characteristics of coating film in contact with the quartz crystal. Thus, the film must serve as a chemical-to-physical transducer, i.e., the properties of coating film change in response to the presence of the chemical species to be detected. Also, some of the intrinsic physical properties that can be used for detection include mass change, viscoelasticity, electrical conductivity, and viscosity. Generally, the increased mass accumulation on the film is relied upon for a sensor response. However, changes in other film parameters, including elastic and electrical properties can also contribute to the response. Since several mechanisms of physical properties can operate simultaneously to

affect a response, the variety of detection mechanism is a "double-edged sword" (Ballantine, 1997) that leads to both a broad range of detection and difficult interpretation of sensor response.

The ultimate performance of the sensor depends on both the device configuration and the nature and extent of coating-analyte interactions. In this chapter, performance criteria are discussed. Also, the use of sensor arrays containing multiple sensors, each bearing a coating with a different degree of selectivity for the analyte of interest, has been investigated.

5.2 Characterization of coating film materials

Many of the coating film materials have complex properties and performance quite different from those associated with simple ideal substances. Characterizing the properties of the coating film plays an important role in QCM application, since the chemical and physical properties of a film material determine its performance to meet the often stringent specifications required for a given application.

5.2.1 Viscoelastic properties

The viscoelastic properties of a polymer can be described as how the polymer deforms in response to an applied stress. Their properties are between those of a pure elastic solid (stress always directly proportional to strain in small deformations but independent of the rate of strain) and a pure viscous liquid (stress always directly proportional to the rate of strain but independent of strain itself). Rigid materials tend to display elastic behavior, and fluid display viscous behavior. In many polymers, a

combination of liquid-like and solid-like characteristics arises as a direct consequence of viscoelastic properties.

The mechanical properties of a viscoelastic material can be described by the complex shear modulus, $G = G' + jG''$. It can be thought of as the stiffness or rigidity of the polymer. The real part of G is called storage modulus and represents the energy storage and release during the periodic deformation associated with the oscillating stress. The imaginary part is called loss modulus and represents the energy losses due to dissipation, usually as heat.

Generally, the polymeric films applied to QCM devices are considered to be viscoelastic. Acoustic wave based QCM sensors obtain their chemical sensitivity from a coating film, which interacts with the surrounding environment. This interaction leads to a change in the acoustic properties at the interface between the quartz crystal and the coating. This phenomenon, in turn, yields a change in the frequency response of the sensor. Therefore, it has been shown in several publications (Lucklum 1999, Reed 1990, Grate 1992, Buttry 1992, Martin, 1994), that the frequency shift is related to the concentration of a specified analyte and viscoelastic property of coating film.

Behling (1997) showed that if the coating film does not act as thin rigid mass layers, viscoelasticity of the coating film can influence the sensor response compared to a acoustically thin rigid mass layer. 'Acoustically thin' means that the geometric film thickness must be reckoned in context with acoustic wavelength and material properties (Martin 1994). Films that are thick or soft behave as acoustically thick. The upper film portions lag behind the interface between film and quartz crystal, causing non-uniform displacement across the film thickness. Displacement varies not only in the plane of the

film but also across the film due to inertial lag of the upper film area. The viscoelastic properties of the coating film obtain more influence over the sensor response with increasing thickness (Lucklum 1999, Bandey 1997, Wolff 1997).

5.2.2 QCM response of viscoelastic polymer coating film

To better understand the QCM performance with coating film, it is necessary to study the mechanism of the viscoelastic influence on the electrical response of acoustic wave sensors.

The behavior of QCM sensor from the physical point of view includes two aspects: first, the transformation of the acoustic values into the electrical signal including the sensor interface electronics; and second, a specific feature of polymer material properties.

An equivalent circuit model can be derived to describe the electrical response. Figure 5.1 shows the modified equivalent circuit, which describes the propagation of acoustic waves in the sensor and the adjacent media. The model is modified form of the Butterworth-van-Dyke equivalent circuit. The equivalent treatments can be done with models regarding the one-dimensional problem of acoustic wave propagation. To illustrate the equivalence with the equivalent circuit, the following analogy relates the acoustic and electrical properties to each other (Behling, 1997):

mechanical tension T	electrical voltage U
particle velocity v	electrical current I
acoustic impedance $Z=T/v$	electrical impedance $Z=U/I$

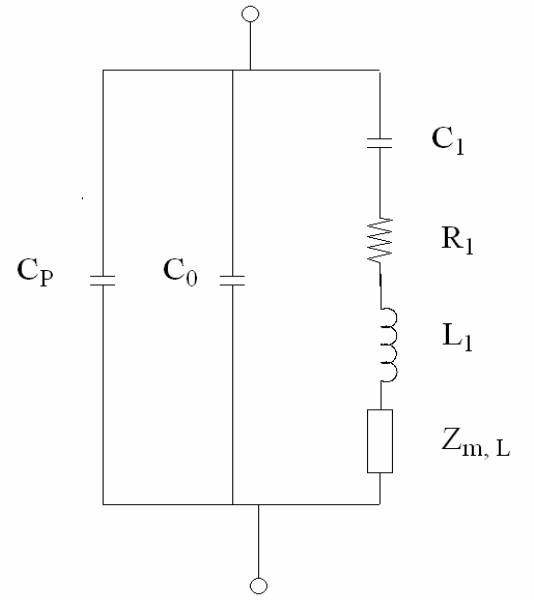

Figure 5.1. Equivalent circuit for a QCM under mass and liquid loading.

The acoustic load concept is a general description of acoustic wave propagation. The acoustic impedance acting at the surface of the quartz crystal is described by transmission line model.

The acoustic transmission line has two ports. The acoustic properties at one port of the transmission line are transformed to the other port introducing the acoustic properties within the transmission line. The piezoelectric quartz crystal is another transmission line, which also has an electrical port. The transmission line consists of distributed and lumped elements, which describe the geometric and material properties of the quartz crystal and its loading. Details of the transmission line model are published in several papers (Lucklum 1997, Behling 1997, Lucklum 2000). It is not the author's intention to introduce the model. Therefore, only the useful conclusions are mentioned here for the application of QCM with acoustic and/or viscoelastic loading.

The relation between acoustic load impedance Z_L, and electrical impedance, Z^e , can be described as

$$Z^e = \frac{j\chi_1(\omega,q) + \chi_2(\omega,q)Z_L}{1 - j\chi_3(\omega,q)Z_L} \qquad (5\text{-}1)$$

where, χ is a parameter dependent only on the angular frequency, ω, and quartz constants, q, which are not independent of acoustic load. This formula can be transformed into a parallel circuit of C_0 and the so-called parallel motional impedance Z_m. C_0 is the static capacitance formed by the electrodes on the quartz crystal, while Z_m represents the mechanical properties of the vibrating quartz crystal. The motional impedance Z_m itself consists of two additive parts

$$Z_m = Z_m^0 + Z_m^L \qquad (5\text{-}2)$$

where Z_m^0 is the motional impedance of the unperturbed quartz crystal, which only depends on the frequency and the quartz constants. Z_m^L is the motional load impedance. It reflects the surface acoustic impedance of the system, which is part of the motional part. An approximation can be applied near resonance of the unloaded quartz crystal and Z_m^0 can be rearranged in a simplified form that results in the well-known Butterworth-van-Dyke (BVD) equivalent circuit (Rosenbaum, 1988)

$$Z_m^0 = R + j\omega L + \frac{1}{j\omega C} + \frac{1}{j\omega(-C_0)} = R + j\omega L + \frac{1}{j\omega C'} \qquad (5\text{-}3)$$

where R, L, and C' are motional elements.

The shear modulus of a viscoelastic film like a polymer can be regarded as a complex quantity $G = G' + jG''$ where G' is the storage modulus representing the elastic properties and G'' is the loss modulus representing the viscous properties of the material.

If the quartz crystal is coated with a single film, which is stress free at its surface, the acoustic load impedance can be calculated. The acoustic load impedance depends on the coating thickness, the density, and the shear modulus as follow (Behling 1997, Lucklum 2000)

$$Z_L = j\sqrt{\rho_c G}\tan\left(\omega\sqrt{\frac{\rho_c}{G}}d_c\right) \tag{5-4}$$

where d_c is the coating thickness, ρ_c is the density, and G is shear modulus.

The acoustic load can be directly related to the frequency shift, Δf and resistance increase, ΔR using the following approximations (Tessier 1994)

$$\frac{\Delta f}{f} = -\frac{\mathrm{Im}(Z_L)}{\pi Z_{cq}} \tag{5-5}$$

$$\frac{\Delta R}{2\omega L} = \frac{\mathrm{Re}(Z_L)}{\pi Z_{cq}} \tag{5-6}$$

where $Z_{cq} = (\rho_q c_q)^{1/2}$ is the characteristic impedance of the quartz, ρ_q is the quartz crystal density, c_q is the piezoelectric stiffened elastic constant. f is the resonance frequency of the bare quartz. L is the motional inductance defined in Eq. (5-3).

A well-known linear relationship between deposited mass and frequency shift for thin rigid films can be obtained as a special case of Eq (5-4). If the tan function approximates to its argument, tan α = α, the shear modulus cancels out of the equation and the acoustic load impedance becomes

$$Z_L = j\omega\rho_c d_c \tag{5-7}$$

Then the film is called acoustically thin and this condition is fulfilled for small thickness of coating (small d_c) and rigid material (large G). These are the requirements formulated by Sauerbrey (1959) that lead directly to the linear relationship for thin rigid films.

$$\frac{\Delta f_{rigid}}{f} = -2 f \frac{\rho h}{Z_{cq}} \tag{5-8}$$

The deviation from the linear relationship becomes more obvious for soft polymer. Applying Eq. (5-4) and Eq. (5-5) results in (Tessier 1994, Behling 1997)

$$\frac{\Delta f}{f} = -\frac{\mathrm{Im}(j\sqrt{\rho_c G}\tan\left(\omega\sqrt{\frac{\rho_c}{G}}d_c\right))}{\pi Z_{cq}} \tag{5-9}$$

Figure 5.2 shows the dependence of the frequency shift on the shear parameters G' and G'', for a coating thickness of 1 μm.

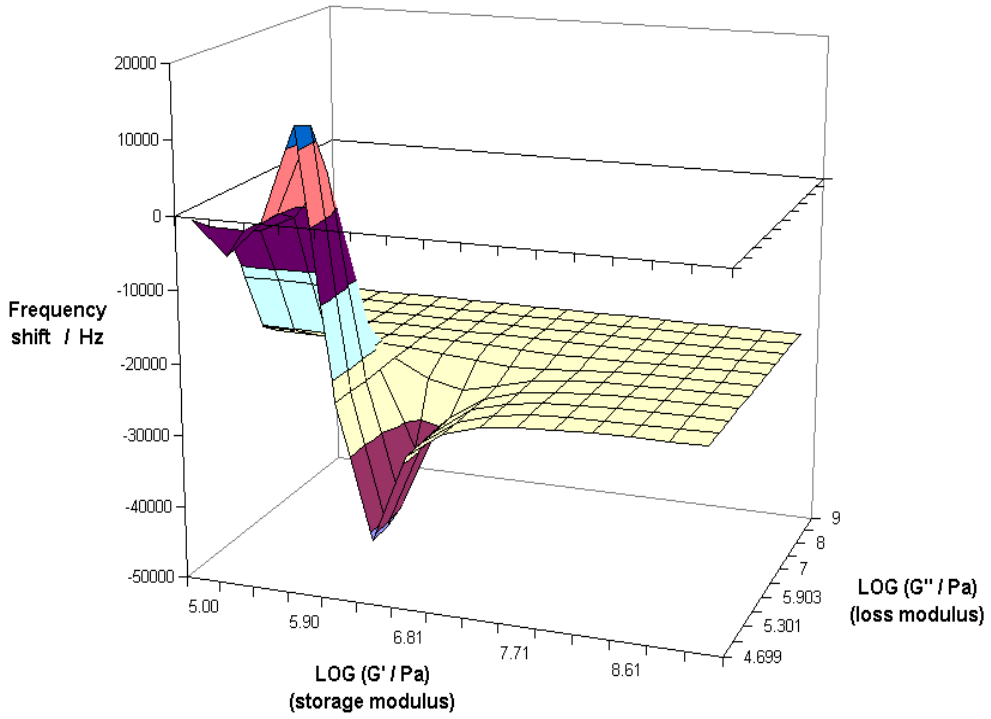

Figure 5.2. Dependence of the frequency shift on the viscoelasticity parameters for a polymer coating thickness of 1 μm.

The left area demonstrates that a soft polymer coating with low values of the shear moduli will lead to frequency changes compared with a thin rigid coating film. With higher storage modulus value, the right area represents glassy-like polymers, which has little influence on the frequency change. Meanwhile, calculation of Eq (5-9) shows that increasing the coating thickness will change the high sensitivity region to higher shear moduli area.

5.2.3 Temperature effects on polymeric films

Temperature can have a considerable influence on film viscosity, stiffness, and volume. At a certain high temperature, the polymer ceases to show glassy characteristics,

and becomes more rubbery. When the temperature increases, the thermal motion of individual chains and chain segments also increases and the polymer swells. When a film stays above the transition temperatures, thermally induced swelling will allow faster diffusion and a greater mass uptake of target. Thus, it is quite possible that as the target concentration increases, nonlinear calibration curves, frequency shift, and unusual attenuation may be observed. Thus, for many practical applications, thermostatting the sensor may be necessary.

5.2.4 Viscoelastic behavior of adsorption phenomena

Adsorption of solute into coating film can profoundly affect the viscoelastic behavior of the polymer. The polymer film may undergo significant changes in its viscoelastic properties. The magnitude of this effect depends on the nature of the solute/polymer interactions and on the amount of solute adsorbed. The adsorption of solute onto polymer film may include from simple dispersion to hydrogen-bonding and other specific interactions. This phenomenon is because the presence of adsorbed solute molecules between the polymer chains can act as a lubricant (Ballantine, 1997). This results in a decrease of glass transition temperature, T_g, of the coating polymer, which is dependent on the concentration of adsorbed solution (Kettle 1977, Deopura 1983). —This effect is called polymer plasticization. Consequently, mass changes of coating film associated with solute adsorption can result in QCM frequency change without significant attenuation of the wave. And polymer material modulus changes associated with the glass transition can result in both frequency and attenuation changes.

5.3 QCM response to viscous liquid loading

It has been shown that QCM sensors can be operated in contact with liquids (Nomura, 1980), which enable their use as solution-phase microbalances. Kanazawa and Gordon (1985) have shown that QCM operating in liquid are sensitive to the viscosity and density of the contacting solution. Viscous loading of the liquid medium to the quartz crystal surface results in both a decrease in the resonant frequency of the QCM and damping of the resonance. The sensitivity of QCM vibration frequency to liquid properties necessitates close control of liquid properties when trying to measure mass accumulation from solution (Bruckenstein, 1985).

Figure 5.3 depicts the cross-sectional geometry of the QCM loaded from above by a coating film and a contacting liquid. Displacement is maximum at the surfaces and varies sinusoidally across the thickness. When liquid contacts the vibration surface, the acoustic waves propagate in a direction perpendicular to the quartz crystal particle displacement, which is parallel to the disc surface in Figure 5.3. In some acoustic wave sensor applications, the liquid load is used to determine density and viscosity of the liquid. It has been shown from previous session that if the shear modulus is high, the material is rigid and vibrates synchronously with the quartz. Otherwise, the coating film is soft and the vibration of the upper film surface lags behind the quartz crystal surface. Here, the liquid (acoustic) loading is discussed from the measurement of the electrical admittance and frequency change of the quartz crystal.

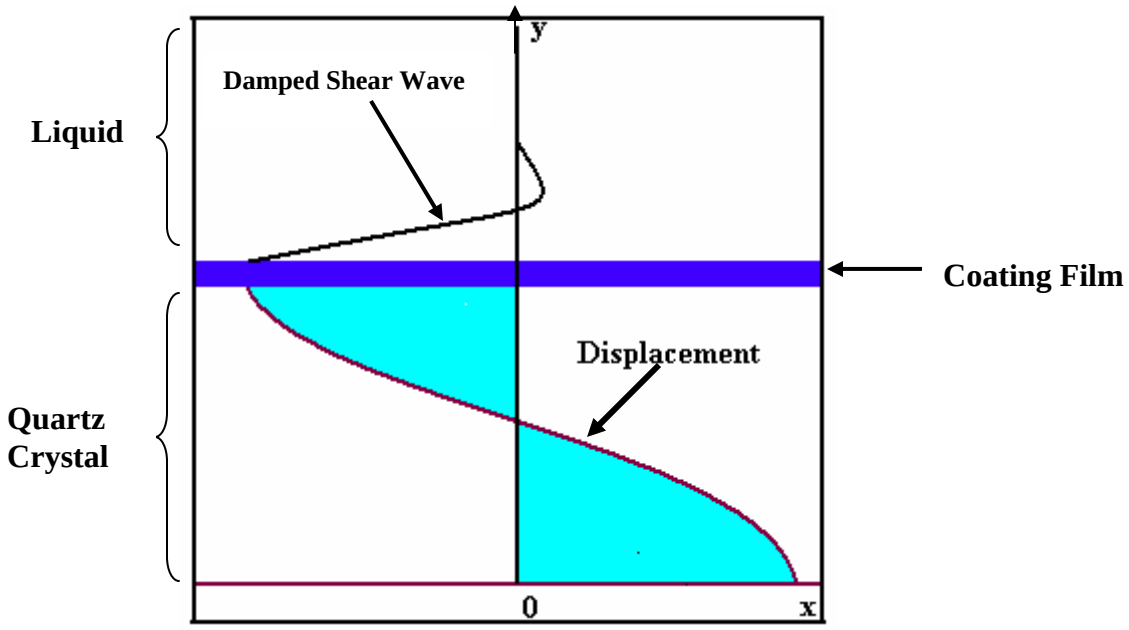

Figure 5.3. Cross-sectional view of a QCM simultaneously loaded on one side by a coating film and a contacting Newtonian liquid. QCM surface displacement causes synchronous motion of the coating film and contacting liquid.

The transmission line model of a quartz crystal with a single coating and a liquid load on top of this coating can be used to describe the acoustic and vibration properties. The acoustic impedance of the *i*th transmission line is given by (Lucklum 1997, Behling 1997)

$$Z_i = Z_{ci}\frac{Z_{i+1} + jZ_{ci}\tan[\omega(\rho_i / Z_{ci})h_i}{Z_{ci} + jZ_{i+1}\tan[\omega(\rho_i / Z_{ci})h_i} \qquad (5\text{-}10)$$

where $Z_{ci} = (\rho_i G_i)^{1/2}$ is the characteristic impedance of the ith layer and G is the shear modulus. Z_{ci} is a material parameter and is different from the acoustic impedance Z_i, which also depends on the relation between film thickness and wavelength of the acoustic

wave. The acoustic impedance, Z_{i+1} represents the acoustic loading acting on the top of the ith layer.

If the quartz crystal coated with thin and rigid film is in contact with liquid, the second term of the denominator in Eq (5-10) is small compared with Z_{ci}. The acoustic loading can be simplified to

$$Z_{rig,liq} = j\omega\rho h + (1+j)\sqrt{\frac{\omega\rho_l\eta_l}{2}} \qquad (5\text{-}11)$$

Combining Eq (5-11) and Eq (5-5) result in the frequency response of acoustic liquid loading.

$$\Delta f = -\frac{2f^2}{Z_{cq}}\left(\rho h + \sqrt{\frac{\rho_l\eta_l}{4\pi f}}\right) \qquad (5\text{-}12)$$

Eq (5-12) is same with Eq (3-1) which is derived by Martin (1991) using modified Butterworth-van-Dyke (BVD) equivalent circuit method.

Figure 5.4 shows negative frequency shift of QCM with mass and liquid viscous loading. From the figure, the negative frequency shift increases for high viscous liquid and high mass loading. For comparison, it is worth noting that when liquid viscosity η_l=0, Eq (5-12) is simplified to Sauerbrey's (1959) equation. It is obvious from Figure 5.4 that without considering viscosity, frequency shift is only related to mass loading from the coating film. The deviation in the frequency shift from Sauerbrey's equation is attributed to the acoustic loading of the contacting liquid. Generally, the acoustic liquid loading contribution to the frequency shift has the same direction as the mass loading. Therefore, it can be understood as amplification of the mass effect.

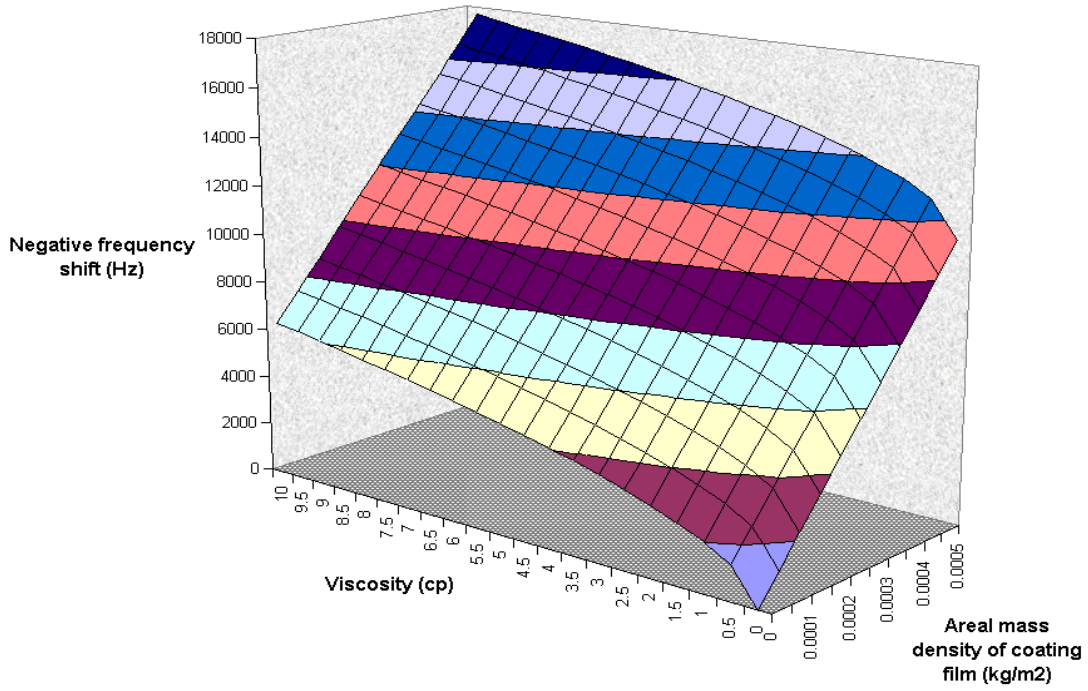

Figure 5.4. Three-dimensional plot of the negative frequency shift dependent on viscosity of contacting liquid and mass loading.

5.4 Coating film and coating-analyte interactions

The QCM response is a function of the nature of the interaction between the analyte and the sensor coating film. A fundamental understanding of the characteristic of interactions is necessary to interpret sensor responses and to design useful sensor coating for analytical application.

Measurements of small fractions of a single molecular monolayer have been reported (Ricco 1989, Sun 1991). For vapor phase detection, adsorption onto an uncoated sensor surface is usually inadequate for sensitive detection. Because of lack of specificity and low sensitivity established as two major drawbacks of uncoated surfaces, the important factor to the performance of adsorption based QCM sensor is the adsorbent coating materials. A coating film with higher surface area results in a larger number of

analyte molecules being adsorbed for a given ambient phase analyte concentration. Therefore, the consequences of coating film are enhanced sensitivity and limit of detection. For reactive and irreversible adsorptive coatings film, higher surface area can translate to higher capacity and thus greater dynamic range. Thus, many of the coating materials used in acoustic wave sensor are porous, with high internal surface areas (Ballantine, 1997).

For vapor phase concentrations, several mechanisms can be applied to achieve selectivity and sensitivity. Physical adsorption has the tendency to favor the deposition of low vapor pressure species, because such molecules have a large vaporization heat and are easier to remain condensed upon surfaces. A high degree of discrimination can be achieved by the use of size specific materials, having a tightly controlled pore size. When the pore size is just larger than the kinetic diameter of the target analyte, it completely excludes all larger species from the pores. Meanwhile, although molecules significantly smaller than the chosen analyte can fit into the pores, they have a smaller interaction energy due to the size mismatch. Additional physical discrimination can be obtained by controlling the polarity and hydrogen-bonding. The selectivity for analyte is dependent on the film structure and subsequent surface modification. In liquid-phase applications, metal ions can be detected via deposition on the sensor surface as a result of electrostatic adsorption (Yao, 1990).

Sensor coatings based on chemisorption are particularly attractive because of the selectivity afforded by analyte/coating chemical interaction. However, this mechanism usually results in irreversible response and limited lifetime. In real application, if the concentrations and adsorptions over a given detection interval are small compared to

coating capacity, and when a equilibrium state record is important, irreversibility is actually beneficial and a limited lifetime is unimportant. Table 5.1 lists some examples of coating and application.

Table 5.1. Some typical examples of coating and their application

Application	Coating film	Comments	Ref.
H_2	Pd		D'Amico, 1982
NH_3	Pt		D'Amico, 1987
H_2S	WO_3	high temperature condition	Vetelino, 1987
Ozone	polybutadiene	Irreversible chemical reaction	Fog, 1985
NO_2	MnO_2		Edmonds, 1988
SO_2	triethanolamine (TEA)	Reversible charge transfer	Bryant, 1983
Explosives	Carbowax 1000	Some interference from perfumes, solvents	Tomita, 1979

5.5 Biochemical interactions and coating film

The increasing development of QCM technology as biochemical and immunological investigation makes the bio application as a unique subset of QCM sensor. Biosensors are similar to chemosensors, but they use biological molecules as the selective coating. The high selectivity of this application is from the three-dimensional structure of biomolecules and the specific arrangement or location of functional groups. The coating film functional group located within the 3-D structure engage in selective interactions with molecules. A good analogy illustration is that of a lock-and-key

configuration. The geometry of the molecules acts to screen out substances that do not fit into the "lock".

The selectivity and sensitivity of active compounds can be achieved by employing antigen-antibody, enzyme-substrate, and other receptor protein pair. The receptor protein (e.g., enzyme, antibody) can be immobilized directly on the quartz crystal surface, or it can be suspended in a suitable film. Table 5.2 lists some examples of biochemically-based QCM coating and application.

Table 5.2. Examples of biochemical acoustic wave sensors

Application	Coating film	Comments	Ref.
Gluocose	Hexokinase		Lasky, 1989
Human IgG	Goat antihuman IgG	Siliane-immobilized antibody	Roederer, 1983
Human serum albumin	Anti-HAS		Muratsuga, 1993
Urea	Urease membrane		Kondoh, 1993

5.6 Coating materials and methods

In terms of coating materials, by far the majority employed in QCM sensor applications are polymer materials based on the analyte solubility. Other typical examples include metal and metal oxide film for small gas molecules such as hydrogen and nitrogen dioxide. Although cyclophane and C60 (buckminsterfullerene) have been reported, cage structures have not been exploited extensively for acoustic wave sensor.

The choices of coating methods are basically determined by the coating materials. The principle coating methods include Langmuir-Blodgett deposition, solvent evaporation, self-assembly, covalent attachment, physical entrapment (Thompson, 1997).

Langmuir-Blodgett deposition:

Langmuir-Blodgett film method achieves the deposition of molecular structures onto flat surface. It has been widely used for producing organized thin films on a variety of substrates. This class of materials is characterized by having distinct hydrophilic and hydrophobic regions referred to as the headgroup and tail, respectively. Basically, a small quantity of the material is dissolved in a nonpolar solvent (such as hexane or chloroform) and allowed to spread across a water surface. Solvent evaporation results in the formation of a monolayer in which the head-groups are immersed in the aqueous phase and the tails orientated away from it. Then, a moving barrier can be used to compress the film until a close-packed ordering of the molecules is obtained. However, over compression of the film results in collapse of the monolayer. Multilayer structures can be built up by successive passes through the interface. Mixed monolayers can also be employed, in which transfer of the desired material is aided by the addition of a second material which promotes film formation and deposition. The general classes of compounds capable of forming Langmuir-Blodgett films include fatty acids, phospholipids, porphyrins, phthalocyanines, dyes, polycyclic aromatic compounds, and various polymers.

Solvent evaporation:

Solvent evaporation techniques are commonly employed with polymeric materials, and include casting, dip coating, and spin coating. Typically, dilute solutions

of the coating are prepared in volatile solvents such as methanol, chloroform, acetone, or toluene and coated onto the device surface.

It is important to clean the sensor surface to ensure a good quality film in intimate contact with the substrate. The techniques of cleaning include sonicating in chloroform, washing with strong acid, or plasma cleaning. The solvent evaporation may give a variety of morphological features in the film. For spin coating, the required coating material is dissolved in a suitable solvent. Then the material is spun to spread the coating across the device surface. This technique depends on the viscosity of the coating solution and the volatility of the solvent.

Self-Assembly:

Self-assembled monolayers (SAMs) are one of many approaches to producing organized thin films of organic material on surfaces. Applications of SAMs include fatty acids, long-chain alkyl thiols and disulphides, and reactive silanes. SAMs form spontaneously at a solid-liquid interface through a combination of specific headgroup-surface reactions and chain-chain packing interactions. These monolayers can be used as the sensor coating itself, or as basis for subsequent surface reactions. Because of formation mechanism, self-assembled films have extensive application. They offer great prospects for the controlled and reproducible production of chemically and physically stable selective films.

Covalent attachment:

The main difference between covalent attachment and the SAMs is the resulting organization and packing density. Two of the most widely used materials are glycidoxypropyl-trimethoxysilane (GOPMS) and aminopropyltriethoxysilane (APTES).

Typical methods for coupling to a silica or metal oxide surface require the use of a 5-20% solution of freshly distilled silane in dry toluene. The resulting polymer film known functional groups can therefore be used either as the coating film itself, or as a means for further immobilizing other species.

Physical entrapment:

Physical entrapment is usually used in bio-detection to immobilize species such as antibodies and enzymes. Basically, the molecularly recognitive function group is trapped within a cross-linked medium which is permeable to the analyte of interest. This method is to simply mix the required compound with a suitable monomer and to initiate polymerization around it. The physical entrapment coating matrix is more robust and stable than covalent attachment. The principle advantage proposed for this method is that selective binding species, especially biomolecules, can be immobilized without the loss of binding activity. However, in practice, a disadvantage is the slow response time and recovery time. This phenomenon is because of the small pore size which reduces the rate of analyte diffusion in and out of the matrix.

Inorganic coatings:

Metal and metal oxide films, for example, tungsten trioxide, can be deposited using thermal evaporation or sputtering techniques. For example, a typical sol might be formed from tetraethoxy silane in a water-ethanol mixture with trace hydrochloric acid. Then, a continuous solvated cross-linked silicate network, the gel, is formed. The resulting solvent is evaporated under controlled conditions until the required viscosity is obtained. The film is then deposited by dip coating. The inorganic coating can also be prepared by entrapment in a thin membrane, which is similar to the physical entrapment.

5.7 QCM sensor performance criteria

In the development of a sensor for a given application, many factors influencing sensor performance must be considered. Among these are selectivity, sensitivity, reversibility, response time, stability, reliability, dynamic range, and environmental (e.g., temperature) effects. The performance criteria play a large role in the design and application of sensor system. Some of these concerns are important in the selection of the coating or in establishing optimal operation conditions.

5.7.1 Selectivity

Selectivity coefficients give an idea of the degree of discrimination between the analyte of interest and possible interferences. The smaller the coefficient, the better the sensor selectivity. For QCM sensor, this criterion is largely determined by the properties of the coating material. The ideal coating film can exhibit high sensitivity toward the target analyte, and low sensitivity toward other species.

The focus of much of the work in QCM application has been achieving selectivity through the use of different types of coating materials. This concept can be illustrated in Figure 5.5 and 5.6 for two quartz crystal sensor coated with fluoropolyol (FPOL), a polyfluorinated polymer of moderate-to-high polarity, and polyisobutylene (PIB), a non-polar hydrocarbon polymer. It is obvious that the FPOL coated sensor exhibits good response to butanone, but significantly less response to isooctane. Thus, FPOL exhibits greater selectivity toward the butanone. In contrast, the PIB coated sensor exhibits greater selectivity toward the isooctane. Comprehensive testing of selectivity for most

target analytes has been limited. The issue of selectivity continues to represent a most active area of research for QCM sensor (Ballantine, 1997).

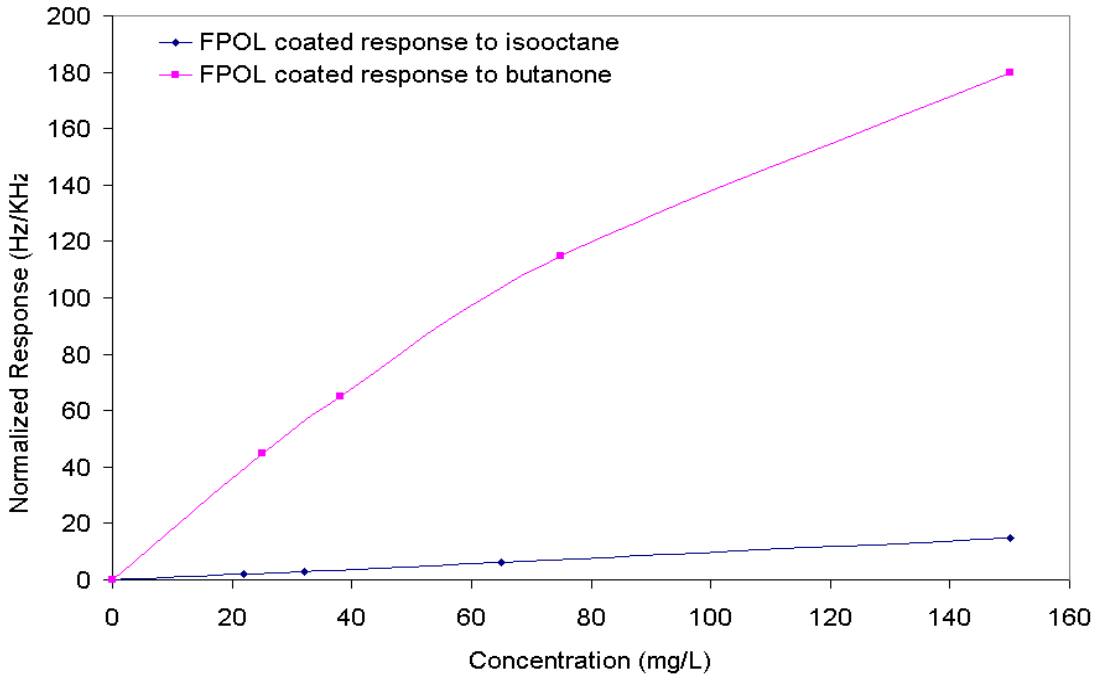

Figure 5.5. Comparison of selectivity of QCM sensor coated with FPOL to butanone and isooctane. Responses have been normalized by the amount of coating deposited (Rose-Pehrsson, 1988).

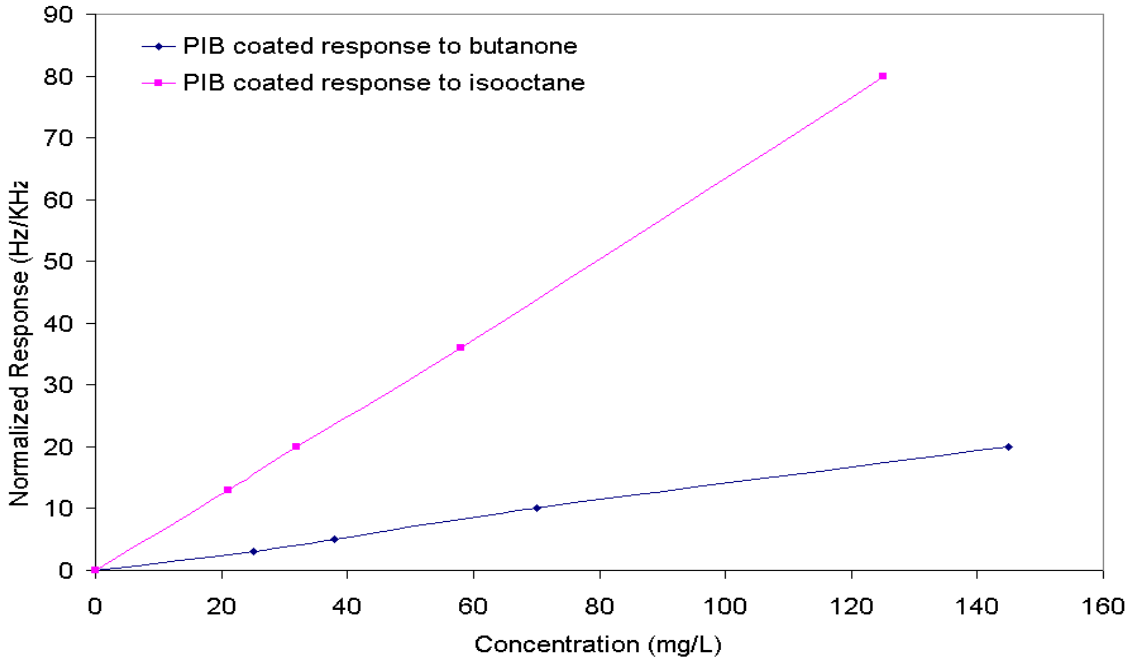

Figure 5.6. Comparison of selectivity of QCM sensor coated with PIB to butanone and isooctane. Responses have been normalized by the amount of coating deposited (Rose-Pehrsson, 1988).

5.7.2 Sensitivity

Sensitivity is defined as the change in sensor output signal obtained for an incremental change in the concentration or mass of the analyte. The value of sensitivity can be shown as the slope of the response-vs-concentration curve. The sensitivity should not be confused with detectability. Detectability, or the limit of detection (LOD), is the smallest amount or concentration of a substance required to produce a sensor response which can be differentiated from zero. For a QCM sensor, sensitivity to an analyte is determined by the amount of coating and the strength of the analyte-coating interaction. As discussed previously, coating-analyte interaction strength has paramount importance in determining overall sensitivity and detection limits. Sensitivity for a reversible QCM sensor typically has units of [frequency change]/[concentration change]. For an

irreversible sensor, the sensitivity is more appropriately defined in terms of [frequency change]/[integrated exposure].

5.7.3 Response time

The response time depends on the properties of the sensor coating, the sensor design, and the properties of analyte/coating interaction. For reactive coating, reactive rates can be affect by a few factors, such as reagent surface area, small particle sizes, and highly porous structure that can maximize the ratio of area and volume and yield a larger response in a shorter period of time. Thus, fast response requires that the coating is sufficiently thin and/or has high enough diffusivity that permeation is comparatively rapid.

Most of the QCM sensor coatings utilize polymer films. In this application, the rate of transport within the film affects response times. For polymeric films, those in the glassy or crystalline state generally exhibit lower diffusion rates than rubbery, amorphous polymers. If assume Fickian diffusion within the polymer film, the time to reach equilibrium is proportional to the square of film thickness. Therefore, thinner films respond more rapidly at the same sensitivity and limit of detection. Also, it is worth noting high temperature invariably improves the response time regardless of the rate limiting mechanism.

The response time should be within the appropriate range for the application for which it is intended. For example, if the sensor is designed for chemical weapon or toxic substance detection, ideally, the response time should be faster than the toxicological response. This will require an extremely fast response, probably within a few seconds.

Meanwhile, for water pollutes environmental monitoring, the application may have the flexibility to response from a few minutes to several days.

5.7.4 Dynamic range

Dynamic range is the concentration interval over which a sensor can provide a continuously changing response. Dynamic range is bounded by the limit of detection (LOD) at the low end and by saturation effects at the upper end, which is often termed the saturation limit.

Limit of detection depends on the inherent sensitivity of the device itself and the properties of the coating-analyte interaction of coating. Also, limit of detection depends on the system noise level. Generally, limit of detection is defined as signal-to-noise ratios of two or three, where the signal roughly exceeds the noise at statistical confidence levels of 95% or 99% respectively. Thus, the limit of detection can be expressed in units of concentration. For a given amount of coating, there is an upper end to the concentration that can be adsorbed before the capacity of the coating is reached. The saturation limit also depends on the coating properties. Any coating material that is significantly inelastic has an upper limit of thickness beyond which sensor detection becomes impractical due to excessive attenuation. Furthermore, the sorption of an analyte can result in significantly more attenuation, especially for viscoelastic polymer films, where sorption of an analyte plasticizes the coating film and increases the attenuation significantly. Thus, the dynamic range is determined by these properties. Analyte concentrations below the limit of detection give no detectable response, and concentrations above the saturation limit all give the same response.

5.7.5 Repeatability, reproducibility, and stability

Repeatability is the degree to which an individual coated sensor repeatability yields the same response for the same sample under the same operating conditions. Repeatability also depends on stability.

Repeatability should not be confused with reproducibility, which quantifies the extent to which two nominally identical coated sensors yield the same response to a given stimulus. The two nominally identical coated sensors means the sensors are fabricated according to the same set of procedures, but at different times and/or at different facilities. A high degree of reproducibility means that a single sensor from a large batch can be used to obtain same response and calibration data for all other sensors in that batch.

Stability is closely related to noise and drift, both in short term and long term. Noise describes positive and negative fluctuations about an unchanging average value. In contrast, drift describes a unidirectional change in signal that results in the average value changing monotonically with time.

Short-term drift is often associated with short-term changes in ambient parameters such as temperature, pressure, and relative humidity. In the short term, drift can exceed oscillator noise and dictates the limit of detection. Long-term aging of the sensor components generally results in drift and may also necessitate recalibration. The long-term baseline drift results from slow temperature variations or physicochemical properties change, including the coating, the device, and the electronic circuit. The long-term baseline drift can be compensated using baseline subtraction strategies.

Another method to compensate the baseline drift effect, both in long-term and in short-term, is performing a differential measurement using a dual device configuration for detection and reference respectively, provided the observed drifts are comparable for the two devices. However, if the environmentally induced aging of the coating is the main source of drift, the differential measurements are not very helpful, since the reference device in this configuration is not constantly exposed to the same ambient as the sensing device.

5.8 Sensor array and pattern recognition

The concept of using sensor arrays for chemical and biochemical analysis obtained widespread recognition in the 1980s and has continued vigorously in the 1990s. The advantages that sensor arrays offer over individual sensors are sensitivity to a wider range of analytes, simultaneous multicomponent analysis, improved selectivity, and the capability for analyte recognition rather than only detection. An analytical instrument with a sensor-array detector and data analysis can be applied to a host of different detection problems. The responses of each sensor are related to the interactions between analyte molecules and sensing materials. Understanding those interactions and designing arrays to take advantage of them have been two of the central themes in sensor array development, especially in the field of quartz crystal microbalance sensor arrays. The first investigations of acoustic wave sensor arrays were reported by researchers at the Naval Research Laboratory and at the University of Washington (Carey 1986c, 1987, 1988).

5.8.1 Sensor coating selection

The sensitivity and selectivity of a chemical sensor to an individual analyte can be improved by taking advantage of selective molecular interactions as discussed before. A great variety of materials have been employed as coating film on the surfaces of QCM devices. Materials applied range from polymer to structured materials such as bullfrog olfactory receptor proteins, dendrimers, and cavitands (Grate, 2000).

The most important issue with regard to coating film for individual sensors is the extent to which the applied materials enhance the sensitivity and selectivity of the sensor, while affording reversibility and reproducibility. In the context of arrays, the materials should maximize the collection of relevant chemical information for detecting and discriminating analytes. Ideally, each material should provide useful information that is not already supplied by other materials in the array, i.e., different materials will not simply be redundant, although real materials can not provide responses that are orthogonal to one another.

Figure 5.7, for example, graphically displays coating properties from the work of Carey (1986 a) in the form of a dendrogram. The data set was analyzed using hierarchical cluster analysis, and the results were displayed in a dendrogram that grouped coatings according to how similar their response patterns were across the data set. The dendrogram is a graphical representation of the similarity of coatings. Such clustering simplifies the process by identifying difference and similarities among coating films. When the coatings have been grouped, a single coating can be selected from each group based on practical considerations such as sensitivity, selectivity, or cost.

Each line in the dendrogram represents a numbered coating whose position indicates where that line merges with another coating or set of coatings. Lines that merge close to the left edge (similarity value = 1.00) demonstrate similar properties, whereas lines that merge far to the right (similarity value = 0.00) demonstrate very different properties. Therefore, coating films 11 and 13 are not similar and merge at a value of 0.30. On the other hand, coating films 3 and 6 are very similar, since their lines merge at a value of 0.85.

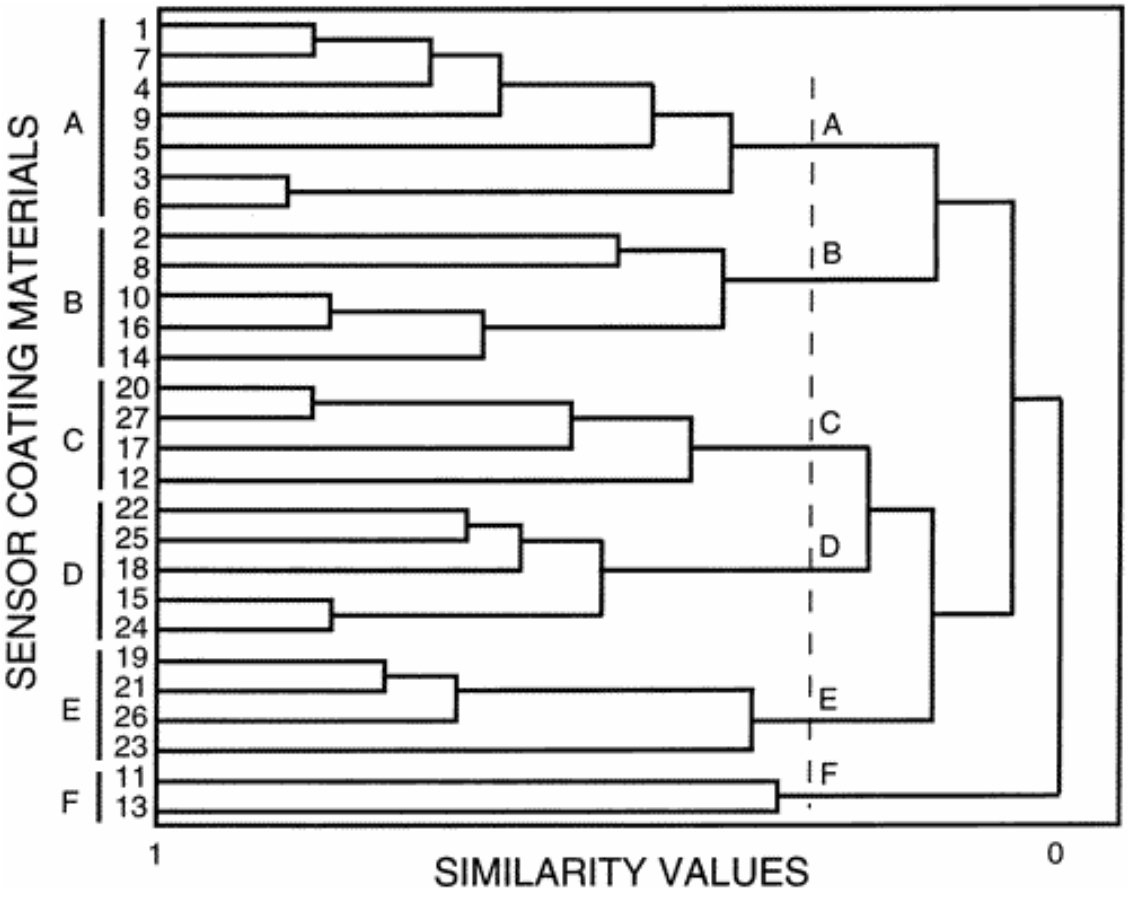

Figure 5.7. Dendrogram illustrating hierarchical cluster analysis results for 27 coating set based on similarities of response. Six dissimilar groups of films are indicated with letters. Adapted from Carey's (1986 a) study.

Coating materials can be selected on the basis of diversity in structures and properties. It is not surprising that coatings in a given cluster exhibit similarities in structure. Coating films with similar structure can display similarities in analyte-coating interactions. In Figure 5.7, Group A consists mostly of poly(butadiene)-based coating and Group B consists mostly of vinyl polymers. The individual coating films are listed, as Group A – E, in Table 5.3.

Table 5.3. Cluster classification of coatings for application in a QCM sensor array

Group	*ID*	*Compound*	*Comments*
A	1	Poly(butadieneacrylonitrile)	Generally exhibited highest sensitivity to test analytes, especially phosphonates (DMMP, DIMP) and octane
	7	Poly(butadiene) (- OH term, liquid)	
	4	Poly(butadiene) (- OH terminated)	
	9	Octadecylvinyl ether/maleic anhydride copolymer blend	
	5	Poly(vinyl stearate)	
	3	Poly(butadiene methacrylate)	
	6	Poly(1-butadiene)	
B	2	Poly(p-vinyl phenol)	Exhibit some selectivity to dimethyl phosphite, and esters
	8	Methyl vinyl ether	
	10	Polystyrene	
	16	Poly(vinyl butyral)	
	14	Poly(vinyl carbazole)	
C	20	Poly(ethylene glycol methyl ether)	Semi-selective response to water vapor
	27	Phenoxy resin	
	17	Poly(methyl methacrylate)	
	12	Poly(vinyl chloride)	
D	22	Poly(caprolactone)triol	Exhibit sensitivity/selectivity for DIMP; collodion exhibits greatest response to phosphonates of all coatings in the set of 27 coatings
	25	Abietic acid	
	18	Polyethylene	
	15	Collodion	
	24	Carnuba wax	
E	19	Ethyl cellulose	Some selectivity for dichloropentane vs. most test analytes
	21	Poly(caprolactone)	
	26	DC 11	
	23	Poly(caprolactone)trion 2X	
F	11	Poly vinyl isobutyl ether	Generally poor sensitivity/ selectivity for test analytes
	13	Poly-1-butene	

Based on data in Ballantine (1997) work. Numbers provide locations of coatings as shown in Figure 5.7.

5.8.2 Pattern recognition

The critical feature with regard to array-based sensing is that the sorption of an analyte varies with the structure and properties of the applied chemical coating. Therefore, an array of several devices with different coatings can produce several responses of different magnitude upon exposure to a particular analyte. The resultant combination of responses can have a unique fingerprint for each analyte. The response of each sensor in an array represents an axis in N-space. The sensor response can be thought of as encoding chemical information about the analytes in numerical form. Identification of the analyte is obtained by the appropriate pattern or fingerprint in the array data. Examples of the response patterns of a sensor array toward different analytes are given in Figure 5.8. The sensor array consists of six sensors in response to four different analytes. Judicious selection of coating leads to patterns for different analytes that can be distinguished from one another, providing a basis for selectivity and classification.

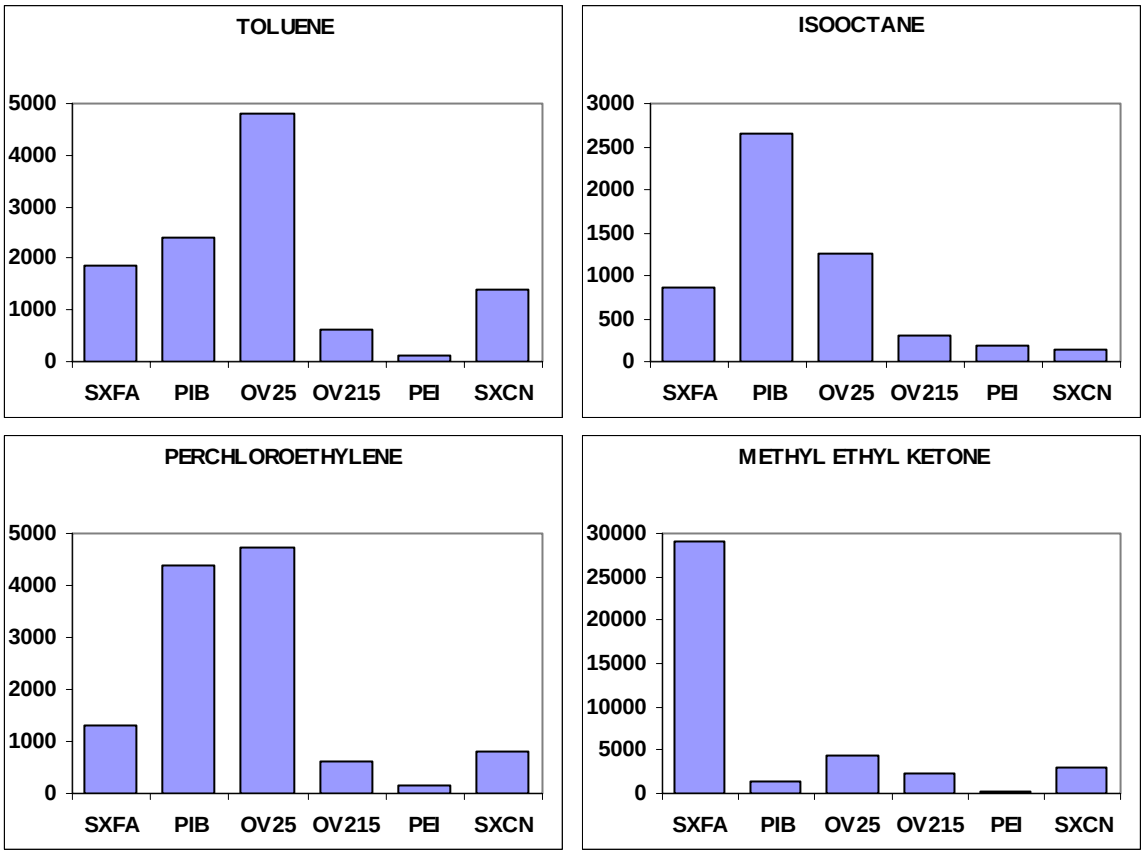

Figure 5.8. Bar graphs depicting different patterns to different analytes as detected by six sensor array. Figure adapted from Grate's (2000) work.

Several methods have been developed for obtaining correlations between the pattern of responses from an array of chemical sensors and the identity of the corresponding analyte (Massart 1988, Sharaf 1986, Carey 1986 b). One problem that must be addressed in the interpretation of sensor array data is the reliability of the final result. Each sensor response contains a certain degree of error. The propagation of error for a sensor array system is not trivial. This fact has important effect in terms of identification of an analyte in the presence of interferences. The efficacy of the sensor

array depends on the uniqueness of coating response. When colinearity of coating film increases, error in the final result is amplified and the detection limit is adversely affected.

CHAPTER 6

CONCLUSIONS

This dissertation examines theoretical issues in using quartz crystal microbalance (QCM) to rapidly predict analyte concentrations. Its specific contributions to the theory and applications of QCM sensor are delineated below.

In Chapter 1, starting from a rather general concept of sensor technology, we listed desirable characteristics for a sensor. An ideal sensor requires fast response time, good signal-to-noise ratio, high selectivity and sensitivity, and no hysteresis. Trends in sensor research showed a steady increase in the number of sensor papers. Significant increase of QCM papers from 1995 demonstrated a huge research effort, underlining the importance of current research, and the future application from it. It was also shown that the increasing interest in sensor technology is supported by the high demand of sensor either from military or non-military sources. We showed that QCM technology is an application of acoustic wave sensor. The QCM devices are conveniently small, relatively inexpensive, high sensitive and selectivity, and inherently capable of measuring a wide variety of different input quantities.

In Chapter 2 we presented the basic theories and principles of QCM sensor. QCM operates based on the converse piezoelectric effect. It was shown that the cut of

the quartz crystal has an effect on the resonance frequency. The standard AT-cut quartz crystal has nearly zero frequency drift with temperature around room temperature. This is a highly desirable feature for applications that requires the resonator to operate at, or near, room temperature. For the application of piezoelectric quartz resonators for quantitative mass measurements, it is necessary to develop a quantitative relationship between the relative shift of the resonant frequency and the added mass. Therefore, we introduced Sauerbrey equation as the starting point of the modeling work. Also, it is convenient to use an equivalent circuit model to describe the electrical and mechanical behavior of the quartz crystal vibration. It was also shown that, although QCM has traditionally been used exclusively in vacuum deposition systems, the applications of the QCM are constantly expanding.

In Chapter 3, a new ion exchange kinetics expression was derived based on a parabolic film concept. The ion exchanger film was assumed to be composed of an inner film with homogeneous concentration distribution and an outer film with parabolic concentration distribution. This expression provides a simple approximation for solid phase ion exchange processes. The simplified model was tested by the numerical model of ternary ion exchange system. All of the cases examined resulted in good agreement. The concepts and techniques of the new approach can be applied to solid phase ion exchange kinetics and complex concentration distribution systems.

The simplified ion exchange model was applied to QCM to predict liquid phase analyte concentration. Several practical cases from industry or literature were simulated. It was shown that the predicted results agree well with experiment data. In addition, simulations demonstrated that the model can predict liquid phase analyte concentration

with continuous step-changes. However, the study showed that frequency response at initially can be complex and may not be fully explained by qualitative arguments.

In Chapter 4 the adsorption process on the quartz crystal microbalance surface were discussed. An adsorption model was proposed to predict the real time analyte concentration. This rate model is based on Glueckauf's (1955) theory. The method proposed by Carslaw et al. (1959) was followed to derive the average adsorbed-phase concentration expressions. The rate model can also be obtained by assuming that the adsorbed phase concentration is parabolic distributed. Then, the adsorption model was applied to quartz crystal microbalance to predict the concentration of target analyte from QCM frequency response. This method is able to specifically predict the analyte concentration with continuous step changes. The predicted analyte concentrations were demonstrated for several literature data. The result showed that the model can generally predict the analyte concentration with less than 15% error, although, at the beginning phase, there may be significant error. This model also confirmed that quartz crystal microbalance system can quantify the components of a bio-adsorption.

In Chapter 5 we studied the characterization of coating film materials. Generally, the polymeric films applied to QCM devices are considered to be viscoelastic. It was shown that if the coating film does not act as thin rigid mass layers, viscoelasticity of the coating film can influence the sensor response compared to an acoustically thin rigid mass layer. We related the acoustic load of coating film and the frequency shift of QCM. We also showed the dependence of the frequency shift on the shear parameters G' (storage modulus) and G'' (loss modulus). We studied the QCM response to viscous liquid loading. It was shown that the deviation in the frequency shift from Sauerbrey's

equation is attributed to the acoustic loading of the contacting liquid. We also found that the acoustic liquid loading contribution to the frequency shift has the same direction as the mass loading. Finally, we explored the coating-analyte interactions, performance, and sensor array of QCM.

In conclusion, the study of quartz crystal microbalance sensor is still a young field. The success of integrated circuits has resulted in the availability of QCM sensors moving from the research laboratories into development, commercialization, and application. Due to its inherent ability to detect analytes in real time, the QCM sensor has found a wide range of applications. This work has demonstrated that the proposed method can rapidly predict analyte concentration with continuous step-changes, which will significantly strengthen the QCM sensor technology.

BIBLIOGRAPHY

Aberl, F., Wolf, H., Kößlinger, C., Drost, S., Woias, P., Koch, S. (1994). HIV serology using piezoelectric immunosensors, Sensors and Actuators B, 18-19, 271-275

Adamson, A. W. (1982). Physical Chemistry of Surface, 4th Ed., John Wiley & Sons: New York, Chapter XVI

Alder, J.F., McCallum, J.J. (1983), Piezoelectric crystals for mass and chemical measurements. A review, Analyst, 108, 1169

Aslanoglu, M., Houlton, A., Horrocks, B.R. (1998). Functionalized monolayer for nucleic acid immobilization on gold surfaces and metal complex binding studies, Analyst 123 (4), 753-754

Attili, B. S., Suleiman, A. A. (1996). A piezoelectric immunosensor for detection of cocaine. Microchem. J., 54 (2), 174-179

Bajpai, R. K., Gupta A. K., and Rao, M. G. (1974). Single particle studies of binary and ternary cation exchange kinetics, AIChE J., 20, 989

Ballantine, D.S. (1997). Acoustic wave sensors: theory, design, and physico-chemical applications, Academic Press, MA

Bandey, H.L., Hillman, A.R., Brown, M.J., Martin, S.J. (1997). Viscoelastic characterization of electroactive polymer films at the electrode/solution interface, Faraday Discuss, 107, 105-121

Bao, M.L., Barbieri, K., Burrini, D., Criffini, O., Pantani, F. (1996). Traces determination of phenols in water by solid phase extraction followed by pentafluorobenzoylation, Ann. Chim. 86, 343-356

Barnes, C. (1991). Development of quartz crystal oscillators for under-liquid sensing, Sens. Actuators, A29, 59

Beck, R., Pittermann, U., Weil, K. G. (1988). Impedance analysis of quartz oscillators, contacted on one side with a liquid, Berichte der Bunsen-Gesellschaft, 92, 1363

Behling, C., Lucklum, R., Hauptmann, P. (1997). Possibilities and limitations in quantitative determination of polymer shear parameters by TSM resonators, Sensors and Actuators A, 61, 260-266

Benes, E., Gröschl, M., Burger, W., Schmid, M. (1995). Sensors based on piezoelectric resonators, Sensors and Actuators A, 48, 1-21

Bottom, V.E. (1982). Introduction to quartz crystal unit deisgn, Van Nostrand Reinhold, New York

Bruckenstein, S., Shay, M. (1985). Experimental aspects of use of the quartz crystal microbalance in solution, Electrochimica Acta, 30, 1295-1300

Bryant, A., Poirier, M., Riley, D.L., Vetelino, J.F. (1983). Gas detection using surface acoustic wave delay lines, Sensors & Actuators, 4, 105

Bunde, R.L., Jarvi, E.J., Rosentreter, J.J. (1998). Piezoelectric quartz crystal biosensors, Talanta, 46, 1223-1236

Buttry, D.A., Ward, M.D. (1992). Measurement of interfacial processes at electrode surfaces with the electrochemical quartz crystal microbalance, Chem. Rev., 92, 1355

Carey, W.P., Beebe, K.R., Kowalski, B.R., Illman, D.L., Hirschfeld, T. (1986 a). Selection of adsorbates for chemical sensor arrays by pattern recognition, Anal. Chem., 58, 149-153

Carey, W.P., Beebe, K.R., Sanchez, E., Geladi, P., Kowalski, B.R. (1986 b). Chemometric analysis of multisensor arrays, Sensors and Actuators, 9, 223

Carey, W.P., Kowalski, B.R. (1986 c). Chemical piezoelectric sensor and sensor array characterization, Anal. Chem., 58, 3077-3084

Carey, W.P., Beebe, K.R., Kowalski, B.R. (1987). Multicomponent analysis using an array of piezoelectric crystal sensors, Anal. Chem., 59, 1529-1534

Carey, W.P., Kowalski, B.R. (1988). Monitoring a dryer operation using an array of piezoelectric crystals, Anal. Chem., 60, 541

Carslaw, H. S., and Jaeger, J. C. (1947). Conduction of Heat in Solids, Oxford University Press, Oxford

Carslaw, H. S., and Jaeger, J. C. (1959). Conduction of Heat in Solids, 2nd ed., Oxford University Press, Oxford

Carta, G. and Cincotti, A. (1998). Film model approximation for nonlinear adsorption and diffusion in spherical particles, Chemical Engineering Science, 53, 3483-3488

Carta, G., Lewus, R. K. (1999). Film model approximation for particle-diffusion-controlled multicomponent ion exchange, Separation Science and Technology 34(14), 2685-2697

Caruso, F., Rodda, E., Furlong, D.N. (1997). Quartz crystal microbalance study of DNA immobilization and hybridization for nucleic acid sensor development, Anal. Chem., 69, 2043-2049

Chung, Y., Lee, K. (2001). Separation and determination of eleven environmental protection agency priority phenols by reversed-phase capillary high-performance liquid chromatography with indirect fluorophotometric detection and solid phase extraction, Microchem. J., 69, 143-152

Crank, J. (1975). The mathematics of Diffusion, Clarendon Press: Oxford, Chaps. 2 and 4

Curie, P. and Curie, J. (1880). Développement, par pression, de l`électricité polaire dans les cristaux hémièdres à faces inclinées C. R. Acad. Sci., Paris, 91, 294

Deopura, B. L., Sengupta, A. K., Verma, A. (1983). Effect of moisture on physical properties of nylon, Polymer Communications, 24(9), 287-8

Diamond, D. (1998). Principles of chemical and biological sensors, Wiley, New York

Dolgonosov, A. M., Khamizov, R. K., Krachak, A. N., Prudkovsky, A. G. (1995). Macroscopic model for multispecies ion-exchange kinetics, React. Polym., 28, 13

D'Amico, A., Palma, A., Verona, E. (1982). Palladium-surface acoustic wave interaction for hydrogen detection, Appl. Phys. Lett., 41, 300

D'Amico, A., Petri, A., Veradi, P., Verona, E. (1987). NH_3 surface acoustic wave gas detector, Proc. IEEE Ultrason. Symp., 633

Edmonds, T.E., Hepher, M.J., West, T.S. (1988). Studies on the adsorption of nitrogen dioxide onto manganese dioxide-coated quartz piezoelectric crystals, Analy. Chim. Acta, 207, 67

Fawcett, N.C., Evans, J.A., Chen, L.C., Drozda, K.A., Flowers, N. (1988). A quartz crystal detector for DNA, Anal. Lett., 21, 1099-1110

Ferrari, M., Ferrari, V., Marioli, D., Taroni, A., Suman, M., Dalcanale, E. (2004). Cavitand-coated PZT resonant piezo-layer sensors: properties, structure, and comparison with QCM sensors at different temperatures under exposure to organic vapors, Sensors and Actuators B. 103, 240

Fog, H.M., Reitz, B. (1985). Piezoelectric crystal detector for the monitoring of ozone in working environments, Anal. Chem., 57, 2634

Fontana, F. (1777). Memorie Mat. Fis. Soc. Ital. Sci., 1, 679

Franzreb, M., Holl, W.H. and Sontheimer, H. (1993). Liquid-side mass transfer in multicomponent ion exchange: I. System without chemical reactions in the film. Reactive Polymer, 21, 117-133

Glueckauf, E. and Coates, J. E. (1947). Theory of chromatography. Part IV. The influence of incomplete equilibrium on the front boundary of chromatograms and on the effectiveness of separation, J. Chem. Soc., 1315

Glueckauf, E. (1949). Theory of chromatography. VII. The general theory of two solutes following non-linear isotherms, Discuss Fraday Soc., 7, 12

Glueckauf, E. (1955 a). Theory of chromatography. IX. Theoretical plate concept in column separations, Trans. Faraday Soc., 51, 34

Glueckauf, E. (1955 b). Theory of chromatography. X. Formulas for diffusion into spheres and their application to chromatography, Trans. Faraday Soc., 51, 1540

Grate, J.W., Klusty, M., McGill, R.A., Abraham, M.H., Whiting, G., Andonian-Haftvan, J. (1992). The predominant role of swelling-induced modulus changes of the sorbent phase in determining the responses of polymer-coated surface acoustic wave vapor sensors, Anal. Chem., 64, 610-624

Grate, J.W. (2000). Acoustic wave microsensor arrays for vapor sensing, Chem. Rev. 100, 2627-2648

Guilbault, G.G. (1983). Determination of formaldehyde with an enzyme-coated piezoelectric crystal detector, Anal. Chem., 55, 1682-1684

Guilbault, George G., Jordan, James M. (1988). Analytical uses of piezoelectric crystals: a review, Critical Reviews in Analytical Chemistry, 19(1), 1-28

Guilbault, G.G., Hock, B., Schmid, R. (1992). PZ immunosensor for atrazine in drinking water, Biosensors Bioelectron., 7, 411-419

Hauden, D., Michel, M., Bardeche, G., and Gagnepain, J.-J. (1977). Temperature effects on quartz-crystal surface-wave oscillators, Appl. Phys. Lett., 31, 315

Hauden, D., Jaillet, G., and Coquerel, R. (1981). Temperature sensor using SAW delay lines, IEEE Ultrason. Symp. (Proc.), 148

Heising, R.A. (1946). Quartz crystals for electrical circuits, their design and manufacture, Van Nostrand, New York

Helfferich, F. and Plesset, M. S. (1958). Ion-exchange kinetics. A nonlinear diffusion problem, J. Chem. Phys., 28, 418

Helfferich, F. (1962). Ion Exchange, McGraw-Hill, New York

Hiemenz, P. C. (1986). Principles of Colloid and Surface Chemistry, 2nd Ed., Marcel Dekker: New York

Hwang, Y-L. and Helfferich, F. (1987). Generalized model for multispecies ion-exchange kinetics including fast reversible reactions, React. Polym., 5, 237

Janata, J., and Bezegh, A. (1988). Chemical sensors, Anal. Chem., 60(12), 62R

Janata, J., Josowic, M., DeVaney, D.M. (1994). Chemical Sensors, Anal. Chem., 66, 207R

Jauregui, O., Galceran, M.T. (1997). Determination of phenols in water by on-line solid disk extraction and liquid chromatography with electrochemical detection, Anal. Chim. Acta, 340, 191-199

Kanazawa, K. K., Gordon, J. G. (1985). Frequency of a Quartz Microbalance in Contact with Liquid, Anal. Chem. 57, 1770

Kennard, E. H. (1938). Kinetic Theory of Gases, McGraw-Hill, New York

Kettle, G.J. (1977). Variation of the glass transition temperature of nylon-6 with changing water content, Polymer, 18(7), 742-3

King, W.H. Jr. (1964). Piezoelectric Sorption Detector, Anal. Chem., 36, 1735

Konash, P. L., Bastiaans, G. J. (1980). Piezoelectric crystals as detectors in liquid chromatography, Anal. Chem. 52, 1929

Kondoh, J., Matsui, Y., Shiokawa, S. (1993). New biosensor using shear horizontal surface acoustic wave device, Jpn. J. Appl. Phys. 32, 2376

Kwong, T.C. (1985). Free drug measurements: Methodology and clinical significance, Clin. Chem. Acta, 151, 193-216

Lai, C. C. and Tan, C. S. (1991). Approximate models for nonlinear adsorption in a packed bed adsorber, AIChE J, 37, 461-465

Lasky, S.J., Buttry, D.A. (1989). in Chemical sensors and microinstrumentation, ACS symposium series #403, Murray, R.W., Dessy, R.E., Heineman, W.R., Janata, J., Seitz, W.R., Eds. Amer. Chem. Soc., Washington D.C., pp. 208-221

Lasky, Steven J., Meyer, Howard R., and Buttry, Daniel A. (1990). Quartz microbalance studies of solvent and ion transport in thin polymer films in sensor applications of the QCM, Solid-State Sensor and Actuator Workshop, 4th Technical Digest, IEEE, 4-7 June 1990

LeVan, M. D., Carta, G. and Yon, C. M. (1997). Adsorption and ion exchange in Perry's Chemical Engineers Handbook, Section 16, ed. D. W. Green, 7th Ed. McGrawHill, New York

Liaw, C. H., Wang, J. S. P., Greenkorn, R. H. and Chao, K. C. (1979). Kinetics of fixed-bed adsorption: a new solution. AIChE J. 54, 376-381

Louter, A.J.H., Jones, P.A., Jorritsma, J.D., Vreuls, J.J., Brinkman, U.A.T. (1997). Automated derivatization for online solid phase extraction gas chromatography phenolic compounds. HRC-J. High Resolut. Chromatogr. 20, 363-368

Lu, C. and Czanderna, A.W. (Eds.). (1984). Applications of piezoelectric quartz crystal microbalances, Elsevier

Lucklum, R., Henning, B., Hauptmann, P., Schierbaum, K.D., Vaihinger, S. and Göpel, W. (1991). Quartz microbalance sensors for gas detection, Sensors and Actuators A, 25-27, 705-710

Lucklum, R., Behling, C., Cernosek, R.W., Martin, S.J. (1997). Determination of complex shear modulus with thickness shear mode resonators, J. Phys. D. Appl. Phys., 30, 346

Lucklum, R., Behling, C., Hauptmann, P. (1999). Role of mass accumulation and viscoleastic properties for the response of acoustic-wave-based chemical sensors, Anal. Chem., 71, 2488-2496

Lucklum, R., Hauptmann, P. (2000). The $\Delta f - \Delta R$ QCM technique: an approach to an advanced sensor signal interpretation, Electrochimica Acta, 45, 3907-3916

Mao, Y., Wei, W., Zhang, J., Zhang, S., Rao, X. (2001). Real-time monitoring of formaldehyde-induced DNA-lysozyme cross-linking with piezoelectric quartz crystal impedance analysis. Analyst, 126, 1568-1572

Mao, Y., Wei, W., He, D., Nie, L., Yao, S. (2002). Monitoring and kinetic parameter estimation for the binding process of berberine hydrochloride to bovine serum albumin with piezoelectric quartz crystal impedance analysis, Analytical Biochemistry, 306, 23-30

Martin, S., Granstaff, V. E., Frye, G. C. (1991). Characterization of a Quartz Crystal Microbalance with Simultaneous Mass and Liquid Loading, Anal. Chem., 63, 2272

Martin, S.J., Frye, G.C., Senturia, S.D. (1994). Dynamics and Response of Polymer-Coated Surface Acoustic Wave Devices: Effect of Viscoelastic Properties and Film Resonance, Anal. Chem., 66, 2201-2219

Masque, N., Pocurull, E., Marce, R.M., Borrull, F. (1998). Determination of 11 priority EPA phenolics at ng L^{-1} levels by online solid phase extraction and liquid chromatography with UV and electrochemical detection, Chromatographia, 47, 176-182

Massart, D.L., van Deginste, B.G.M., Demming, S.N., Michotte, Y., Kaufman, L. (1988). Chemometrics: A Textbook, Elsevier Science, Amsterdam, pp403-407

McCallum, J.J. (1989). Piezoelectric devices for mass and chemical measurements: an update. A review, Analyst, 114, 1173

McSkimin, H.J., Andreatch, P.Jr., and Thurston, R.N. (1965). Elastic Moduli of Quartz versus Hydrostatic Pressure at 25° and – 195.8°C, J. Appl. Phys., 36, 1624

Mirmohseni, A., Oladegaragoze, A. (2004). Application of the quartz crystal microbalance for determination of phenol in solution, Sensors and Actuators B, 98, 28-36

Mueller, R.M. and White, W. (1968). Direct Gravimetric Calibration of a Quartz Crystal Microbalance, Rev. Sci. Instrum., 39, 291

Mueller, R.M. and White, W. (1969). Areal Densities of Stress Producing Films Measured by Quartz Crystal Microbalance, Rev. Sci. Instrum., 40, 1646

Muller, R.S., Howe, R.T., Senturia, S.D., Smith, R.L., White, R.M. Eds. (1990). Microsensors, IEEE Press, New York

Muramatsu, H., Dicks, J.M., Tamiya, E., Karube, I. (1987). Piezoelectric crystal biosensor modified with protein A for determination of immunoglobulins, Anal. Chem., 59, 2760

Muramatsu, H., Tamiya, E., Suzuki, M., and Karube, I. (1988). Viscosity monitoring with a piezoelectric quartz crystal and its application to determination of endotoxin by gelation of limulus amebocyte lysate, Anal. Chem. Acta., 215, 91-98

Muramatsu, H., Suda, M., Ataka, T., Seki, A., Tamiya, E., and Karube, I. (1990). Piezoelectric resonator as a chemical and biochemical sensing device, Sensors and Actuators, A21-A23, 362-368

Muratsuga, M., Ohta, F., Miza, Y., Hosokawa, T., Kurosawa, S., Kamo, N., Ikeda, H. (1993). Quartz crystal microbalance for the detection of microgram quantities of human serum albumin: relationship between the frequency change and the mass of protein adsorbed, Anal. Chem., 65, 2933

Mussmann, P., Levsen, K., Radeck, W. (1994). Gas-chromatographic determination of phenols in aqueous samples after solid phase extraction, Fresenius J. Anal. Chem. 348, 654-659

Neumeister, J., Thum, R., and Lüder, E. (1990). A SAW Delay-line oscillator as a high-resolution temperature sensor, Sens. Actuators A, A21-23, 670

Niedermayer, R. (1966). Vacuum Microbalance Techniques, Vol. 5, Plenum, New York, NY. pp.217

Nomura, T. and Minemura A. (1980). Behavior of a piezoelectric quartz crystal in an aqueous solution and the application to the determination of minute amounts of cyanide, Nippon Kagaku Kaishi, 1621-1625

Nomura, T., Ando, M. (1985). Determination of iron (III) and aluminum in solution with a piezoelectric quartz crystal coated with silicone oil, Anal. Chim. Acta, 172, 353

Nomura, T., Okahara, T., Hasegawa, T. (1986). Determination of lead in solution with a piezoelectric quartz crystal coated with copper oleate, Anal. Chim. Acta, 182, 261

Nye, J.F. (1957). Physical properties of crystals, Clarendon Press, Oxford

O'Sullivan, C.K., and Guilbault, G.G. (1999). Commercial quartz crystal microbalances – theory and applications, Biosensors & Bioelectronics, 14, 663-670

Reed, C.E., Kanazawa, K.K., Kaufmann, J.H. (1990). Physical description of a viscoelastically loaded AT-cut quartz resonator, J. Appl. Phys., 68, 1993-2001

Ricco, A.J. Frye, G.C., Martin, S.J. (1989). Determination of BET surface areas of porous thin films using surface acoustic wave devices, Langmuir, 5, 273

Rice, R. G. (1982). Approximate solutions for batch, packed tube and radial flow adsorbers—comparison with experiment, Chem. Eng. Sci., 37, 83

Roederer, J.E., Bastiaans, G.J. (1983). Microgravimetric immunoassay with piezoelectric crystals, Anal. Chem., 55, 2333

Rosenbaum, J.F. (1988). Bulk acoustic wave theory and devices. Artech House, Boston

Rose-Pehrsson, S.L., Grate, J.W., Ballantine, D.S.Jr., Jurs, P.C. (1988). Detection of hazardous vapors including mixtures using pattern recognition analysis of responses from surface acoustic wave devices, Anal. Chem., 60, 2801

Ruthven, D.M. (1984). Principles of Adsorption and Adsorption Process. Wiley, New York

Sauerbrey, G.Z. (1959). Verwendung von Schwingquarzen zur Wägung dünner Schichten und zur Mikrowägung, Z. Phys, 155, 206.

Schröder, N. (1999). SENSOR MARKETS 2008: Worldwide Analyses and Forecasts for the Sensor Markets until 2008, Intechno Consulting, Basle, Switzerland

Scott, D. S. and Dullien, F. A. L. (1962). Diffusion of ideal gases in capillaries and porous solids, AIChE J. 8, 113

Sharaf, M.A., Illman, D.L., Kowalski, B.R. (1986). Chemometrics, Wiley, New York

Shons, A., Dorman, F., Najarian, J. (1972). The piezoelectric quartz immunosensor., J. Biomed. Mater. Res., 6, 565-570

Stockbridge, C.D. (1966). Vacuum Microbalance Techniques, Vol.5, Plenum, New York, NY. pp.193

Storri, S., Santoni, T., Mascini, M. (1998). A piezoelectric biosensor for DNA hybridization detection. Anal. Lett., 31 (11), 1795-1808

Sun, L., Thomas, R.C., Crooks, R.M., Ricco, A.J. (1991). Real-time analysis of chemical reactions occurring at a surface-confined organic monolayer, J. Am. Chem. Soc., 113, 8550

Svensson, C.K., Woodruff, M.N., Baxter, J.G., Lalka, D. (1986). Free drug concentration monitoring in clinical practice: Rationale and current status. Clin. Pharmacokinet., 11, 450-469

Tessier, L., Patat, F., Schmitt, N., Pourcelot, L., Frangin, Y., Guilloteau, D. (1993). AT-cut quartz crystal biosensor for blood assay, Proc. Ultrasonics Int. '93, Vienna, Austraia, pp. 627-630

Tessier, L., Patat, F., Schmitt, N., Lethiecq, M., Frangin, Y., and Guilloteau, D. (1994). Significance of mass and viscous loads discrimination for an AT-quartz blood group immunosensor, Sensors and Actuators B, 18-19, 698-703

Thompson, M. Dhaliwal, G.K., Arthur, C.L. and Calabrese, G.S. (1987). The potential of the bulk acoustic wave device as a liquid-phase immunosensor, IEEE Trans. Ultrasonics, Ferroelectr., Freq. Control, UFFC-34, 127-135

Thompson, M., Stone, D.C. (1997). Surface-launched acoustic wave sensors: chemical sensing and thin-film characterization, John Wiley & Sons, New York

Tien, C. (1994). Adsorption calculations and modeling. Butterworth-Heinemann, Newton, Maryland

Tomita, Y., Ho, M.H., Guilbault, G.G. (1979). Detection of explosives with a coated piezoelectric quartz crystal, Anal. Chem., 51, 1475

Vermeulen, T., Hiester, N. K. (1954). Ion-exchange and adsorption-column kinetics with uniform partial presaturation, Journal of Chemical Physics, 22, 96-101

Vetelino, J.F., Lade, R., Falconer, R.S. (1987). Hydrogen sulfide surface acoustic wave gas detector, IEEE Trans. Ultrason. Ferro. & Freq. Control, UFFC-34, 156

Viens, M. and Cheeke, J.D.N. (1990). Highly sensitive temperature sensor using SAW resonator oscillator, Sens. Actuators A, A24, 209

Vold, R. D., Vold, M. J. (1983). Colloid and Interface Chemistry, Addison-Wesley: Reading, MA

White, R.M., Voltmer, F.W. (1965). Direct piezoelectric coupling to surface elastic waves, Appl. Pys. Lett., 7, 314

Willoughby, S. L. (1998). Effective diffusion coefficients for toluene in calcium carbonate filled poly(vinyl acetate) from quartz crystal microbalance sorption experiments, Thesis, Oklahoma State University

Wissiack, R., Rosenberg, E., Grasserbauer, M. (2000). Comparison of different sorbent materials for on-line solid phase extraction with liquid chromatography-atmospheric pressure chemical ionization mass spectrometry of phenols, J. Chromatography A., 896, 159-170

Wolff, O., Seydel, E., Johannsmann, D. (1997). Viscoelastic properties of thin films studied with quartz crystal resonators, Faraday Discuss, 107, 91-104

Yang, R. T. (1987). Gas Separation by Adsorption Processes. Butterworths, Boston

Yao, S.H., Mo, Z.H., Nie, L.H., (1990). Titrations with piezoelectric monitoring : Part 2. Complexiметric titrations and precipitation titrations, Analy, Chim. Acta, 230, 51

Yao, C. and Tien, C. (1993). Approximations of uptake rate of spherical adsorbent pellets and their application to batch adsorption calculations. Chem. Engng. Sci., 48, 187-198

Zhang, R. and Ritter, J. A. (1997). New approximate model for nonlinear adsorption and diffusion in a single particle. Chem. Engng Sci., 52, 3161-3172

APPENDIX A

Average Adsorbed-phase Concentration Expressions

A quantitative representation of adsorbate uptake rate requires the solution of the appropriate intraparticle diffusion equation. Several earlier researchers (Vermeulen and Hiester 1954, Glueckauf and Coates 1947) have independently employed linear driving force expressions. In this work, the method proposed by Carslaw et al. (1959) is followed to derive the average adsorbed-phase concentration expressions. This method was originally derived for heat conduction in solids.

Considering a region $0 < x < l$; ends kept at zero temperature; initial temperature *f(x)*, the differential equation to be solved is

$$\frac{\partial v}{\partial t} = k \frac{\partial^2 v}{\partial x^2}, \; 0 < x < l , \tag{A-1}$$

with $v = 0$, when $x = 0$ and $x = l$, (A-2)

and $v = f(x)$, when $t = 0$. (A-3)

If the initial distribution were

$$v = A_n \sin \frac{n\pi x}{l} , \tag{A-4}$$

it is clear that $v = A_n \sin\frac{n\pi x}{l} e^{-kn^2\pi^2 t/l^2}$ would satisfy all the conditions (1), (2), (3) of the problem.

If we suppose that the initial temperature, *f(x)*, is a bounded function in the interval (0, *l*) so that it can be expanded in the sine series

$$\sum_{n=1}^{\infty} a_n \sin\frac{n\pi x}{l}, \tag{A-5}$$

where $a_n = \frac{2}{l}\int_0^l f(x')\sin\frac{n\pi x'}{l}\,dx'$ (A-6)

Now consider the function *v* defined by the infinite series

$$v = \sum_{n=1}^{\infty} a_n \sin\frac{n\pi x}{l} e^{-kn^2\pi^2 t/l^2} \tag{A-7}$$

This series, owing to the presence of the convergency factor $e^{-kn^2\pi^2 t/l^2}$, is uniformly convergent for any interval of *x*, when $t > 0$; and, regarded as a function of *t*, it is uniformly convergent when $t \geq t_0 > 0$, t_0 being any positive number.

Thus the function *v*, defined by the Eq. (A-7), is a continuous function of *x*, and a continuous function of *t*, in these intervals. It is easy to show that the series obtained by term-by-term differentiation of Eq. (A-7) with respect to *x* and *t* are also uniformly convergent in these intervals of *x* and *t* respectively. Thus they are equal to the differential coefficients of the function *v*. Hence

$$\frac{\partial v}{\partial t} = -\sum_{1}^{\infty} \frac{kn^2\pi^2}{l^2} a_n \sin\frac{n\pi x}{l} e^{-kn^2\pi^2 t/l^2} \tag{A-8}$$

and $$k\frac{\partial^2 v}{\partial x^2} = -\sum_{1}^{\infty} \frac{kn^2\pi^2}{l^2} a_n \sin\frac{n\pi x}{l} e^{-kn^2\pi^2 t/l^2} \tag{A-9}$$

when $t > 0$, and $0 < x < l$.

Thus the equation, $\frac{\partial v}{\partial t} = k\frac{\partial^2 v}{\partial x^2}$, is satisfied at all points of the rod, when $t > 0$, by the function defined by Eq. (A-7).

Since the series is uniformly convergent with respect to x in the interval $0 \le x \le l$, when $t>0$, it represents a continuous function of x in this interval.

Thus,

$\lim_{x\to 0} v$ = the value of the sum of the series when $x = 0$

= 0,

and $\lim_{x\to l} v$ = the value of the sum of the series when $x = l$

= 0.

Hence the boundary conditions are satisfied. With regard to the initial conditions, the sine series for $f(x)$,

$$a_1 \sin\frac{\pi x}{l} + a_2 \sin\frac{2\pi x}{l} + \cdots, \qquad \text{(A-10)}$$

converges, and its sum is $f(x)$ at every point between 0 and l where $f(x)$ is continuous, and $\frac{1}{2}\{f(x+0) + f(x-0)\}$ at all other points.

When v is defined by Eq. (A-7), we have

$$\lim_{t\to 0} v = \lim_{t\to 0} \sum_1^\infty a_n \sin\frac{n\pi x}{l} e^{-kn^2\pi^2 t/l^2} \qquad \text{(A-11)}$$

$= f(x)$ at a point of continuity

$= \frac{1}{2}\{f(x+0) + f(x-0)\}$ at all other points

Thus Carslaw et al. have shown that if the initial temperature is continuous from $x = 0$ to $x = l$, while $f(0) = f(l) = 0$, the function defined by Eq. (A-7) satisfies all the conditions of the problem.

If the initial temperature has discontinuities, the function defined by Eq. (A-7) at these points tends to $\frac{1}{2}\{f(x+0) + f(x-0)\}$ as $t \to 0$. If t is taken small enough, v will bridge the gap from $f(x-0)$ to $f(x+0)$, and the temperature curve will pass close the point $\frac{1}{2}\{f(x+0) + f(x-0)\}$.

The following special case of Eq. (A-7) is of interest:

(i) Constant initial temperature $f(x) = V_0$, constant.

$$v = \frac{4V_0}{\pi}\sum_{n=0}^{\infty}\frac{1}{(2n+1)}e^{-k(2n+1)^2\pi^2 t/l^2}\sin\frac{(2n+1)\pi x}{l} \qquad \text{(A-12)}$$

(ii) The slab $-l < x < l$ with constant initial temperature V_0.

Changing the origin in Eq. (A-12) to the mid-point of the slab and replacing $\frac{1}{2}l$ by l gives

$$v = \frac{4V_0}{\pi}\sum_{n=0}^{\infty}\frac{(-1)^n}{(2n+1)}e^{-k(2n+1)^2\pi^2 t/4l^2}\cos\frac{(2n+1)\pi x}{2l} \qquad \text{(A-13)}$$

$$= V_0 - V_0\sum_{n=0}^{\infty}(-1)^n\left\{erfc\frac{(2n+1)l - x}{2(kt)^{1/2}} + erfc\frac{(2n+1)l + x}{2(kt)^{1/2}}\right\} \qquad \text{(A-14)}$$

The average temperature v_{av} in the slab at time t is

$$v_{av} = \frac{8V_0}{\pi^2}\sum_{n=0}^{\infty}\frac{1}{(2n+1)^2}e^{-k(2n+1)^2\pi^2 t/4l^2} \qquad \text{(A-15)}$$

(iii) This method can be applied to diffusion into or out of a planar thin film or spherical particle. The fundamental case to consider is a planar thin film exposed to step changes in adsorbate concentration at the external surface of the film at time zero. If the diffusivity is constant, the diffusion equation simplifies to

$$\frac{\partial q}{\partial t} = D\frac{\partial^2 q}{\partial x^2}, \quad 0 < x < L, \tag{A-16}$$

where D is the diffusion constant in the adsorbent and $q(r,t)$ is the adsorbed phase concentration. The bulk adsorbate concentration is assumed to remain essentially constant following the step change. Therefore, the appropriate initial boundary conditions are

$$q(x,0) = q_0 \text{ when time t = 0} \tag{A-17}$$

$$q(L,t) = q_1 \text{ when time t > 0} \tag{A-18}$$

$$\left(\frac{\partial q}{\partial x}\right)_{x=0} = 0 \tag{A-19}$$

For planar thin film, the average internal concentration of the coating film, $\bar{q}$, can be defined by

$$\bar{q} = \frac{1}{L}\int_0^L q\,dx \tag{A-20}$$

Applying the solution given by Carslaw and Jaeger (1959), the average internal concentration can be described as

$$\bar{q} = q_0 + (q_1 - q_0)\left\{1 - \frac{8}{\pi^2}\sum_{n=0}^{\infty}\frac{1}{(2n+1)^2}\exp\left[-(2n+1)^2\pi^2 Dt/4L^2\right]\right\} \tag{A-21}$$

where D = diffusion constant in the coating film

L = coating film thickness

Using the same method, the average internal concentration of spherical particles can be described as (Glueckauf, 1955 b)

$$\bar{q} = q_0 + (q_1 - q_0)\left\{1 - \frac{6}{\pi^2}\sum_{n=0}^{\infty}\frac{1}{n^2}\exp\left[-n^2\pi^2 Dt / r^2\right]\right\} \qquad \text{(A-22)}$$

where D = diffusion constant in the particle

L = the particle radius

APPENDIX B

Error Propagation Analysis

To estimate the uncertainty in the calculated analyte concentration, q_i, a differential method must be utilized to find how uncertainties are propagated. The relative error in q_i means the actual error in calculating q_i divided by the calculated concentration, q_i. Recall that differentials represent infinitesimal changes, and that small finite changes are approximately equal to the infinitesimal changes. That is,

$$dq_i \approx \Delta q_i \tag{B-1}$$

as long as Δq_i is small. The analyte concentration can be related to frequency change,

$$q_i = \frac{EXP(k_2 t_n)\Delta f_n - \Delta f_{n-1}}{\left[EXP(k_2 t_n) - 1\right]k_1} \tag{B-2}$$

where Δf_{n-1} is the frequency change from baseline at the moment of exposure to (n-1)th analyte. Δf_n is the online frequency change from baseline after time t_n exposure to nth analyte. t_n is the time after exposure to nth analyte. To avoid confusing the frequency change with the infinitesimal concept, we use F_n and F_{n-1} to represent Δf_n and Δf_{n-1}, respectively. Thus, Eq. (B-2) changes to

$$q_i = \frac{EXP(k_2 t_n)F_n - F_{n-1}}{\left[EXP(k_2 t_n) - 1\right]k_1} \tag{B-3}$$

The experimental quantities used to calculate q_i were the measured frequency change F_n and F_{n-1}. Time was measured with an ultra stable clock, so the uncertainty in time is assumed to be zero. The estimated uncertainties of these quantities are as follows,

$$F_n = \pm 10 \text{ Hz} \tag{B-4}$$

$$F_{n-1} = \pm 10 \text{ Hz} \tag{B-5}$$

To find the uncertainty Δq_i, the differential dq_i is taken, then all the differentials are replaced by their appropriate small finite changes. In order to simplify the taking of the differential, the logarithm is taken first, then the differential. From Eq. (B-3),

$$\ln q_i = \ln\left(e^{k_2 t_n} F_n - F_{n-1}\right) - \ln\left(e^{k_2 t_n} - 1\right) - \ln k_1 \tag{B-6}$$

Then, the differential of this expression is

$$\frac{dq_i}{q_i} = \frac{d(e^{k_2 t_n} F_n - F_{n-1})}{e^{k_2 t_n} F_n - F_{n-1}} - \frac{d(e^{k_2 t_n} - 1)}{e^{k_2 t_n} - 1} - \frac{dk_1}{k_1} \tag{B-7}$$

Recall that the term $-\dfrac{d(e^{k_2 t_n} - 1)}{e^{k_2 t_n} - 1} - \dfrac{dk_1}{k_1}$ is zero because $e^{k_2 t_n} - 1$ and k_1 are constant, then

$$\frac{dq_i}{q_i} = \frac{d(e^{k_2 t_n} F_n - F_{n-1})}{e^{k_2 t_n} F_n - F_{n-1}} \tag{B-8}$$

The differential term, $d(e^{k_2 t_n} F_n - F_{n-1})$, is

$$d(e^{k_2 t_n} F_n - F_{n-1}) = \frac{\partial(e^{k_2 t_n} F_n - F_{n-1})}{\partial F_n} dF_n + \frac{\partial(e^{k_2 t_n} F_n - F_{n-1})}{\partial F_{n-1}} dF_{n-1}$$

$$= e^{k_2 t_n} dF_n - dF_{n-1} \tag{B-9}$$

The maximum value of relative error in q_i is then

$$\text{Largest } \left|\frac{dq_i}{q_i}\right| = \left|\frac{e^{k_2 t_n} dF_n}{e^{k_2 t_n} F_n - F_{n-1}}\right| + \left|\frac{dF_{n-1}}{e^{k_2 t_n} F_n - F_{n-1}}\right| \tag{B-10}$$

Sample calculation

With the errors in QCM frequency changes as given above, the relative error in analyte concentration was calculated for a sample run based on the data from Brims Ness Corporation.

$$k_2 = 3.3333 \times 10^{-4}\ \text{s}^{-1} \tag{B-11}$$

$$t_n = 762.70\ \text{s} \tag{B-12}$$

$$F_n = 7613.1\ \text{Hz} \tag{B-13}$$

$$F_{n\text{-}1} = 3466.4\ \text{Hz} \tag{B-14}$$

Thus, the error propagation due to experimental uncertainty can be calculated using Eq. (B-10).

$$\text{Largest}\left|\frac{dq_i}{q_i}\right| = \left|\frac{e^{k_2 t_n} dF_n}{e^{k_2 t_n} F_n - F_{n-1}}\right| + \left|\frac{dF_{n-1}}{e^{k_2 t_n} F_n - F_{n-1}}\right|$$

$$= \left|\frac{e^{3.3333\times10^{-4}\times762.70} \times 10}{e^{3.3333\times10^{-4}\times762.70} \times 7613.1 - 3466.4}\right| + \left|\frac{10}{e^{3.3333\times10^{-4}\times762.70} \times 7613.1 - 3466.4}\right|$$

$$= 0.3605\% \tag{B-15}$$

The small error from Eq. (B-15) is at least partially because of the large frequency change. Another example from Caruso's (1997) study with smaller frequency change is shown as follows:

$$k_2 = 0.300\ \text{min}^{-1} \tag{B-16}$$

$$t_n = 5.00\ \text{mins} \tag{B-17}$$

$$F_n = -80.0\ \text{Hz} \tag{B-18}$$

$$F_{n\text{-}1} = 0.00\ \text{Hz} \tag{B-19}$$

Thus,

$$\text{Largest } \left|\frac{dq_i}{q_i}\right| = \left|\frac{e^{k_2 t_n} dF_n}{e^{k_2 t_n} F_n - F_{n-1}}\right| + \left|\frac{dF_{n-1}}{e^{k_2 t_n} F_n - F_{n-1}}\right|$$

$$= \left|\frac{e^{0.300\times 5.00} \times 10}{e^{0.300\times 5.00} \times (-80.0) - 0.00}\right| + \left|\frac{10}{e^{0.300\times 5.00} \times (-80.0) - 0.00}\right|$$

$$= 15.3\,\% \qquad \text{(B-20)}$$

APPENDIX C

Calibration

The methodology for the calibration of QCM model considering uncertainties is comprised of three basic steps: data collection, parameter estimation and assessment of the calibration.

Data collection

The purpose of data collection effort is to provide sufficient and reliable field test to be used as input data in the estimation of model parameters. Before being accepted as a valid profile and used to estimate model parameter, the collected data needs to be filtered to identify and reject gross errors. This screening process determines if the measurements satisfy the physical constrains of the system. For QCM application, it is necessary to pay special attention to repeatability, stability, and frequency drift.

Parameter estimation

This process aims to determine the best values for the parameters such that model outputs agree with field measurements. Parameters that must be calibrated are k_1 and k_2, shown as Eq. (C-1).

$$q_i = \frac{EXP(k_2 t_n)\Delta f_n - \Delta f_{n-1}}{\left[EXP(k_2 t_n) - 1\right]k_1} \qquad \text{(C-1)}$$

where Δf_{n-1} is the frequency change from baseline at the moment of exposure to (n-1)th analyte. Δf_n is the online frequency change from baseline after time t_n exposure to nth analyte. t_n is the time after exposure to nth analyte.

The parameters, k_1 and k_2, describe the equilibrium and rate caused by the adsorption on the QCM coating film. It should be pointed out that at this stage empirical determination of these parameters is necessary. This is because the frequency response is not stable and the parameters should match the initial curve instead of the entire curve, if not both. Parameter k_1 is determined by the equilibrium curve over an infinite time interval. When time interval is infinite, Eq. (C-1) becomes

$$q_i = \frac{\Delta f_n}{k_1} \tag{C-2}$$

hence,

$$k_1 = \frac{\Delta f_n}{q_i} \tag{C-3}$$

Parameter k_2 describes the adsorption rate on the QCM coating film. The value of parameters, k_1 and k_2, are determined experimentally. The materials and procedures listed below is an example of industrial applications. The materials and procedures used will be extended by the applications and requirements.

Materials:

1. NaCl and $NaNO_3$ salts.
2. DI water.
3. QCM sensor.
4. Analytical balance capable of measuring to nearest 0.0001 gram.
5. Large beakers, size depends on flow volume of QCM.

Procedures:

1. Gather the materials needed for the calibration test.
2. Prepare a 0.400 g/L NaCl and a 0.200 g/L $NaNO_3$ solutions.
3. Put the ion exchanger on the crystal in the chloride form by flowing 0.400 g/L NaCl in DI solution and allow it to flow for at least half hour, but not stopping until the crystal has a flat, baseline frequency.
4. With as little disturbance as possible to the system as possible, stop adding NaCl solution and allow 0.200 g/L $NaNO_3$ solution to flow through the sensor until a baseline value is achieved.
5. Record all frequency change and time onto Excel spreadsheets and graph frequency change versus time. (Figure C.1 shows an example of frequency change curves after the adding of $NaNO_3$ solution.)
6. Parameter k_1 is determined by the equilibrium frequency change. At equilibrium, k_1 can be obtained using Eq. (C-3).

$$k_1 = \frac{\Delta f_n}{q_i} = \frac{-100Hz}{0.200g/L} = -500Hz \cdot L/g \qquad \text{(C-4)}$$

7. The typical range of k_2 is from 0.1 to 3 min^{-1}. Thus, make an initial guess $k_2 = 1$. The trial frequency change can be calculated for arbitrary time using a transformed expression of Eq. (C-1).

$$\Delta f_n = \frac{q_i\left(e^{k_2 t_n} - 1\right)k_1 + \Delta f_{n-1}}{e^{k_2 t_n}} = \frac{0.200\left(e^{1t_n} - 1\right)(-500) + 0}{e^{1t_n}} \qquad \text{(C-5)}$$

Record the trial frequency change and time onto Excel spreadsheets and graph frequency change versus time. Compare the initial slope of the trial frequency change curve with the experimental data. Adjust the value of k_2

to make the calibration curve match the initial slope of the experimental data. Figure C.2 shows the calibration curves of the initial trial and after the adjustment of the value of k_2.

8. After the calibration, the values of parameters, k_1 and k_2, can be obtained as follows

k_1 = -500 Hz L/g from Eq. (C-4)

k_2 = 0.25 min^{-1} by trial and adjustment.

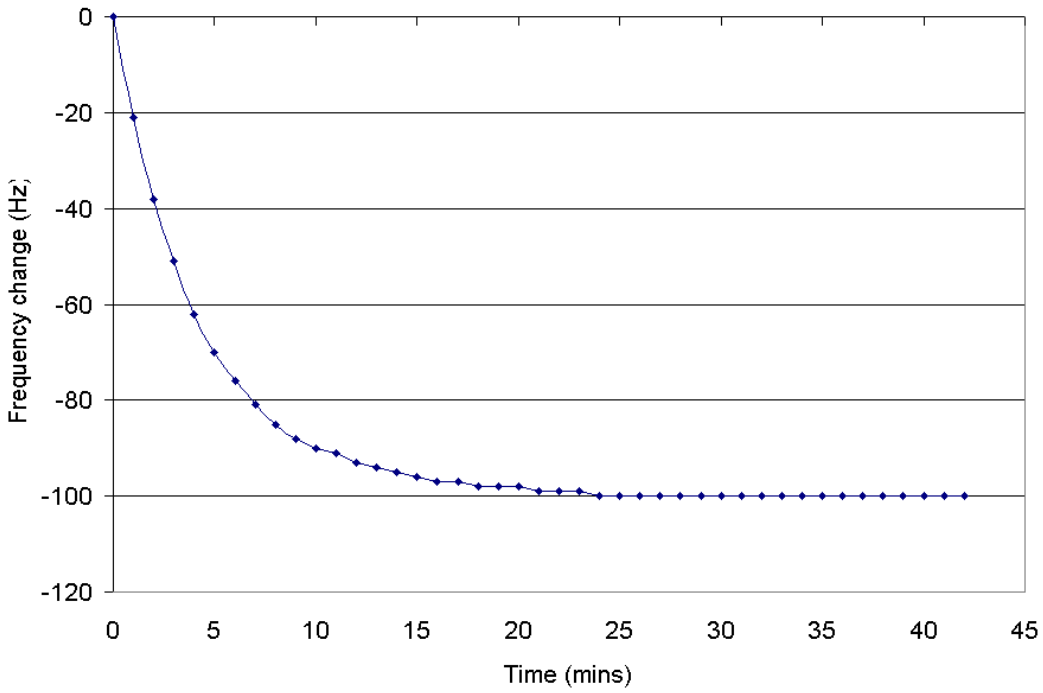

Figure C. 1. An example of frequency change curves after the adding of $NaNO_3$ solution.

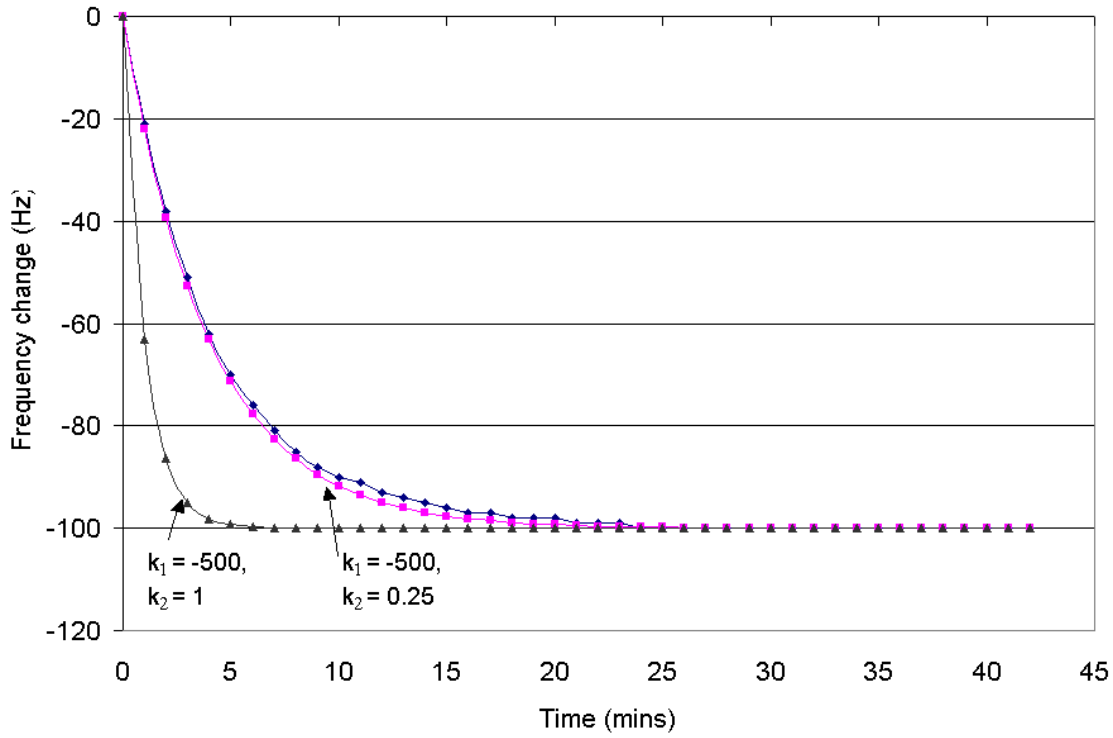

Figure C.2. Calibration curves of the initial trial and after the adjustment of the value of k_2.

Assessment of the calibration

The third step of the calibration procedure consists of assessing the impact of the calibrated parameters on model predictions. It has been demonstrated in Appendix B that the error propagation for equipment is small. The assessments of the calibration accuracy in Chapter 3 and 4 show that the predictions are generally within 20% error of the exact experiment value. However, at the initial phase, there may be significant error because of the time lag from the sensor.

Sample calculation

Example from Caruso's (1997) study is shown as follows

k_1 = -500 Hz L/g (C-6)

$k_2 = 0.300\ \text{min}^{-1}$ (C-7)

$t_n = 5.00$ mins (C-8)

$\Delta f_n = -80.0$ Hz (C-9)

$\Delta f_{n-1} = 0.00$ Hz (C-10)

Thus, the analyte concentration can be calculated using Eq. (C-1).

$$q_i = \frac{EXP(k_2 t_n)\Delta f_n - \Delta f_{n-1}}{\left[EXP(k_2 t_n) - 1\right]k_1} = 0.206 \text{ mg/mL} \quad \text{(C-11)}$$

$$\text{Relative error} = \frac{0.206 - 0.200}{0.200} \approx 3\% \quad \text{(C-12)}$$

APPENDIX D

Comparison of Approximate Ion Exchange Model with Numerical Solution

In this section we present a new solution for intraparticle ion exchange kinetics for multi-component systems with counterions of arbitrary valences. The solution is a good approximation for complex multi-component systems. The model assumes that the spherical particle is composed of a core with homogeneous concentration distribution and an outer ring with parabolic concentration distribution. The approximate dynamic model of the solid phase is compared with the numerical solution developed by Hwang and Helfferich (1987).

Model assumptions

To simplify the mathematical derivation, the following assumptions were made based on the system conditions.

(1) isothermal, isobaric operation.

(2) negligible swelling and shrinking changes of the ion exchanger.

(3) electrical neutrality.

(4) complete Donnan exclusion, no net co-ion flux within the film.

(5) constant individual diffusion coefficients of the ions.

(6) constant activity coefficients.

(7) quasi-stationary or pseudo steady state liquid film diffusion.

(8) ion exchanger particle is assumed to be composed of a core with homogeneous concentration distribution and an outer ring with parabolic concentration distribution.

Figure D.1 shows a schematic diagram of concentration profiles in the exchanger particle.

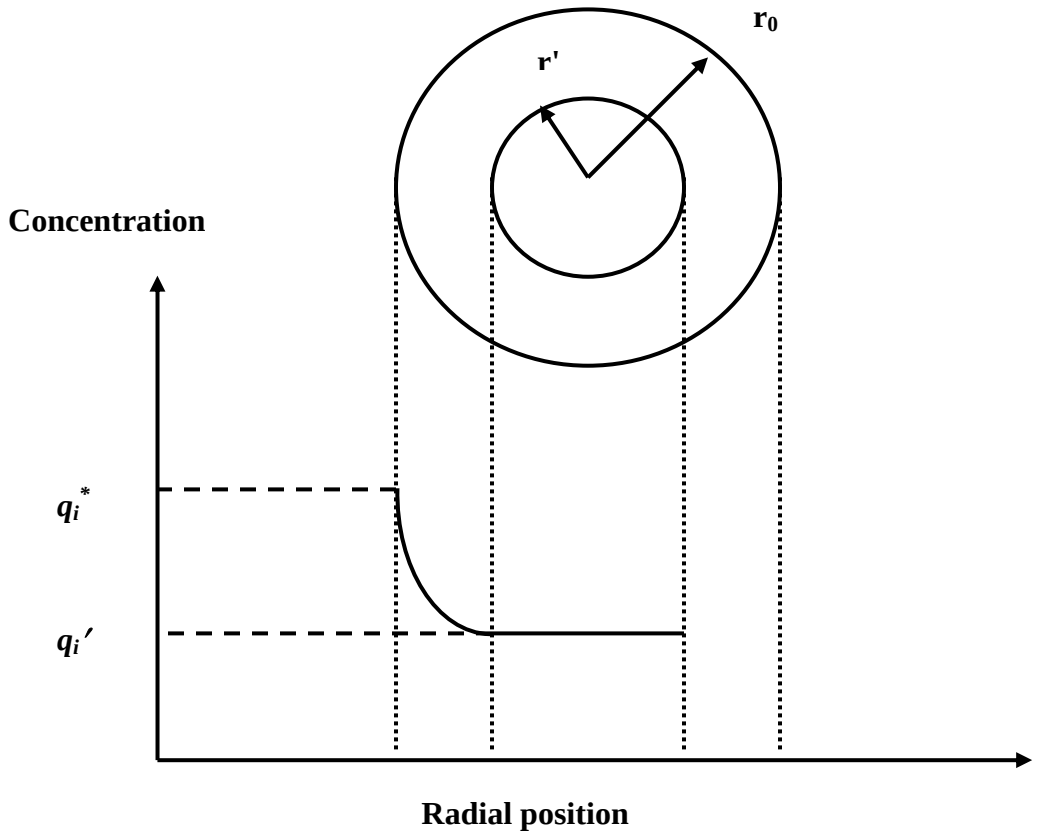

Figure D.1. Schematic diagram of concentration profile in ion exchange particle. The inner core has homogeneous concentration distribution; while the outer ring has parabolic concentration distribution.

Mathematical model

We consider an ion exchange system with n counterions. The flux of ion i in the particle is described by the Nernst-Planck equation

$$J_i = -D_i\left[\frac{\partial q_i}{\partial r} + z_i \frac{q_i F}{RT}\frac{\partial \Phi}{\partial r}\right] \qquad \text{(D-1)}$$

$i = 1, 2,\ldots, n$ counterions

where D_i is the effective diffusivity of ith ions in the exchanger, z_i is the electrochemical valence of ion i, F is Faraday constant, Φ is electric potential, and q_i is the concentration of ith ions in the exchanger.

The condition of no net electric current can be expressed by

$$\sum_{i=1}^{n} z_i J_i = 0 \qquad \text{(D-2)}$$

The corresponding initial conditions are

$$\text{at} \quad t = 0, \qquad q_i = q_i^0 \qquad i = 1, 2,\ldots, n \qquad \text{(D-3)}$$

Boundary conditions are

$$\text{at} \quad r = r', \qquad \frac{\partial q_i}{\partial r} = 0 \qquad \text{(D-4)}$$

$$\text{at} \quad r = r_0, \qquad q_i = q_i^* \qquad i = 1, 2,\ldots, n \qquad \text{(D-5)}$$

where q_i^* is the concentration of ith ions at the boundary condition.

If the ion exchanger is assumed to be composed of a core with homogeneous concentration distribution and an outer ring with parabolic concentration distribution, one has

$$q_i = q_i' + a(r - r')^2 \quad \text{for} \quad r' \le r \le r_0 \qquad \text{(D-6)}$$

where a is arbitrary function of time. On the external surface of ion exchanger, by substituting boundary condition, Eq. (D-6) becomes

$$q_i^{*} = q_i' + a(r_0 - r')^2 \tag{D-7}$$

hence

$$a = \frac{q_i^{*} - q_i'}{(r_0 - r')^2} \tag{D-8}$$

The external surface concentration gradient is

$$\left.\frac{\partial q_i}{\partial r}\right|_{r=r_0} = 2(r_0 - r')\frac{q_i^{*} - q_i'}{(r_0 - r')^2} \tag{D-9}$$

The average concentration of ion *i* in ion exchanger can be obtained by carrying out the integration.

$$\bar{q}_i = \frac{1}{V_0}\int_0^{V_0} q_i dV \tag{D-10}$$

where $\bar{q}_i$ is the average concentration of ion *i* in the exchanger.

In order to illustrate the effect of the thickness of parabolic profile, five examples were calculated with r'=0, 0.2, 0.4, 0.6, $0.8\,r_0$. Table D.1 shows the average concentration and the external surface concentration gradient when r_0 equals to various thickness. In this case, the surface concentration gradient $\left.\frac{\partial q_i}{\partial r}\right|_{r=r_0}$ is represented as a function of surface concentration q_i^{*} and average concentration $\bar{q}_i$.

Table D.1. Average concentration and surface concentration gradient for different r'

$r' =$	$\bar{q}_i =$	$q_i^* - \bar{q}_i =$	$\left.\frac{\partial q_i}{\partial r}\right\|_{r=r_0} =$	
0	$q_i' + \frac{3}{5}(q_i^* - q_i')$	$\frac{2}{5}(q_i^* - q_i')$	$2\frac{(q_i^* - q_i')}{r_0} = 5\frac{(q_i^* - \bar{q}_i)}{r_0}$	(D-11)
$0.2\,r_0$	$q_i' + \frac{332}{625}(q_i^* - q_i')$	$\frac{293}{625}(q_i^* - q_i')$	$\frac{5}{2}\frac{(q_i^* - q_i')}{r_0} = \frac{3125}{586}\frac{(q_i^* - \bar{q}_i)}{r_0}$	(D-12)
$0.4\,r_0$	$q_i' + \frac{276}{625}(q_i^* - q_i')$	$\frac{349}{625}(q_i^* - q_i')$	$\frac{10}{3}\frac{(q_i^* - q_i')}{r_0} = \frac{6250}{1047}\frac{(q_i^* - \bar{q}_i)}{r_0}$	(D-13)
$0.6\,r_0$	$q_i' + \frac{204}{625}(q_i^* - q_i')$	$\frac{421}{625}(q_i^* - q_i')$	$5\frac{(q_i^* - q_i')}{r_0} = \frac{3125}{421}\frac{(q_i^* - \bar{q}_i)}{r_0}$	(D-14)
$0.8\,r_0$	$q_i' + \frac{113}{625}(q_i^* - q_i')$	$\frac{421}{625}(q_i^* - q_i')$	$10\frac{(q_i^* - q_i')}{r_0} = \frac{6250}{512}\frac{(q_i^* - \bar{q}_i)}{r_0}$	(D-15)

The flux across the external surface can be described by

$$J_{r_0} = -D_i\left[\left.\frac{\partial q_i}{\partial r}\right|_{r_0} + z_i\frac{q_i F}{RT}\left.\frac{\partial \Phi}{\partial r}\right|_{r_0}\right] \tag{D-16}$$

The time derivative of average concentration is defined as

$$\frac{d\bar{q}_i}{dt} = \frac{3}{r_0}D_i\left[\left.\frac{\partial q_i}{\partial r}\right|_{r_0} + z_i\frac{q_i^* F}{RT}\left.\frac{\partial \Phi}{\partial r}\right|_{r_0}\right] \tag{D-17}$$

The system is subject to the no electric current restriction, i.e., the electric field is completely generated by diffusion of ions within the system. Therefore, the electric potential gradient in Eq. (D-17) can be transformed to concentration gradient by combining Eq. (D-2) and Eq. (D-16).

$$\frac{F}{RT}\frac{\partial \Phi}{\partial r} = -\frac{\sum D_i z_i}{\sum D_i z_i^2 q_i^*}\frac{\partial q_i}{\partial r} \tag{D-18}$$

By substituting Eq. (D-18) and Eq. (D-11, D-12, D-13, D-14, D-15) respectively, Eq. (D-17) can be rearranged as follows

$$r' = 0, \qquad \frac{d\bar{q}_i}{dt} = \frac{15}{r_0^{\,2}} D_i \left[(q_i^* - \bar{q}_i) - z_i q_i^* \frac{\sum z_i D_i (q_i^* - \bar{q}_i)}{\sum z_i^2 D_i q_i^*} \right] \tag{D-19}$$

$$r' = 0.2\, r_0, \qquad \frac{d\bar{q}_i}{dt} = \frac{15.9983}{r_0^{\,2}} D_i \left[(q_i^* - \bar{q}_i) - z_i q_i^* \frac{\sum z_i D_i (q_i^* - \bar{q}_i)}{\sum z_i^2 D_i q_i^*} \right] \tag{D-20}$$

$$r' = 0.4\, r_0, \qquad \frac{d\bar{q}_i}{dt} = \frac{17.9083}{r_0^{\,2}} D_i \left[(q_i^* - \bar{q}_i) - z_i q_i^* \frac{\sum z_i D_i (q_i^* - \bar{q}_i)}{\sum z_i^2 D_i q_i^*} \right] \tag{D-21}$$

$$r' = 0.6\, r_0, \qquad \frac{d\bar{q}_i}{dt} = \frac{22.2684}{r_0^{\,2}} D_i \left[(q_i^* - \bar{q}_i) - z_i q_i^* \frac{\sum z_i D_i (q_i^* - \bar{q}_i)}{\sum z_i^2 D_i q_i^*} \right] \tag{D-22}$$

$$r' = 0.8\, r_0, \qquad \frac{d\bar{q}_i}{dt} = \frac{36.6211}{r_0^{\,2}} D_i \left[(q_i^* - \bar{q}_i) - z_i q_i^* \frac{\sum z_i D_i (q_i^* - \bar{q}_i)}{\sum z_i^2 D_i q_i^*} \right] \tag{D-23}$$

It is worth noting that, for r' = 0, Eq. (D-19) assumes that the concentration distribution in the whole particle is parabolic. Eq. (D-19) is also similar to Glueckauf's (1955 a, b) diffusion equation (Eq. D-24) which was derived for spherical particle adsorption

$$\frac{d\bar{q}_i}{dt} = \frac{15}{r_0^{\,2}} D_i (q_i^* - \bar{q}_i) \tag{D-24}$$

Glueckauf's diffusion equation is derived from Fick equation. The Fick equation takes into account only diffusive terms. The second term of Eq. (D-19) is related to the electric potential in Nernst-Planck equation, which is not considered in adsorption process.

Comparison with numerical solution

Figure D.2 compares uptake curves for spherical particle diffusion with r' = 0, $0.2\,r_0$, $0.4\,r_0$, $0.6\,r_0$, $0.8\,r_0$; $z_A = z_B = z_C = 1$, $D_A : D_B : D_C = 1:5:0.2$; dimensionless concentration at boundary $x_B^* = \frac{q_B^*}{Q} = 0.6$, $x_C^* = \frac{q_C^*}{Q} = 0.4$. The diffusion kinetic curves in Figure D.2 provide expected results. When r' is small, the ion exchange process is slow. This occurs because ions need to transfer through a long diffusion region. An overshoot on the uptake curve is shown for counterion with higher diffusion coefficient. Figure D.2 illustrates that the maximum overshoot is not related to the assumed homogeneous radius r'.

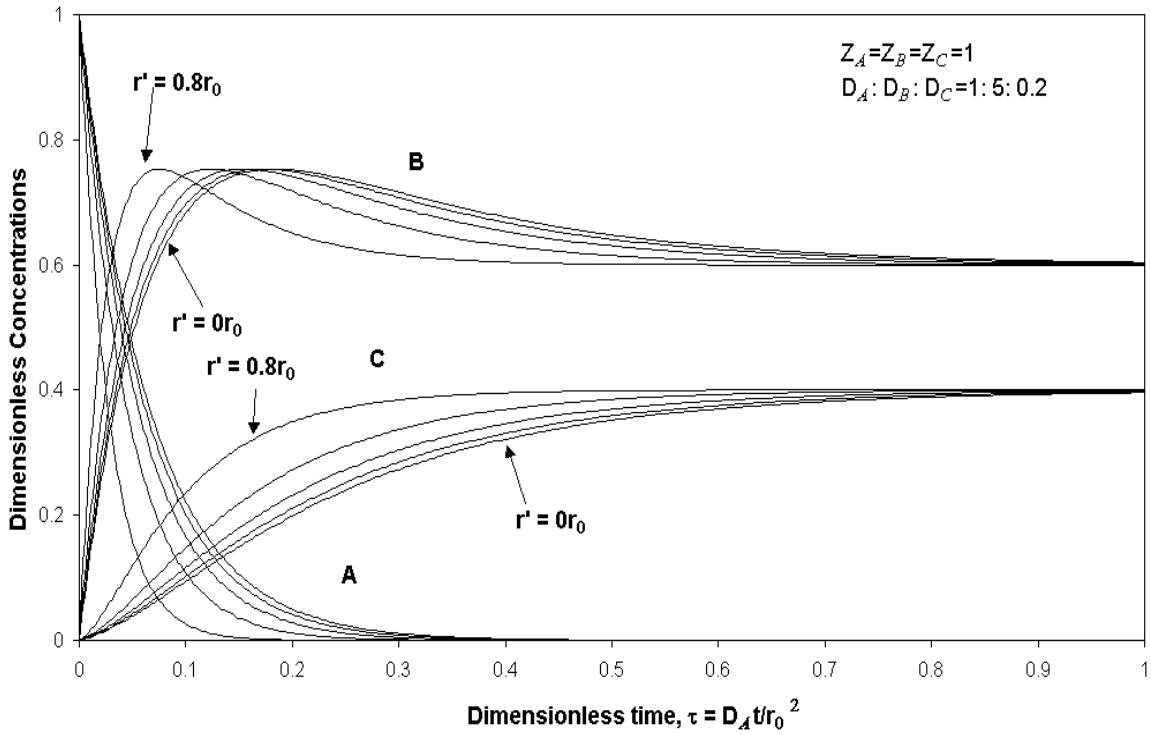

Figure D.2. Sorption uptake curve of ternary ion exchange system with r'=0, 0.2, 0.4, 0.6, 0.8 r_0 respectively. Dimensionless concentration at boundary x_B*=0.6, x_A*=0.4.

In order to test the approximation model for solid phase ion exchange kinetics, the proposed model was compared with the numerical solution submitted by Hwang and Helfferich (1987). A comparison with a ternary system A/B-C is demonstrated in Figure D.3. The parameter for both models is the same as the one used in Figure D.2. In this case, the kinetic curve is based on Eq. (D-19) with $r' = 0$, i.e., the spherical particle is assumed to be a completely parabolic profile. Figure D.3 shows a good agreement between both models. While the agreement is not precise everywhere, the effect of the slope of the isotherm on the sorption uptake curve is captured quantitatively by the proposed model.

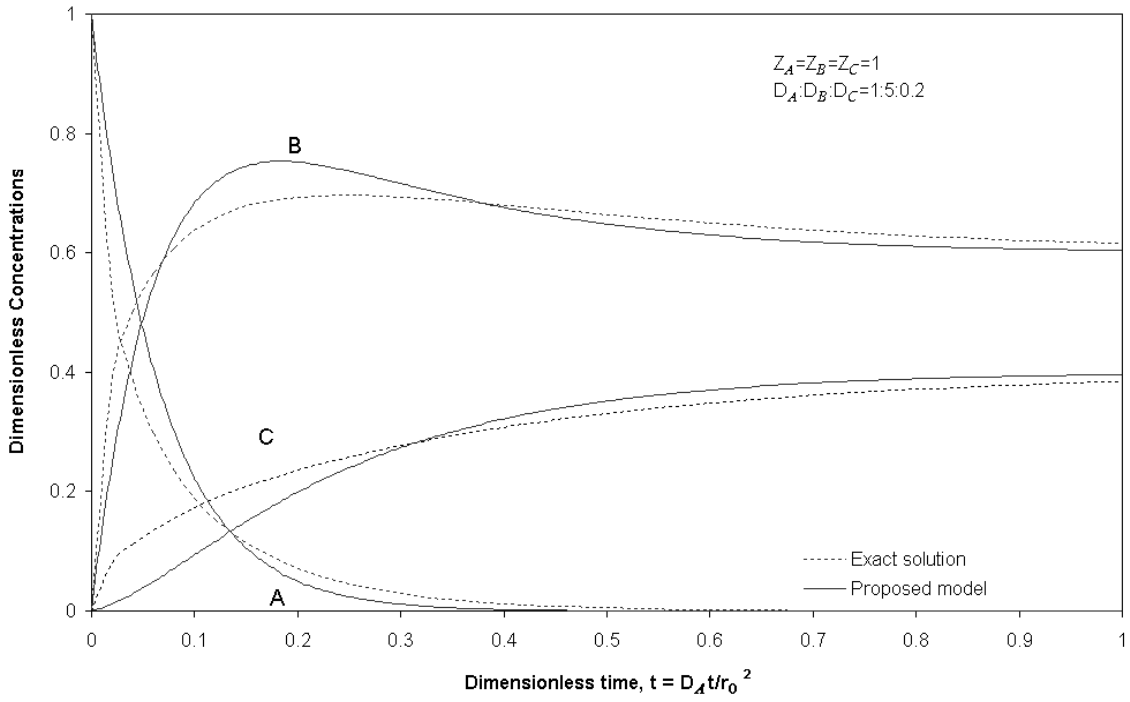

Figure D.3. Comparison of kinetic curves calculated from proposed model with r'=0 and numerical solution for ternary solid phase ion exchange. Dimensionless concentration at boundary x_B*=0.6, x_A*=0.4.

VITA

WANG LIN

Candidate for the Degree of

Doctor of Philosophy

Dissertation: DEVELOPMENT AND APPLICATION OF A PREDICTIVE MODEL TO DETECT ANALYTE CONCENTRATION FROM A QUARTZ CRYSTAL MICROBALANCE

Major Field: Chemical Engineering

Biographical:

Personal Data: Born in Tianjin, China, on January 1, 1978, the son of Yiren Lin and Yun Yu.

Education: Graduated from Nankai High School, Tianjin, China, July, 1996; received Bachelor of Science degree in Chemical Engineering at Nanjing University, Nanjing, China, July, 2000; completed the requirements for the Doctor of Philosophy Degree in Chemical Engineering at Oklahoma State University in May 2005.

Professional Experience: Employed as a teaching associate, School of Chemical Engineering, Oklahoma State University, August 2000 to May 2001; Employed as a research associate, School of Chemical Engineering, Oklahoma State University, May 2001 to June 2004; Employed as a PhD summer intern, The Procter & Gamble Company, June 2004 to September 2004.